Integration of Dynamic Rhizospheric Methane Oxidation into a Process-based Methane Emissions Model

Farnaz Aslkhodapasand

A thesis

submitted in partial fulfillment of the

requirements for the degree of

Master of Science in Civil Engineering

University of Washington

2016

Committee:

Rebecca B Neumann
David Butman
Theodore Bohn

Program Authorized to Offer Degree:

Department of Civil and Environmental Engineering

University of Washington

Abstract

Integration of Dynamic Rhizospheric Methane Oxidation into a Process-based Methane Emissions Model

Farnaz Aslkhodapasand

Chair of the Supervisory Committee:
Rebecca B Neumann
Civil and Environmental Engineering

Global methane models predict that wetlands contribute 20 to 39% of global methane emissions. Wetland plants can contribute fuel for methane production by exuding carbon into the soil, but they also introduce oxygen which would oxidize the produced methane (known as rhizospheric methane oxidation). They can also provide conduits for methane to escape to the atmosphere through their aerenchyma tissues. Previous process-based global-scale models have assumed that a constant fraction of methane in the rhizosphere is oxidized, while experimental studies have found that rhizospheric methane oxidation is not a static process and changes with environmental factors.

In this study, a mechanistic rhizosphere-scale model was developed in order to understand the relationship between rhizospheric methane oxidation and environmental factors.

The mechanistic model results showed that rhizospheric methane oxidation not only can change with availability of carbon from roots and root gas transport capacity, but that it also is a function of microbial competition between microbial populations that live in methanogenic environments. These results were incorporated into a large-scale process-based methane emissions model in form of a dynamic rhizospheric methane oxidation process and plot-scale model simulations were performed for four study sites located in Western Siberia. Future simulations using both static and dynamic models showed that methane emissions would increase by a median factor of 1.7 by the end of century. Switching from static to dynamic model resulted in reduction of total annual methane emissions by 4% and reduction of plant-mediated methane transport by 17% in the four study sites. The reduction is more pronounced for sites with higher density of aerenchymatous plants (such as sedges) due to higher root zone methane oxidation. The dynamic model showed that higher coverage of aerenchymatous plants in a wetland can lead to lower plant-mediated methane transport and lower methane emission. As a result, current approach of global methane emission models could potentially be overestimating methane emissions from such sites due to neglecting the effect of high root transport capacity on P_{ox} as it is proposed in this study.

TABLE OF CONTENTS

LIST OF FIGURES

LIST OF TABLES

ACKNOWLEDGEMENTS

I would like to thank my adviser Dr. Rebecca Neumann for consistently supporting me during my master's studies at UW. This thesis would not have been possible without her helping me grow ideas into actual modeling experiments. I would also like to thank Dr. David Butman for being on my supervisory committee and Dr. Theodore Bohn for all the insightful meetings and helping me with performing modeling simulations.

I am very thankful to my fellow graduate students and postdoctoral researchers in the UW Hydro-Biogeochemistry research group. It was such a great pleasure to be team-mates with you guys, I learned a lot from you in research and writing.

I appreciate the help and support from my parents who have always supported me in pursuing my goals. Thank you for always so patient and caring, even when you were thousands of miles away. I miss you so much.

And last but not least, I would like to say thank you to my dear husband Abbas, who has been there by my side all along, in ups and downs. Abbas, you are my biggest source of inspiration. You are my best friend. Thank you for helping me grow up, to be a better person.

Chapter 1. INTRODUCTION

1.1 BACKGROUND AND MOTIVATION

Atmospheric methane is an important greenhouse gas, with 25 times higher warming effect per mass compared to CO_2 in a time horizon of 100 years (Boucher et al., 2009; IPCC 2013). Atmospheric methane concentrations have increased more than 100% over the last 200 years (Boucher et al., 2009). Although methane concentrations are on average only 0.5% of atmospheric CO_2 concentrations (IPCC 2013), methane currently contributes almost 17% of greenhouse radiative forcing globally (IPCC 2013). Wetlands are the largest sources of natural methane emission to the atmosphere. However, due to high variability of wetland areas and variability in measured methane emissions, uncertainty in the magnitude of wetland methane emission is large, with current estimates ranging from 20 to 40% of total global methane emissions (Bohn et al., 2015; Melton et al., 2013).

Methane emission from wetlands is the result of microbial processes in wetland soils, including methane production by methanogens, methane oxidation by methanotrophs and aerobic respiration by heterotrophs. Wetlands have water-logged anoxic soil and large deposits of potentially labile organic carbon due to slow decomposition of organic matter in anoxic conditions. These conditions make wetlands suitable habitats for methanogens which are anaerobic microbes that use organic carbon to produce methane (acetoclastic methanogens) or use H_2 gas to reduce CO_2 to CH_4 (hydrogenotrophic methanogens). Wetland plants also contribute to methane emission via input of carbon to soils around their root (the rhizosphere). Some plants provide emission pathways for methane to escape to the atmosphere through their

aerenchematous tissues (Aulakh et al., 2001; Walter and Heimann, 2000; Whalen and Reeburgh, 1988).

Methane produced in the anoxic zone of wetlands has three main pathways of emission to the atmosphere. First pathway is diffusion through the water column; methane produced in the deeper anoxic soil diffuses through the soil and is emitted to the atmosphere. Since methane diffusion in water is a very slow process (methane diffusion coefficient in water is 1.84E-9 m^2/s (Jähne et al., 1987)), this emission pathway contributes a small portion of total emissions (Lai, 2009; Kiene 1991). Second pathway is ebullition: bubbles of methane form when water becomes saturated with dissolved methane. These bubbles then travel upwards and are released to the atmosphere. This pathway can transport methane to the atmosphere much faster than diffusion and is capable of contributing 48 to 63% of total methane emission (Bartlett et al., 1988). The third pathway is plant-mediated transport: hollow tissues inside wetland plant roots, also known as aerenchymatous tissues, can directly transport methane from the deep anoxic soil to the atmosphere. Plant-mediated transport is usually the dominant pathway of methane emission to the atmosphere and can contribute up to 90% of total emissions during the growing season (Bhullar et al., 2013; Laanbroek, 2010).

Plant roots require oxygen for respiration and they usually receive this oxygen from the small air spaces in soil. However, this is not possible in wetlands since the soil is saturated with anoxic water. As a result, wetland plants develop aerenchyma to allow diffusion of oxygen down to the root tips. The diffusive gradient that drives this transport process extends outside the roots into the soil, so oxygen typically leaks out into the soil to form an oxic layer around plant roots (Armstrong, 1964). Carbon can also be exuded from wetland plant roots and be a potential source of carbon for methanogens (Aulakh et al., 2001; Koelbener et al., 2009). Plant-exuded

carbon can also be taken up by heterotrophic bacteria that use oxygen to oxidize organic carbon into CO_2 (Hütsch et al., 2002). The oxic layer around the plant roots is a suitable environment for heterotrophic respiration since both oxygen and carbon is provided to heterotrophic bacteria from plant roots (Gerard and Chanton, 1993; King, 1994; Nat and Middelburg, 1998). Due to methane concentration gradient between the soil and atmosphere, methane can diffuse through the aerenchymatous tissues and be emitted to the atmosphere. Methanotrophs (methane oxidizing bacteria) also reside in this oxic zone around the roots and oxidize a significant portion of the methane that is diffusing towards the roots to travel to the atmosphere. P_{ox} is defined as the ratio of methane that is oxidized in the rhizosphere when it is diffusing towards the roots to travel to the atmosphere through the plants. Studies show that P_{ox} values can vary between 39 to 90% (Gerard and Chanton, 1993; Schipper and Reddy, 1996; Schütz et al., 1989).

Inputs of organic carbon and oxygen from the roots make the rhizosphere a microbial hotspot capable of hosting a variety of microbial communities. These inputs trigger competition between different microbial populations for available substrates: methanogens ferment organic carbon into methane, a reaction that is inhibited by oxygen; methanotrophs use oxygen to oxidize methane into carbon dioxide; and heterotrophs use oxygen to oxidize organic carbon. Since plant-mediated methane transport is directly related to the methane concentration gradient between soil and the atmosphere, competition between different microbial processes impacts the amount of methane emitted through plants.

Large scale and global scale methane models are essential tools to estimate methane emissions to the atmosphere. Output from methane models can help policy makers by providing current and predicted future methane emissions. Large-scale methane emission models usually treat rhizospheric methane oxidation as a static process. In other words, they assume a static

portion of methane in the rhizosphere become oxidized (i.e. constant P_{ox}). For example the Walter-Heimann methane emission model assumes that a constant ratio (50%) of methane that travels through the plant is oxidized in the oxic region around roots while studies show a much wider range for this ratio. On the other hand, previous studies show that P_{ox} can actually have a wide range (39 to 90%), presumably due to differing conditions of competition between different microbial activities that occur in methanogenic environments like wetlands (Gerard and Chanton, 1993; Schipper and Reddy, 1996; Schütz et al., 1989). Since methane oxidation is a potentially large sink of methane, P_{ox} could have an important role in large-scale and global-scale methane models. P_{ox} is dependent on the competition between microbial processes and is likely to vary as a function of plant root exudation rates and root gas transport capacity which determines root zone oxygenation.

Mechanistic methane emission models that take into account the biological, chemical and physical processes that take place in the environment are useful for analyzing the competition between the microbial processes. Mechanistic models are helpful for understanding the variation in P_{ox} and the factors that might be contributing to this variation and thus help improve the representation of P_{ox} in large-scale methane models.

In this study, a mechanistic model of wetland plant roots and the biochemical processes occurring in the rhizosphere was developed. This model is capable of modeling methane oxidation ratios with variable root carbon exudation rates, variable root gas transport capacities and different levels of microbe competitiveness (described in more detail in Chapter 2). This study improves understanding of how microbial competition impacts rates of methane oxidation, rhizosphere methane concentration and rates of plant-mediated methane emissions from wetlands. Hence this study can be used to enhance the model representation of the fraction of

methane that is oxidized before traveling through plants. The results of the mechanistic model were used to develop an empirical equation that describes methane oxidation fraction in the Walter-Heimann large scale methane model as a function of plant gas transport capacity and root carbon exudation (known as dynamic P_{ox} in this study) (Walter and Heimann, 2000). Incorporating this new equation could potentially enhance the predictive power of large-scale methane emission models that currently treat methane oxidation as a static process.

1.2 Areas of Investigation and Research Approach

In this study, the following questions were investigated.

1) How is root zone methane oxidation controlled by physical and biological process occurring in the rhizosphere of wetland plants (processes such as root carbon exudation and root gas transport)? Can this question be investigated using a mechanistic model?
2) How can mechanistic rhizosphere-scale models inform the representation of root zone oxidation in a dynamic manner in large-scale methane models compared to the current approach of static methane oxidation rate?
3) How does dynamic rhizosphere methane oxidation in large-scale methane models change current and future estimates of methane emission?

Chapter 2. MECHANISTIC ROOT-SCALE MODEL METHODS

In order to understand the microbial competition in the rhizosphere of wetland plants, a mechanistic root-scale model was developed using the Reactive Transport Code MIN3P (Mayer et al., 2002). MIN3P is a FORTRAN code that solves multi-component reactive transport combined with saturated or unsaturated water flow using finite differences. It allows the user to define specific kinetic rates for each reaction in a defined domain with desired initial conditions and boundary conditions.

The model in this study was a one-dimensional radial model that consisted of a single root of 0.37mm radius (Bodegom et al., 2001) and 10 cm of surrounding soil in which microbial reactions and plant-related processes were simulated. Simulated microbial reactions were methane production (acetoclastic and hydrogenotrophic methanogenesis), methane oxidation (methanotrophy), heterotrophic respiration, glucose fermentation and decomposition of organic matter. Simulated plant-related processes were root carbon exudation, root oxygen leakage and plant-mediated methane transport (aerenchyma methane uptake). Rates of microbial reactions were modeled with Michaelis-Menten kinetics:

$$R = V_{\max} \frac{[S]}{[S] + K_m} \frac{I_x}{I_x + [X]} \qquad 2\text{-}1$$

where *[S]* is the substrate concentration, K_m is the half-saturation (concentration at which reaction rate is equal to half of maximum uptake rate V_{max}) of that specific substrate and V_{max} is the maximum uptake rate for that substrate. *[X]* is the concentration of the inhibitor of the reaction (for example oxygen is an inhibitor of methane production reaction) and I_x the inhibition constant for that specific inhibitor. Values of these parameters were obtained through literature review. The literature review results for collecting kinetic parameters data is available in

Appendix A. Specific values used in this model are shown for each reaction separately in section 2.3.

2.1 Model Domain

The root was modeled as a single node and the soil as a one-dimensional radial domain in which each node is characterized by its distance from the root. Solutes were transported by diffusion across the domain. Figure 2-1 shows a schematic of the model and the represented processes. Root carbon exudation is shown in form of glucose. Oxygen leakage from the root oxygenates a layer around the root (shown in blue). The rest of the domain is anoxic (Shown in orange).

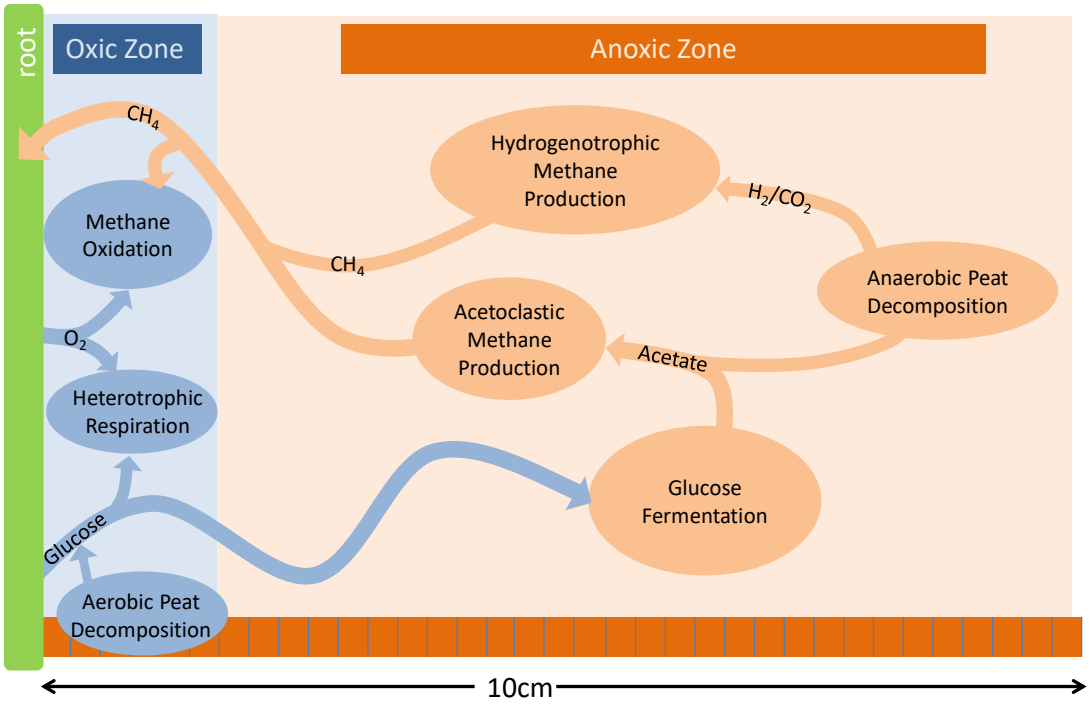

Figure 2-1 Schematic representation of microbial processes in the rhizosphere of wetland plant roots

2.1.1 *Initial conditions*

The initial concentrations were set to mimic the beginning of the growing season in boreal wetlands according to the typical values reported in the literature (see Table 2-1). Simulations were performed for a 3-month period (typical growth season in boreal wetlands).

2.1.2 *Boundary conditions*

The root boundary was closed to solute transport except for root carbon exudation, root oxygen leakage and root methane uptake. Root exudates and oxygen entered the domain from the root at prescribed rates and methane was allowed to diffuse out of the domain throughout the root (see section 2.2.9 for details on root methane uptake). The outer soil boundary was a third-

type (Cauchy) boundary. Concentrations of chemical species were defined on a dummy node outside of the domain according to typical concentration of the species in the environment (shown in Table 2-1) and the solutes were allowed to diffuse based on the concentration difference between inside and outside of the domain and their diffusion coefficient based on Fick's law. A third-type boundary acts like a boundary closed to the inside of the domain, but permeable to the outside such that chemical species can enter the domain in response to concentration gradients but cannot flux out.

Table 2-1 Initial concentration and boundary concentration of chemical species in the model

Species	Initial concentration ($mol \cdot L^{-1}$)	Boundary concentration (typical concentration in environment) ($mol \cdot L^{-1}$)	Reference
CH_3COO^-	1.7E-6	1.7E-6	(Duddleston et al., 2002)
CO_3^{2-}	1.0E-4	1.0E-4	Calculated based on assumption of
$CH_{4(aq)}$	2.0E-4	2.0E-4	(Shoemaker and Schrag, 2010)
H^+	1.0E-5	1.0E-5	(Kotsyurbenko et al., 2007)
$O_{2(aq)}$	1.0E-10	1.0E-10	MIN3P's zero limit
$H_{2(aq)}$	1.0E-8	1.0E-8	(Krämer and Conrad, 1993)
$C_6H_{12}O_6$	1.0E-10	1.0E-10	MIN3P's zero limit

2.2 MICROBIAL PROCESSES

In this section the microbial and plant-related processes included in the model and their rate equations are described. Kinetic parameters used in these equations are described in section 2.3. Note that rates of all microbial reactions were assumed to be independent of biomass; therefore microbial biomass was not modeled.

2.2.1 *Methane production from acetate*

One of the pathways of methane production is acetate fermentation (aka acetoclastic methanogenesis). The stoichiometry of this reaction is shown in Equation 2-2.

$$CH_3COO^- + H_2O \rightarrow CO_3^{2-} + CH_{4(aq)} + H^+ \quad (2\text{-}2)$$

Since methane production is an anaerobic process, an oxygen inhibition factor was included in the rate equation for methane production (Arah and Stephen, 1998). Acetate needed for methanogenesis was supplied by decomposition of peat organic matter (see Figure 2-1 and section 2.2.6). Fermentation of exuded glucose from the root also provided acetate for methane production (see section 2.2.5). The rate of methane production from acetate followed Michaelis-Menten kinetics according to Equation 2-3.

$$R_{prod\_ace} = V_{\max}^{prod\_ace} \frac{[CH_3COO^-]}{[CH_3COO^-] + K_{acetate}^{prod\_ace}} \frac{I_{O_2}^{prod\_ace}}{I_{O_2}^{prod\_ace} + [O_2]} \quad (2\text{-}3)$$

where $K_{acetate}^{prod\_ace}$ is the half-saturation for acetate and $K_{O_2}^{prod\_ace}$ is the inhibition constant for oxygen. $V_{\max}^{prod\_ace}$ is the maximum rate of methane production from acetate in complete abundance of substrate.

2.2.2 *Methane production from CO_2/H_2*

Another pathway for methane production is through microbial utilization of CO_2 and H_2 as substrates (hydrogenotrophic methanogenesis). Stoichiometry of this reaction is shown in Equation 2-4.

$$CO_3^{2-} + 2H^+ + 4H_2 \rightarrow 3H_2O + CH_{4(aq)} \quad (2\text{-}4)$$

The rate of hydrogenotrophic methanogenesis followed Michaelis-Menten kinetics as shown in Equation 2-5. CO_2 and H_2 were produced via anaerobic decomposition of peat (see Equation 2-7). This pathway of methane production is also an anaerobic process. An oxygen inhibition factor was included in the rate equation for methane production from CO_2/H_2.

$$R_{prod\_hyd} = V_{\max}^{prod\_hyd} \frac{[H_2]}{[H_2] + K_{H_2}^{prod\_hyd}} \frac{I_{O_2}^{prod\_hyd}}{I_{O_2}^{prod\_hyd} + [O_2]} \quad (2\text{-}5)$$

where $K_{H_2}^{prod\_hyd}$ is the half-saturation for H_2 and $K_{O_2}^{prod\_hyd}$ is the inhibition constant for oxygen. $V_{\max}^{prod\_hyd}$ is the maximum rate of methane production from hydrogenotrophic methanogenesis.

2.2.3 *Methane oxidation*

Methane oxidizing microbes (methanotrophs) use oxygen to oxidize methane into CO_2, competing with heterotrophs for available oxygen. Stoichiometry of methane oxidation reaction is shown in Equation 2-6.

$$CH_{4(aq)} + 2O_{2(aq)} \rightarrow CO_3^{2-} + 2H^+ + H_2O \quad (2\text{-}6)$$

The rate of methane oxidation reaction follows Michaelis-Menten kinetics as shown in Equation 2-7:

$$R_{oxid} = V_{\max}^{oxid} \frac{[CH_4]}{[CH_4] + K_{CH_4}^{oxid}} \frac{[O_2]}{[O_2] + K_{O_2}^{oxid}} \quad (2\text{-}7)$$

where $K_{CH_4}^{oxid}$ is the half-saturation for methane and $K_{O_2}^{oxid}$ is the half-saturation for oxygen. $V_{\max}^{oxid}$ is the maximum rate of methane oxidation.

2.2.4 *Heterotrophic respiration*

Heterotrophs use oxygen to oxidize organic carbon in the soil to CO_2. Glucose was used as the model carbon source for heterotrophic respiration (Van Bodegom 2001). Stoichiometry of the heterotrophic respiration is shown in Equation 2-8.

$$C_6H_{12}O_6 + 6O_2 \rightarrow 6CO_3^{2-} + 12H^+ \quad (2\text{-}8)$$

Heterotrophic respiration rate follows Michaelis-Menten kinetics as shown in Equation 2-9.

$$R_{hetr} = V_{\max}^{hetr} \frac{[C_6H_{12}O_6]}{[C_6H_{12}O_6] + K_{glu\cos e}^{hetr}} \frac{[O_2]}{[O_2] + K_{O_2}^{hetr}} \quad (2\text{-}9)$$

$K_{glu\cos e}^{hetr}$ is the half-saturation of glucose and $K_{O_2}^{hetr}$ is the half-saturation of oxygen in heterotrophic respiration reaction. $V_{\max}^{hetr}$ is the maximum rate of heterotrophic respiration.

2.2.5 *Glucose fermentation*

In the anoxic zone of the modeled domain glucose fermentation generated acetate, CO_2 and H_2 from available glucose according to the following stoichiometry:

$$C_6H_{12}O_6 + 4H_2O \rightarrow 2CH_3COO^- + 2CO_3^{2-} + 4H_2 + 6H^+ \quad (2\text{-}10)$$

This process is called dark fermentation of glucose, also known as homogenous acetate fermentation. The rate of glucose fermentation was defined using Michaelis-Menten kinetics as shown in Equation 2-11:

$$R_{ferm} = V_{\max}^{ferm} \frac{[C_6H_{12}O_6]}{[C_6H_{12}O_6] + K_{glu\cos e}^{ferm}} \frac{I_{O_2}^{ferm}}{I_{O_2}^{ferm} + [O_2]} \quad (2\text{-}11)$$

where $K_{glu\cos e}^{ferm}$ is the half-saturation of glucose in glucose fermentation reaction. $V_{\max}^{ferm}$ is the maximum rate of glucose fermentation which is defined in order to produce acetate with the same rate as anaerobic peat decomposition (see section2.2.8 for more details on anaerobic peat decomposition).

2.2.6 *Peat decomposition*

Peat decomposition is the process by which microorganisms break down large organic molecules in the soil and produce more labile forms of carbon (Pankratov, 2012). In this model, peat decomposition occurred under both aerobic and anaerobic conditions. Anaerobic peat decomposition is the result of fermentation processes occurring in the soil. In the model, this

process produced acetate, CO_2, and H_2 with ratios of dark fermentation of organic carbon (Ferry 1993) as shown in Equation 2-12. This process was inhibited by oxygen. Equation 2-13 shows the anaerobic peat decomposition rate equation. Note that maximum rate (V_{max}) was a prescribed variable in Equation 2-13.

$$anaerobic\,peat \rightarrow CH_3COO^- + CO_3^{2-} + 2H_2 + 3H^+ \tag{2-12}$$

$$R_{anaer\_peat} = V_{\max}^{anaer\_peat} \frac{I_{O_2}^{anaer\_peat}}{[O_2] + I_{O_2}^{anaer\_peat}} \tag{2-13}$$

Aerobic peat decomposition produced glucose (model non-acetate carbon compound) in oxygenated portion of the model domain as shown in Equation 2-14.

$$aerobic\,peat \rightarrow C_6H_6O_{12} \tag{2-14}$$

Heterotrophic bacteria can directly use this glucose to respire. According to previous research, aerobic peat decomposition can be up to 3 times faster than anaerobic decomposition (D'Angelo and Reddy, 1999). As a result, prescribed aerobic peat decomposition V_{max} was defined to be 3 times larger than the anaerobic peat decomposition V_{max} in the model. While anaerobic peat decomposition was inhibited by oxygen, aerobic peat decomposition depended on oxygen via a defined half-saturation ($K_{O_2}^{aer\_peat}$) value of 2.5E-6 mol.L^{-1}. Aerobic peat decomposition rate is shown in Equation 2-15.

$$R_{aer\_peat} = V_{\max}^{aer\_peat} \frac{[O_2]}{[O_2] + K_{O_2}^{aer\_peat}} \tag{2-15}$$

Maximum rates (V_{max}) of both anaerobic and aerobic peat decomposition were prescribed in order for the model to generate typical rates of methane production observed in wetlands which were 400 to 1000 μmol/L/month (Neumann et al., 2015). These rates were prescribed at three

different levels to mimic high, medium and low levels of peat decomposition across varying simulations as shown in Table 2-2.

Table 2-2 Anaerobic and aerobic peat decomposition maximum rates used in the model

	Anaerobic peat decomposition V_{max} ($mol \cdot L^{-1} \cdot s^{-1}$)	Aerobic peat Decomposition V_{max} ($mol \cdot L^{-1} \cdot s^{-1}$)
Low peat decomposition	2.5E-11	7.5E-11
Medium peat decomposition	5.0E-11	1.5E-10
High peat decomposition	1.0E-10	3.0E-10

2.2.7 *Root carbon exudation*

Organic carbon produced by photosynthesis can leak out of the plant roots into the soil. Previous studies show that labile organic carbon exuded from the roots of wetland plants can significantly enhance methane production in the rhizosphere (King, 1994; Whiting and Chanton, 1993). It can also be used by heterotrophs in the rhizosphere. Varying rates of root carbon exudation was included in this model according to the range of carbon exudation rates reported in the literature (shown in Table 2-3). Exuded carbon was modeled as glucose, a generic non-acetate carbon compound. A range of 0 to 1.2E-9 $mol \cdot (m\ length\ of\ root)^{-1} \cdot s^{-1}$ were used in the mechanistic model simulations.

Table 2-3 Root carbon exudation data collected from literature

Root Carbon Exudation ($mol \cdot (m\ length\ of\ root)^{-1} \cdot s^{-1}$)	Measurement type	Reference
9.4E-12	Site	(Crow and Wieder, 2005)
9.2E-10	site	(Wu et al., 2012)
7.8E-13	Site	(Zhai et al., 2013)
2.1E-11	Plant	(Phillips et al., 2009)
2.0E-11	Plant	(Phillips et al., 2009)
1.1E-12	Plant	(Phillips et al., 2009)
7.6E-13	Plant	(Phillips et al., 2009)
6.9E-10	Plant	(Phillips et al., 2009)
2.09E-10		Average

2.2.8 *Root oxygen release and root oxygen consumption*

Oxygen can diffuse into the aerenchyma tissues of wetland plants and leak out into the soil from the roots. Depending on root respiration rates, some of this diffused oxygen is consumed by the root and as a result decreases the rate at which oxygen leaks out into the rhizosphere from the root. Varying oxygen release rates were defined over a number of simulations in order to mimic a range of possible oxygen concentrations in the root zone (ranging from 0 to 60% saturation) (Armstrong et al., 2000). Root consumption of oxygen was modeled by reducing root oxygen leakage rate by multiplying a variable Root Consumption Fraction variable into the root oxygen leakage rate. Values between 0 and 1 were assigned to this variable to represent 100% and 0% consumption of oxygen by the root.

$$R_{oxygen\ release} = RootConsumption\ Fraction \cdot RootGasTransportCapacity \cdot D_{O_2} \cdot ([O_2]_{atmosphere} - [O_2]_{root}) \quad (2\text{-}16)$$

D_{O_2} is the diffusion coefficient of oxygen in air which is equal to 0.204 $cm^2.s^{-1}$ (He et al., 2010). $([O_2]_{atmosphere} - [O_2]_{root})$ is the oxygen concentration gradient between the atmosphere and the root. $[O_2]_{atmosphere}$ is the oxygen concentration in the atmosphere and $[O_2]_{root}$ is the oxygen

concentration in the model node next to the root which is assumed to be 1E-10 $mol \cdot L^{-1}$ in the initial conditions (see Table 2-1). $R_{oxygen\ release}$ is the rate of oxygen release to the soil in $mol \cdot (m^{-1}).(s^{-1})$. Note that oxygen release rate was a prescribed rate in this model. The rationale behind developing Equation 2-16 -which is a modified Fickian diffusion equation-, was to calibrate plant-mediated methane transport using oxygen release rate because of the fact that both of these processes use the same diffusion path inside the plant. Root Gas Transport Capacity variable in Equation 2-16 is a unitless parameter to describe the level of connectivity of root with the atmosphere. A higher Root Gas Transport Capacity leads to higher methane transport to the atmosphere since there is less resistance.

2.2.9 *Plant-mediated methane transport*

Methane concentration gradient between the rhizosphere and the atmosphere results in diffusion of methane through the aerenchyma and release of methane to the atmosphere (Bhullar et al., 2013; Nouchi et al., 1990). In this model, aerenchyma transport of methane was directly related to root oxygen leakage since both processes involve diffusion of gas through the same aerenchymatous tissues. The rate of methane transport was calculated according to oxygen leakage rate assuming zero root consumption of oxygen. Tissue resistance to diffusion was assumed to be the same for oxygen and methane therefore transfer rates were in proportion to the diffusion coefficients of each of these gases. Diffusion coefficient of O_2 and CH_4 are 0.204 and 0.212 $cm^2 \cdot s^{-1}$ respectively (He et al., 2010). Plant-mediated methane transport rate was directly related to methane concentration gradient between atmosphere (assumed zero methane in atmosphere) and root zone (nearest node to the root). Rate of methane transport through aerenchyma is shown in Equation 2-17.

$$R_{methane\_transport} = RootGasTransportCapacity \cdot D_{CH_4}[CH_4]_{root} \quad (2\text{-}17)$$

Root Gas Transport Capacity is the same parameter as defined in Equation 2-16. D_{CH_4} is the diffusion coefficient of methane in the air which is equal to 0.212 $cm^2 \cdot s^{-1}$ respectively (He et al., 2010). $[CH_4]_{root}$ is the methane concentration at the root. Atmospheric concentration of methane was assumed to be zero. $R_{methane\_transport}$ is the rate of aerenchyma methane transport to the atmosphere in $mol \cdot (m^{-1}).(s^{-1})$.

2.3 KINETIC PARAMETERS

Values of kinetic parameters used in the microbial reaction rates in the model were collected from the literature (see Appendix A). 1st quartile, median and 3rd quartiles (reported in Table 2-4) were then used in simulations to capture possible parameter ranges.

Table 2-4 : 1st quartile, median and 3rd quartile of kinetic parameters used in the model

Reaction	Symbol	Definition	Unit	1st Quartile	Median	3rd Quartile
Methane production from acetate	$K_{acetate}^{prod\_ace}$	Half-Saturation of Acetate	mol·L^{-1}	3.91E-04	2.16E-03	3.50E-03
Methane production from acetate	$I_{O_2}^{prod\_ace}$	Oxygen Inhibition Factor	mol·L^{-1}	2.5E-6	2.5E-6	2.5E-6
Methane production from acetate	$V_{\max}^{prod\_ace}$	Maximum Rate	mol·L^{-1}·s^{-1}	1.48E-10	1.57E-09	4.35E-09
Methane production from H_2/CO_2	$K_{H_2}^{prod\_hyd}$	Half-Saturation of H_2	mol·L^{-1}	2.31E-06	5.78E-06	1.20E-05
Methane production from H_2/CO_2	$I_{O_2}^{prod\_hyd}$	Oxygen Inhibition Factor	mol·L^{-1}	2.5E-6	2.5E-6	2.5E-6
Methane production from H_2/CO_2	$V_{\max}^{prod\_hyd}$	Maximum Rate	mol·L^{-1}·s^{-1}	1.50E-10	7.60E-09	1.02E-08
Methane oxidation	$K_{CH_4}^{oxid}$	Half-Saturation of CH_4	mol·L^{-1}	2.25E-06	4.13E-06	3.75E-05
Methane oxidation	$K_{O_2}^{oxid}$	Half-Saturation of O_2	mol·L^{-1}	1.06E-06	2.98E-06	1.62E-05
Methane oxidation	$V_{\max}^{oxid}$	Maximum Rate	mol·L^{-1}·s^{-1}	3.97E-10	2.10E-09	5.50E-09
Heterotrophic respiration	$K_{glucose}^{hetr}$	Half-Saturation of Glucose	mol·L^{-1}	9.16E-04	1.21E-03	1.41E-03
Heterotrophic respiration	$K_{O_2}^{hetr}$	Half-Saturation of O_2	mol·L^{-1}	6.90E-06	1.31E-05	2.96E-04
Heterotrophic respiration	$V_{\max}^{hetr}$	Maximum Rate	mol·L^{-1}·s^{-1}	5.79E-11	9.94E-11	1.87E-10
Glucose fermentation	$K_{glucose}^{ferm}$	Half-Saturation of Glucose	mol·L^{-1}	4.0E-02	6.1E-02	1.46E-01
Glucose fermentation	$I_{O_2}^{ferm}$	Oxygen Inhibition Factor	mol·L^{-1}	2.5E-6	2.5E-6	2.5E-6
Glucose fermentation	$V_{\max}^{ferm}$	Maximum Rate	mol·L^{-1}·s^{-1}	1.25E-12	1.25E-12	1.25E-12
Anaerobic peat decomposition	$V_{\max}^{anaer\_peat}$	Maximum Rate	mol·L-1	2.5E-11	5.0E-11	1.0E-10
Anaerobic peat decomposition	$I_{O_2}^{anaer\_peat}$	Oxygen Inhibition Factor	mol·L-1·s-1	2.5E-6	2.5E-6	2.5E-6
Aerobic peat decomposition	$V_{\max}^{aer\_peat}$	Maximum Rate	mol·L-1	5.0E-11	1.0E-10	2.0E-11
Aerobic peat decomposition	$K_{O_2}^{aer\_peat}$	Half-Saturation of O_2	mol·L-1·s-1	2.5E-6	2.5E-6	2.5E-6

2.4 MODEL SIMULATIONS

Table 2-5 shows the performed mechanistic model simulations. For each process, lower and higher rates were chosen according to data collected from literature. Using these simulations, model's response to varying levels of competition between different microbial groups was examined. 1st quartile, median and 3rd quartile of kinetic parameters were determined and used to create scenarios of different competitiveness between microbial groups. In base case (simulation MMM in Table 2-5), all of the kinetic parameters were equal to the median of the range found in the literature. As a result, base case simulation represents median competitiveness for all of the microbial groups. High competitiveness for each microbial group was achieved by selecting a higher-end V_{max} value and a lower-end K_m value (3rd quartile and 1st quartile of the range found in the literature, respectively). Low competitiveness was achieved by selecting a lower-end V_{max} and a higher-end K_m value (1st quartile and 3rd quartile of the range found in the literature, respectively). Different combinations of competitiveness for microbial groups were created and a model simulation was performed for each case (see Table 2-5). All simulations were run for different rates of root carbon exudation, plant gas transport capacity, oxygen root consumption rates and peat decomposition rates.

Table 2-5 Modeling simulations perfromed using the 1-D root-scale mechanistic model

Run Name	Microbial competitiveness of methane production	Microbial competitiveness of heterotrophic respiration	Microbial competitiveness of methane oxidation	Root oxygen consumption	peat decomposition rate
MMM	medium	medium	medium	0 and 95%	low, medium and high
MMH	medium	medium	high	0 and 95%	low, medium and high
MML	medium	medium	low	0 and 95%	low, medium and high
HMM	high	medium	medium	0 and 95%	low, medium and high
LMM	low	medium	medium	0 and 95%	low, medium and high
MHM	medium	high	medium	0 and 95%	low, medium and high
MLM	medium	low	medium	0 and 95%	low, medium and high
MHH	medium	high	high	0 and 95%	low, medium and high
MHL	medium	high	low	0 and 95%	low, medium and high
MLL	medium	low	low	0 and 95%	low, medium and high
MLH	medium	low	high	0 and 95%	low, medium and high
HHH	high	high	high	0 and 95%	low, medium and high
HHL	high	high	low	0 and 95%	low, medium and high
HLH	high	low	high	0 and 95%	low, medium and high
HLL	high	low	low	0 and 95%	low, medium and high
LHH	low	high	high	0 and 95%	low, medium and high
LHL	low	high	low	0 and 95%	low, medium and high
LLH	low	low	high	0 and 95%	low, medium and high
LLL	low	low	low	0 and 95%	low, medium and high

Chapter 3. MECHANISTIC ROOT-SCALE MODEL RESULTS

3.1 MECHANISTIC MODEL RESULTS

Results of root-scale methane model are presented in this chapter. Contour plots consist of outputs from multiple model simulations (described in section 2.4). Each dot in a contour plot represents a single model simulation and the contour lines are created by linear interpolations between the simulations.

Figure 3-1 shows the rates of microbial reactions in the model domain for model run "MMM" (described in Table 2-5) with no root oxygen consumption and an average level of peat decomposition at the end of growing season (t=3 months from the start date of the model simulation). Figure 3-1-a shows that methane production linearly increased with root carbon exudation rate, which is consistent with previous modeling and field studies that suggest root carbon exudation provides fuel for acetoclastic methanogenesis (Aulakh et al 2001, Walter and Heimann, 2000). Total methane production is slightly inhibited by oxygen since only a small portion of the domain is oxygenated (shown in Figure 3-1 a). The modeled methane production rate ranges from 500 to 850 μmol/L/month which is comparable to measured methane production rates in the field (Neumann et al., 2015; Segers, 1998). Figure 3-1-b shows that methane oxidation almost linearly increased with root gas transport capacity. Figure 3-1-c shows the dependence of heterotrophic respiration on root carbon exudation and availability of oxygen from the root. Comparing figures b and c in Figure 3-1 indicates that heterotrophic respiration rate is low compared to rate of methane oxidation in median competitiveness for both processes and although both processes are competing for oxygen that is coming out of the roots, methane oxidation is the dominant user of the oxygen.

Figure 3-1-d shows the rate of plant-mediated methane transport. As observed in this figure, plant-mediated methane transport increases with increased root gas transport capacity and also increases as root carbon exudation rate increases. Note that rates of all the processes discussed in the mechanistic model simulations figures represent the total rates over the spatial domain of the model.

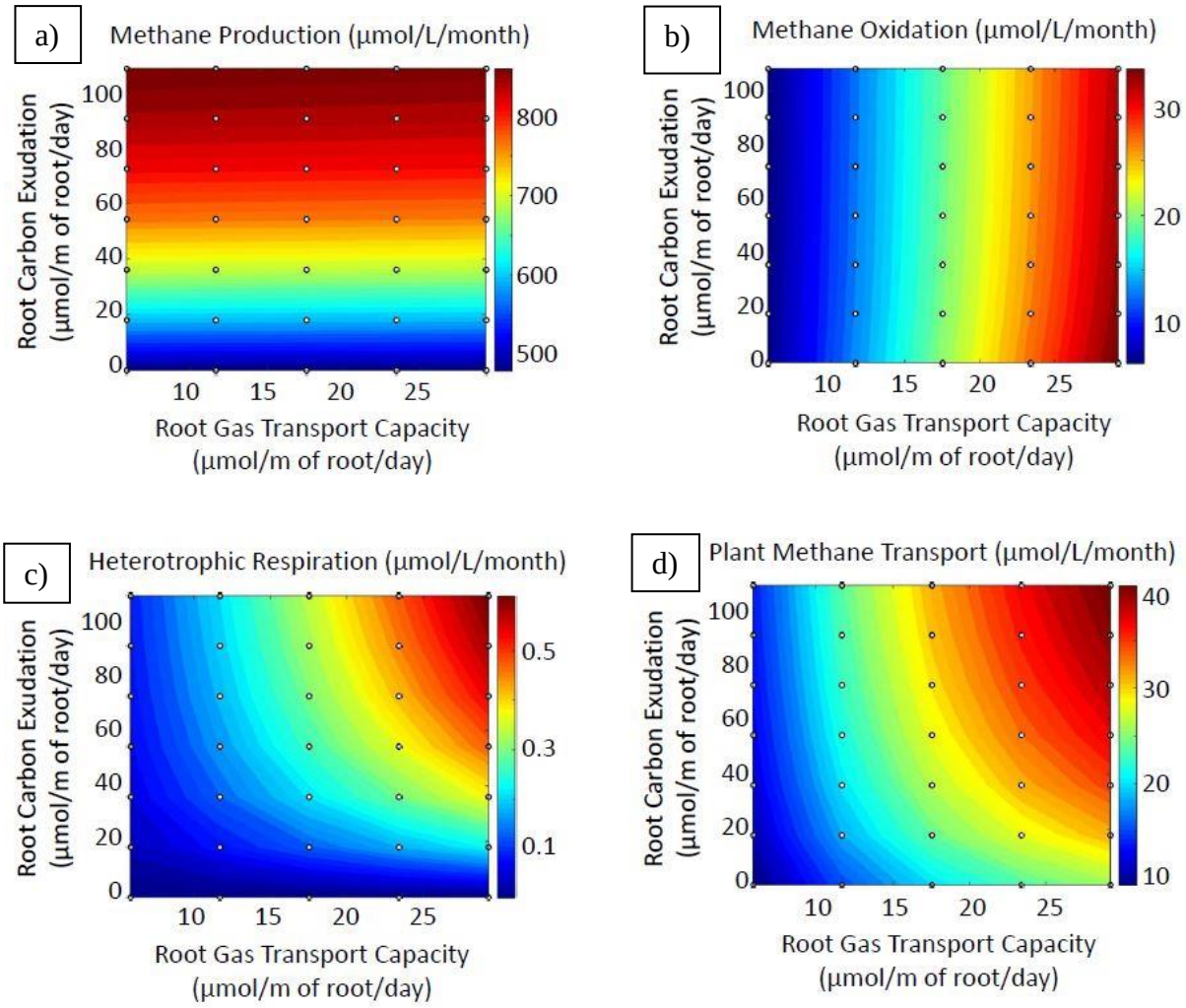

Figure 3-1 Rates of a) methane production, methane oxidation, heterotrophic respiration and plant-mediated methane transport with medium peat decomposition at the end of growing season

Concentration profiles are shown in Figure 3-2 for the simulation with average conditions of root oxygen release and root carbon exudation (the middle point in the contour plots).

Concentrations of chemical species are comparable to typical concentrations in the environment (shown in Table 2-1).

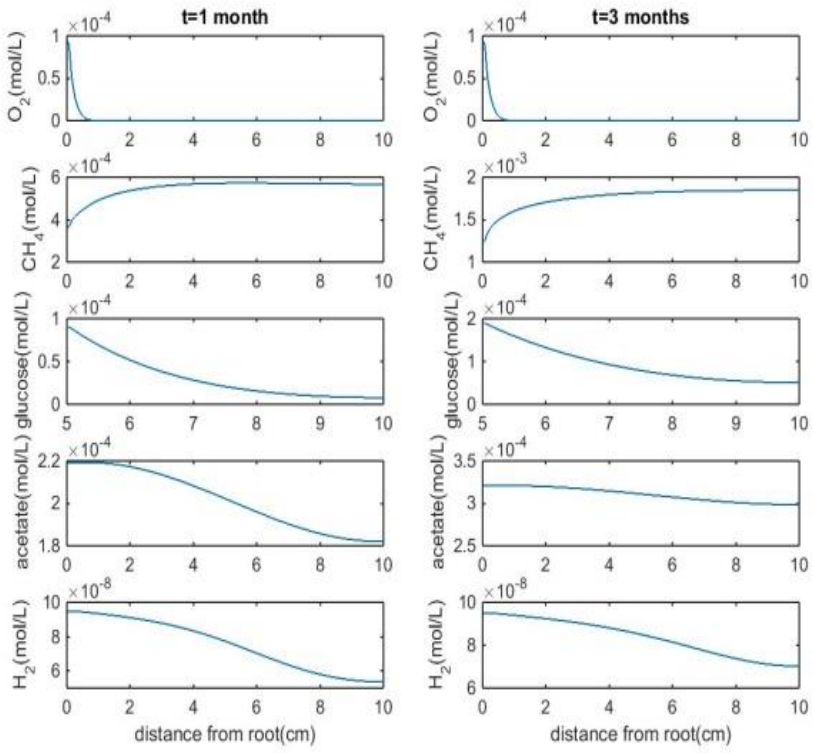

Figure 3-2 concentration profiles for a simulation with average conditions of root oxygen release and root carbon exudation (the middle point in the contour plots) for an average level of peat decomposition at the end of growing season

As described in Chapter 1, an important outcome of the mechanistic model was to understand the impact of competition between different microbial processes (methane production, methane oxidation, heterotrophic respiration) on methane oxidation rates as well as on plant-mediated methane emission. P_{ox} was defined as the ratio of methane produced that is oxidized before traveling through aerenchyma (Walter and Heimann, 2000). P_{ox} is defined according to equation 4-1:

$$P_{ox} = \frac{MethaneOxidationRate}{MethaneOxidationRate + PlantMediatedMethanetransportRate} \quad (4\text{-}1)$$

Figure 3-3 shows the calculated P_{ox} for average peat decomposition rate at the end of growing season. As seen in Figure 3-3, P_{ox} increased with increased root gas transport capacity but decreased with increased root carbon exudation. Looking at figure b and d in Figure 3-1 indicates that the observed trend in P_{ox} was due to the fact that while increasing root carbon exudation significantly increased plant-mediated methane transport, it did not have a significant impact on methane oxidation. Thus the ratio of oxidized methane went down as root carbon exudation increased. Competition of heterotrophic respiration and methane oxidation for oxygen seems to have minimal impact on P_{ox} trend.

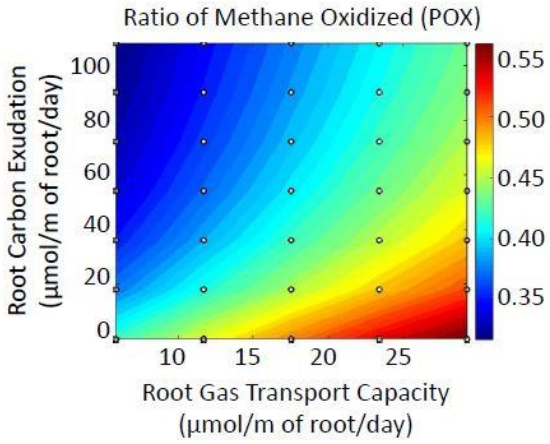

Figure 3-3 contour plot of P_{ox} for average peat decomposition rate at the end of growing season

Figure 3-4 through Figure 3-7 show the rates of methane production, methane oxidation, heterotrophic respiration and plant-mediated methane transport with varying root carbon exudation rates and root gas transport capacities and different levels of microbial competitiveness for three different levels of peat decomposition rates with no root oxygen consumption. Figure 3-8 shows the calculated P_{ox} for the same conditions.

Figure 3-4 shows that methane production is being fueled by both background peat decomposition and carbon exuded from the root. The impact of inhibition by oxygen on methane production rate is very distinct for simulations with low methane oxidation (the left column on Figure 3-4). It can be confirmed by the oxygen concentration profiles for these simulations that methane oxidation uses a larger portion of oxygen compared to heterotrophic respiration as seen in Figure 3-1. This is reasonable taking into account the kinetic parameters of these two reactions. Methane oxidation has a higher maximum rate and a smaller half-saturation for oxygen, both of which indicate it as a competitive process in oxygen consumption. When methane oxidation is high, the inhibition effect on production is smaller because the oxic area is smaller.

Figure 3-5 and Figure 3-6 show the interactions between methane oxidation and heterotrophic respiration. Heterotrophic respiration dominated methane oxidation only when methane oxidation competitiveness was set to low. Heterotrophs thrived in the absence of strong methanotrophs (left column of Figure 3-6) and impacted the rate of methane oxidation by outcompeting methanotrophs for oxygen. This pattern disappeared when competitiveness of methanotrophs increased (right column of Figure 3-5 and Figure 3-6).

Figure 3-7 shows the rate of plant-mediated methane transport as a function of methane concentration at the root (thus methane production and oxidation) and root gas transport capacity. Note that increase in gas transport capacity increases oxygen transport down to the root and plant transport of methane to the atmosphere simultaneously. In spite of higher methane oxidation rate at higher gas transport capacities, plant-mediated methane transport rate is still higher compared to lower gas transport capacities. Plant-mediated transport of methane also increased with higher peat decomposition rates.

Figure 3-8 shows the changes in P_{ox} with varying peat decomposition rate, root carbon exudation rate and root gas transport capacities. P_{ox} is a function of methane oxidation and plant-mediated methane transport. As shown in Figure 3-8, P_{ox} increased with root gas transport capacity and decreased as root carbon exudation rate increased. The non-linear contour lines in the graph show that for a specific root gas transport capacity, there is a limit to the root carbon exudation rate after which P_{ox} does not decrease any more as we increase root carbon exudation (minimum P_{ox}). This result was used in developing the dynamic P_{ox} equation.

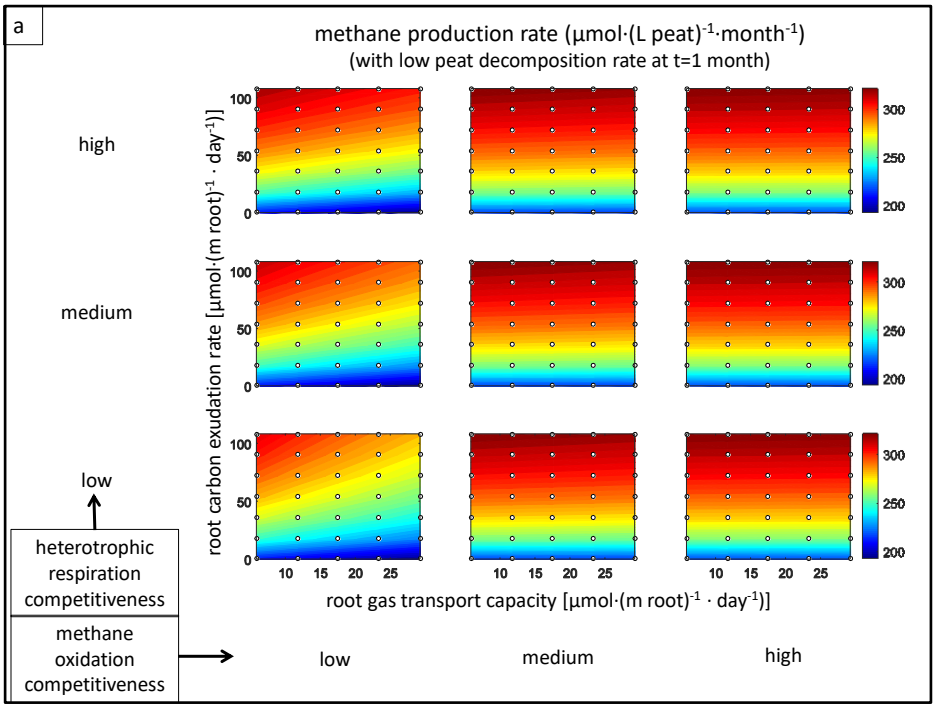

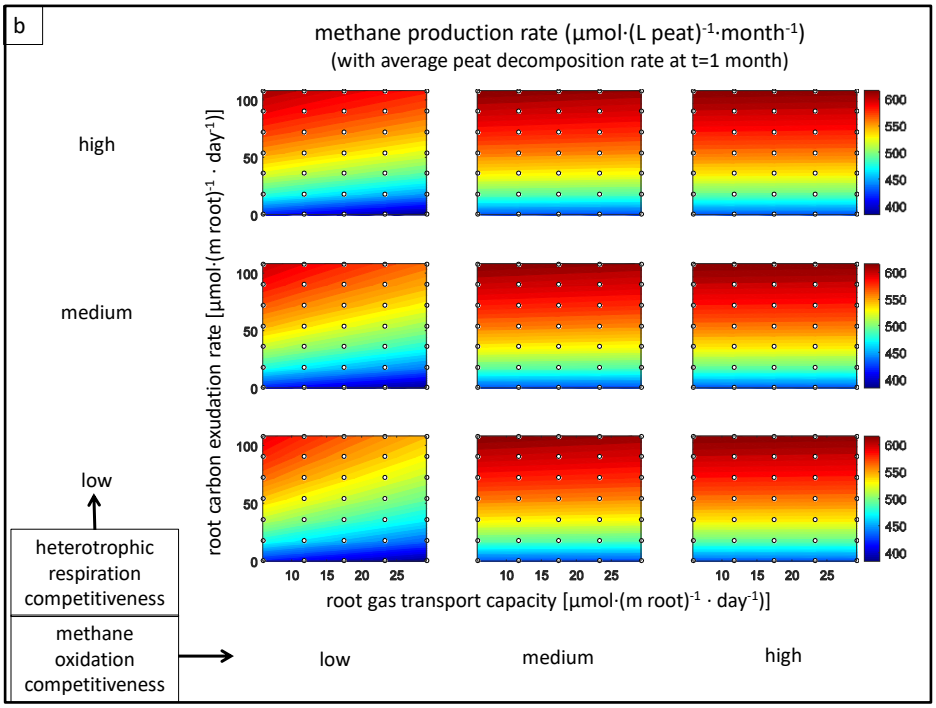

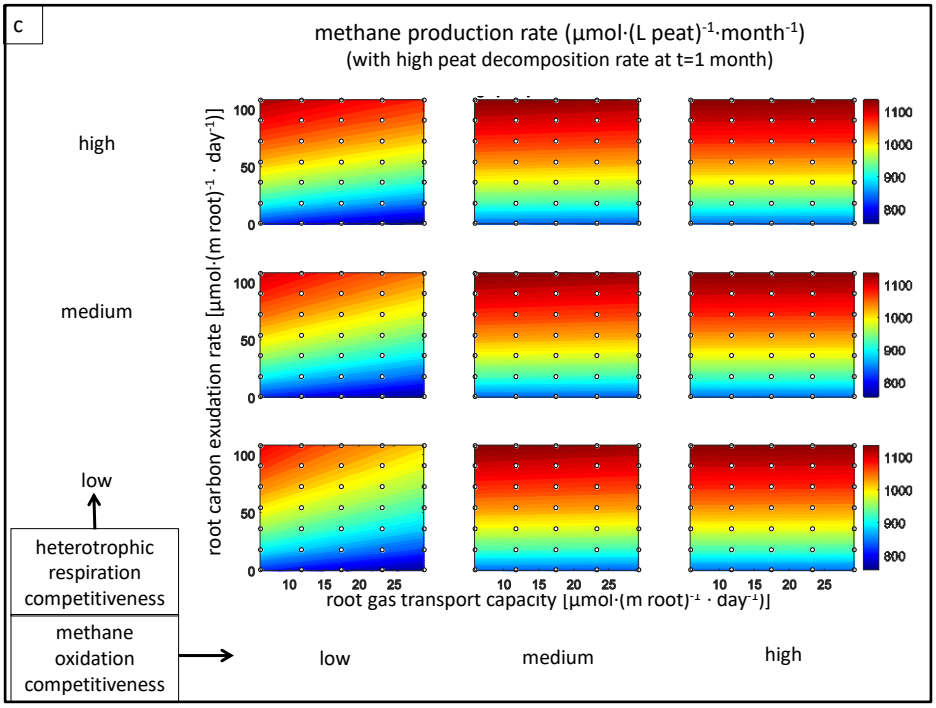

Figure 3-4 Dependence of methane production on root gas transport capacity and root carbon exudation rate in different levels of competition between methanotrophic and heterotrophic bacteria, zero root oxygen consumption and a) low, b) medium and c) high peat decomposition rate at t=1 month

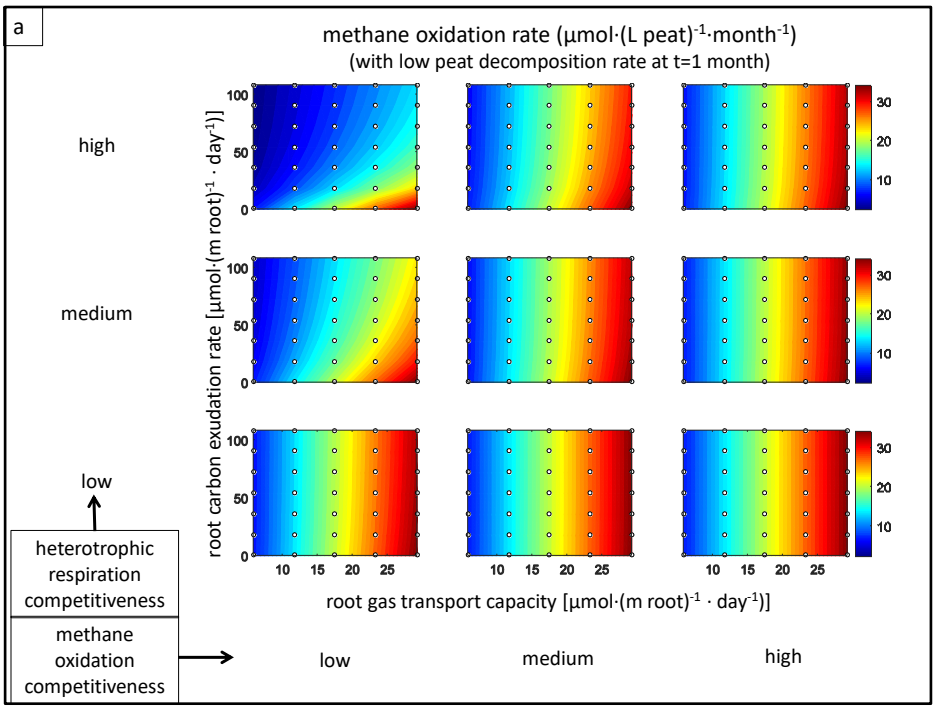
a
methane oxidation rate (µmol·(L peat)-1·month-1)
(with low peat decomposition rate at t=1 month)
high
medium
low
root carbon exudation rate [µmol·(m root)-1 · day-1)]
root gas transport capacity [µmol·(m root)-1 · day-1)]
heterotrophic respiration competitiveness
methane oxidation competitiveness
low
medium
high

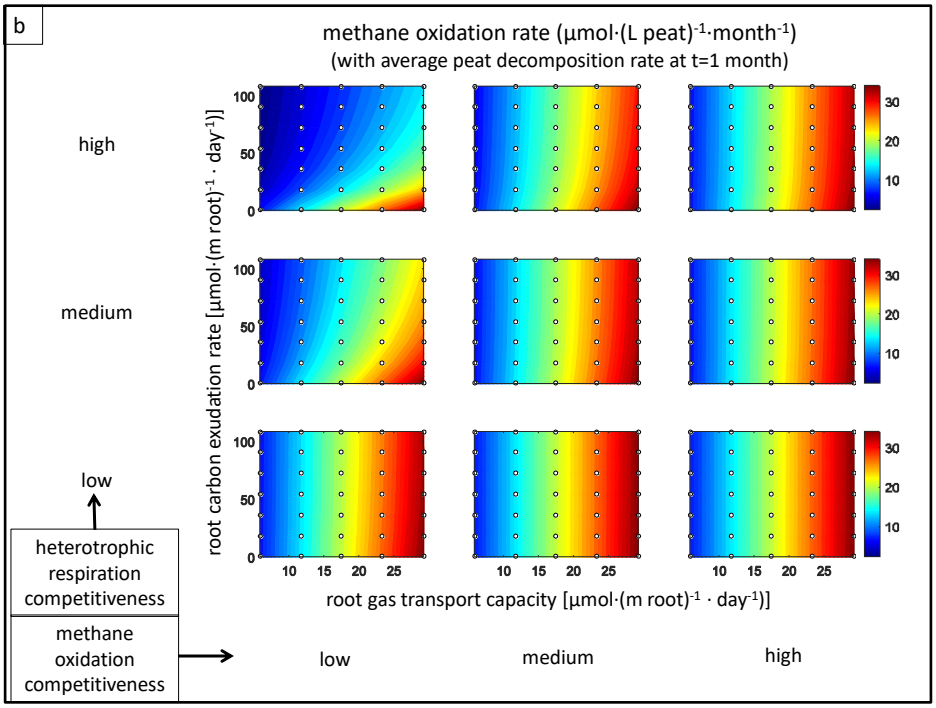
b
methane oxidation rate (µmol·(L peat)-1·month-1)
(with average peat decomposition rate at t=1 month)
high
medium
low
root carbon exudation rate [µmol·(m root)-1 · day-1)]
root gas transport capacity [µmol·(m root)-1 · day-1)]
heterotrophic respiration competitiveness
methane oxidation competitiveness
low
medium
high

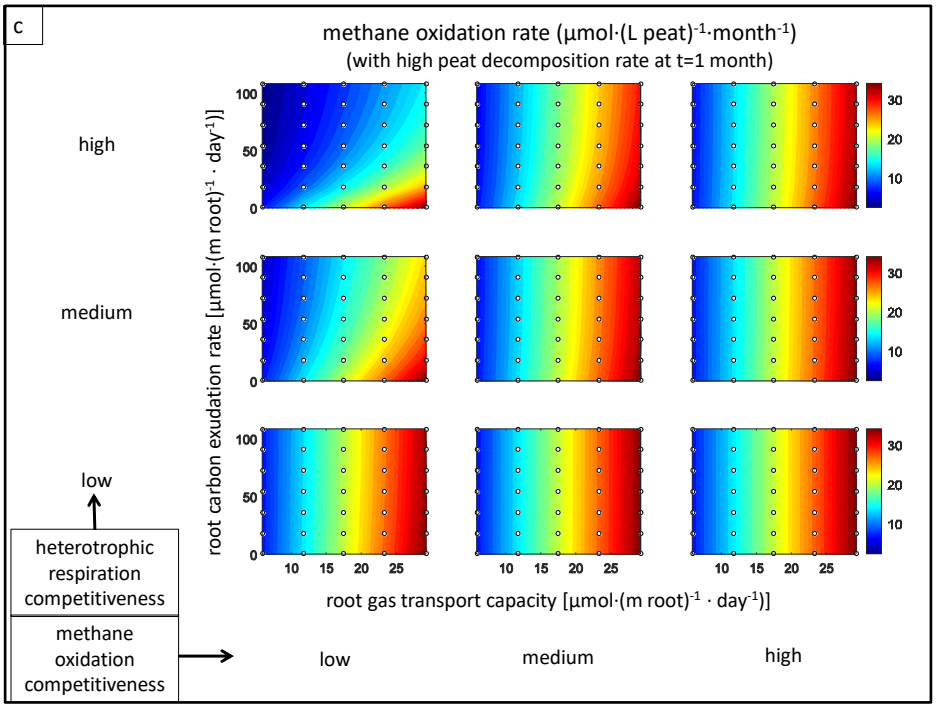

Figure 3-5 Dependence of methane oxidation on root gas transport capacity and root carbon exudation rate in different levels of competition between methanotrophic and heterotrophic bacteria, zero root oxygen consumption and a) low, b) medium and c) high peat decomposition rate at t=1 month

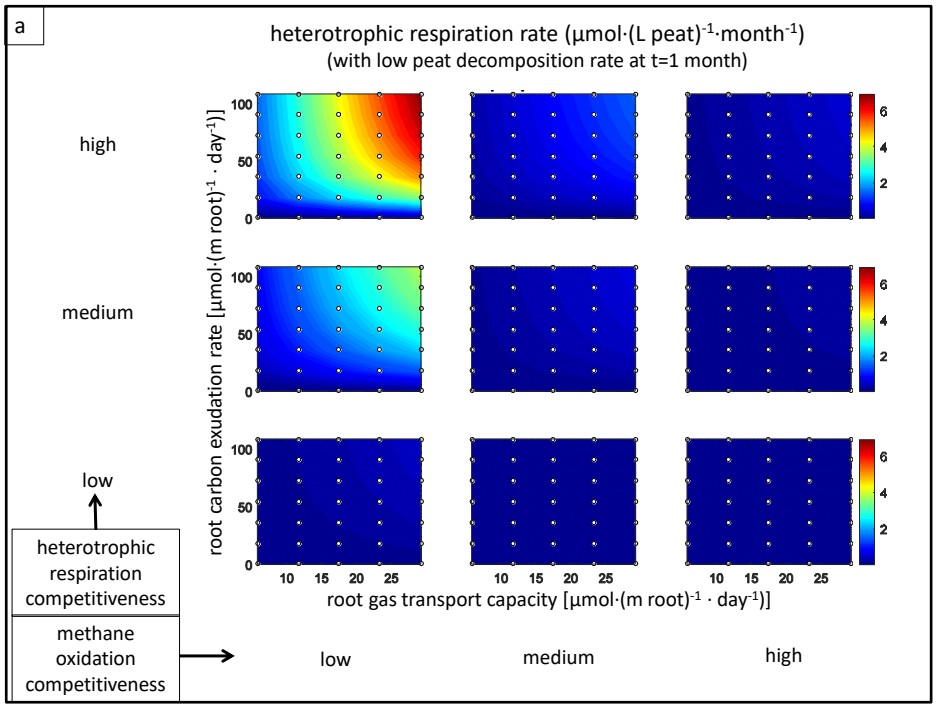
a
heterotrophic respiration rate (µmol·(L peat)-1·month-1)
(with low peat decomposition rate at t=1 month)
high
medium
low
root carbon exudation rate [µmol·(m root)-1 · day-1)]
root gas transport capacity [µmol·(m root)-1 · day-1)]
heterotrophic respiration competitiveness
methane oxidation competitiveness
low
medium
high

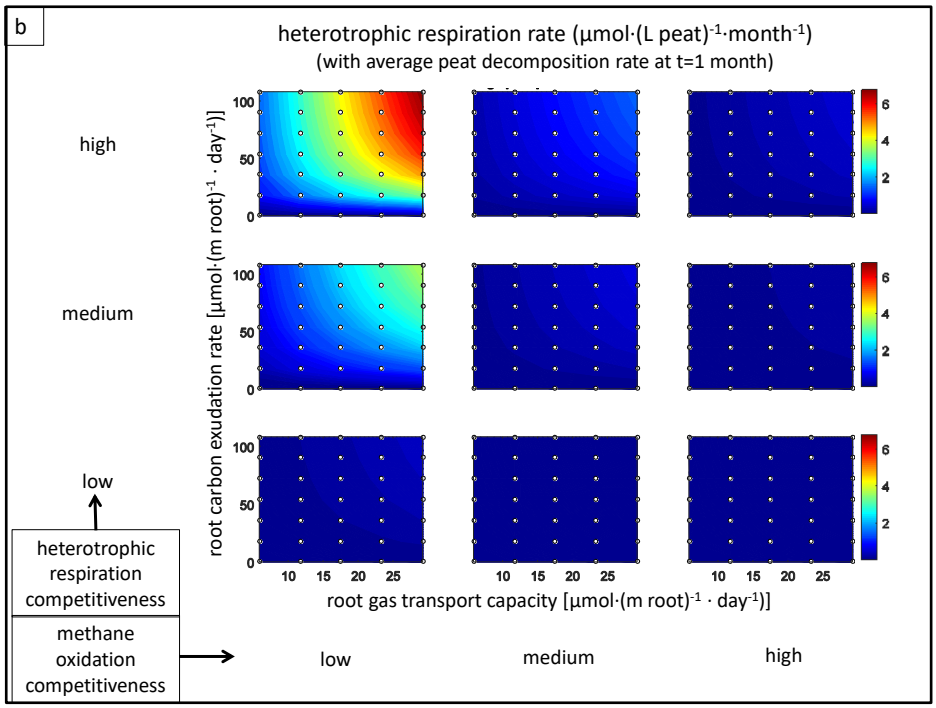
b
heterotrophic respiration rate (µmol·(L peat)-1·month-1)
(with average peat decomposition rate at t=1 month)
high
medium
low
root carbon exudation rate [µmol·(m root)-1 · day-1)]
root gas transport capacity [µmol·(m root)-1 · day-1)]
heterotrophic respiration competitiveness
methane oxidation competitiveness
low
medium
high

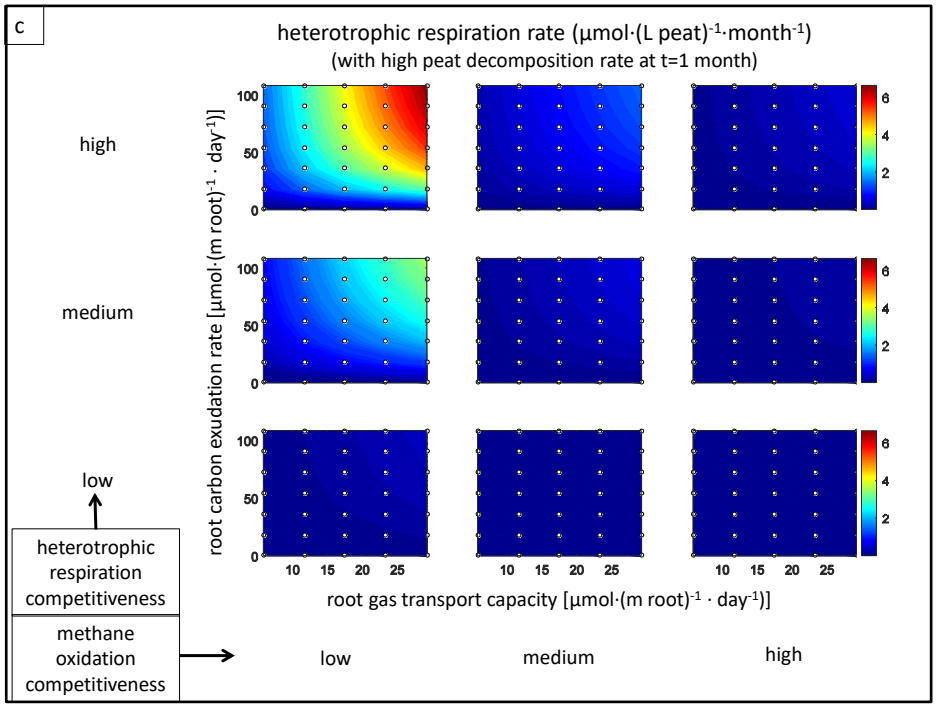

Figure 3-6 Dependence of heterotrophic respiration on root gas transport capacity and root carbon exudation rate in different levels of competition between methanotrophic and heterotrophic bacteria, zero root oxygen consumption and a) low, b) medium and c) high peat decomposition rate at t=1 month

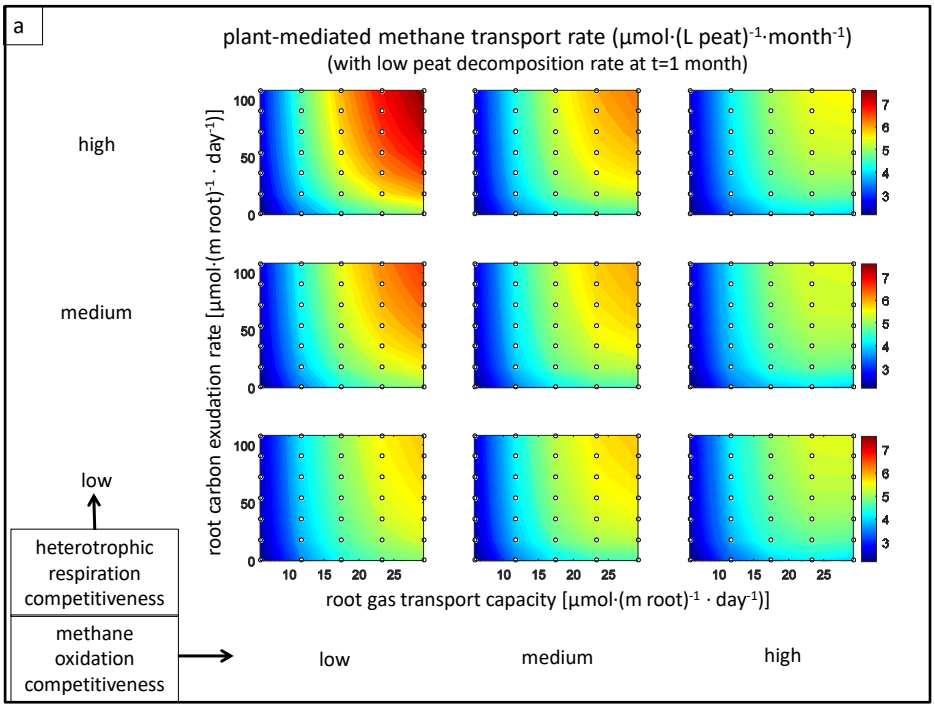
a
plant-mediated methane transport rate (µmol·(L peat)-1·month-1)
(with low peat decomposition rate at t=1 month)
high
medium
low
root carbon exudation rate [µmol·(m root)-1 · day-1)]
root gas transport capacity [µmol·(m root)-1 · day-1)]
heterotrophic respiration competitiveness
methane oxidation competitiveness
low
medium
high

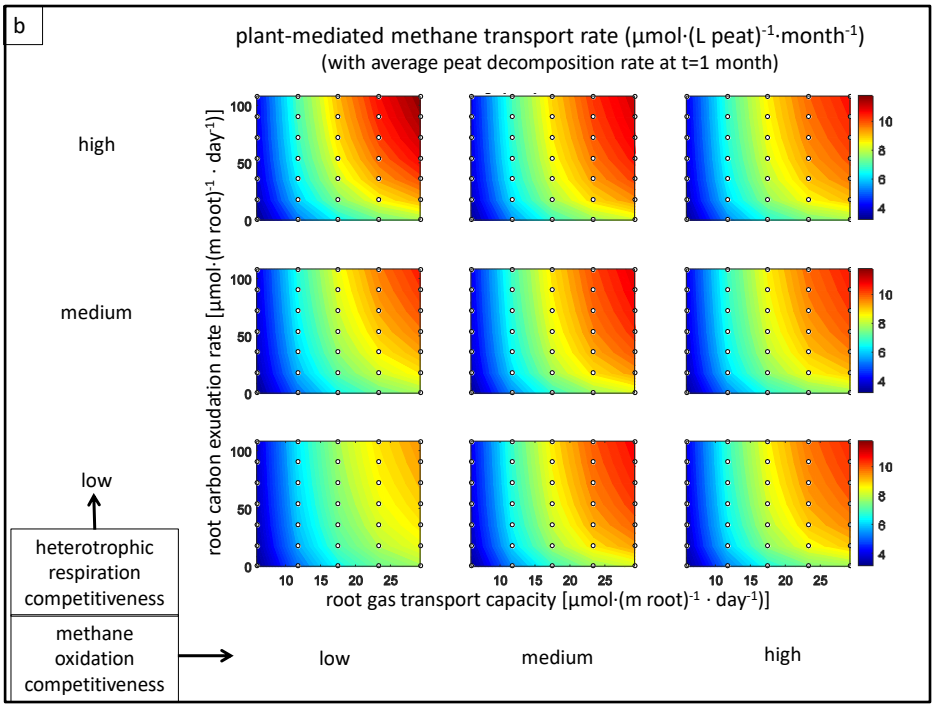
b
plant-mediated methane transport rate (µmol·(L peat)-1·month-1)
(with average peat decomposition rate at t=1 month)
high
medium
low
root carbon exudation rate [µmol·(m root)-1 · day-1)]
root gas transport capacity [µmol·(m root)-1 · day-1)]
heterotrophic respiration competitiveness
methane oxidation competitiveness
low
medium
high

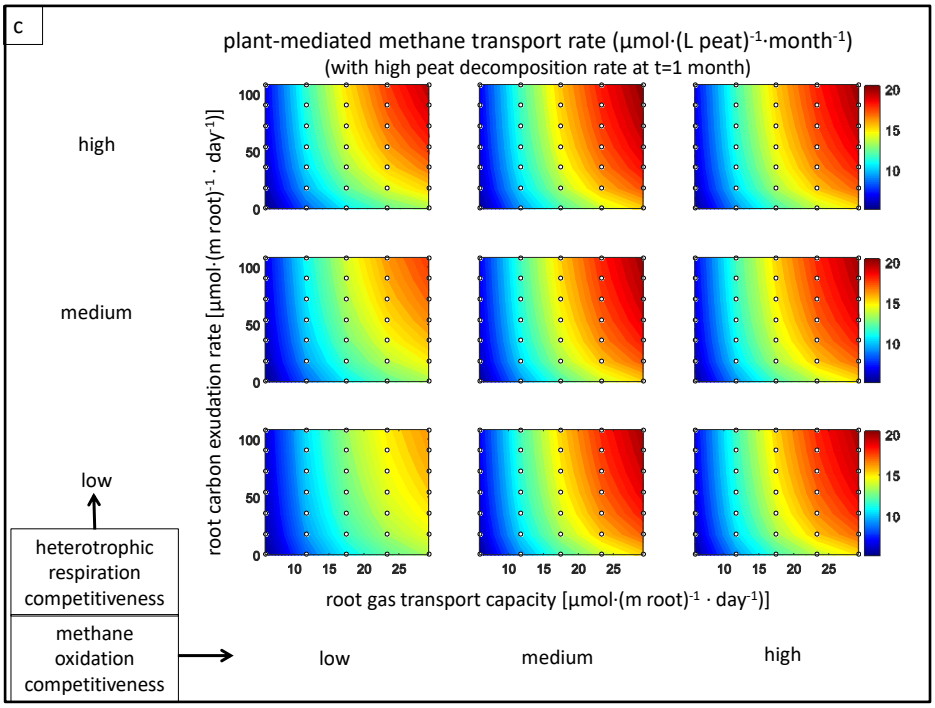

Figure 3-7 Dependence of plant mediated methane transport on root gas transport capacity and root carbon exudation rate in different levels of competition between methanotrophic and heterotrophic bacteria, zero root oxygen consumption and a) low, b) medium and c) high peat decomposition rate at t=1 month

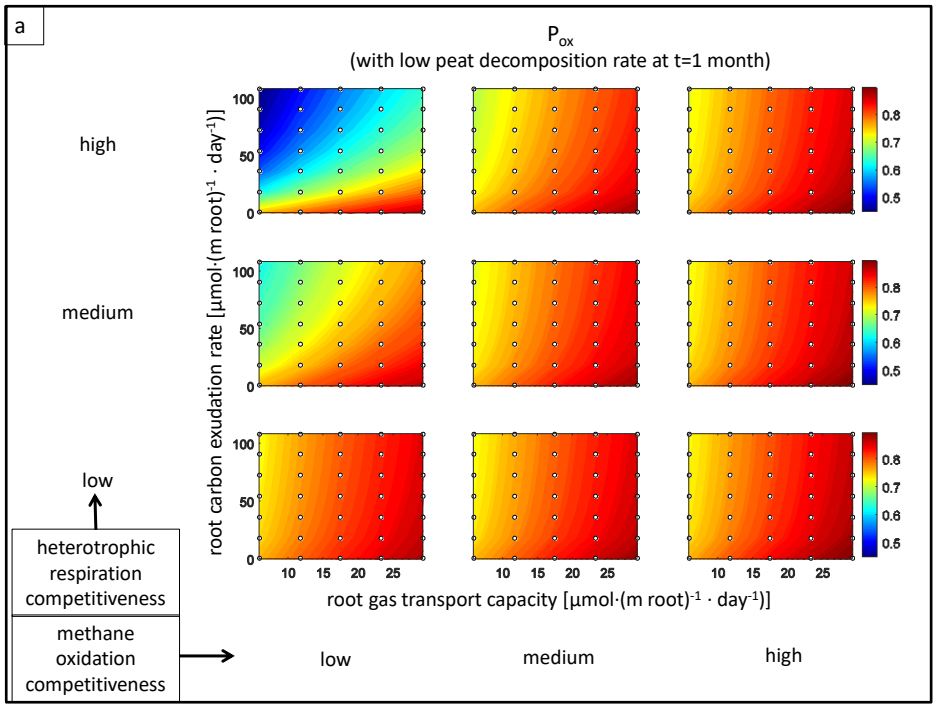
a
P_{ox}
(with low peat decomposition rate at t=1 month)
high
medium
low
root carbon exudation rate [µmol·(m root)$^{-1}$ · day^{-1})]
root gas transport capacity [µmol·(m root)$^{-1}$ · day^{-1})]
heterotrophic respiration competitiveness
methane oxidation competitiveness
low
medium
high

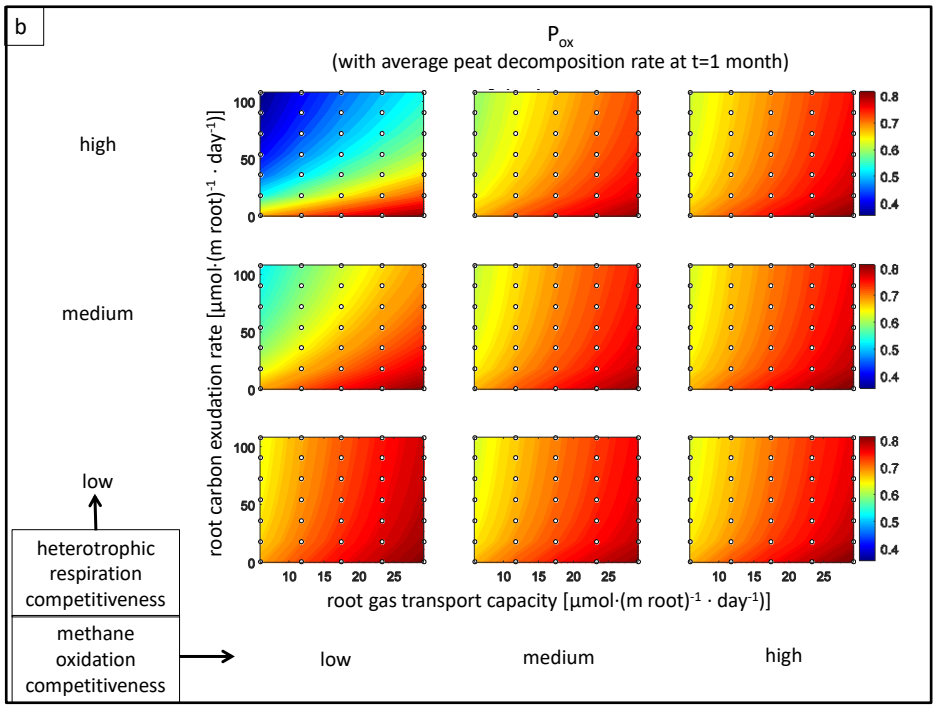
b
P_{ox}
(with average peat decomposition rate at t=1 month)
high
medium
low
root carbon exudation rate [µmol·(m root)$^{-1}$ · day^{-1})]
root gas transport capacity [µmol·(m root)$^{-1}$ · day^{-1})]
heterotrophic respiration competitiveness
methane oxidation competitiveness
low
medium
high

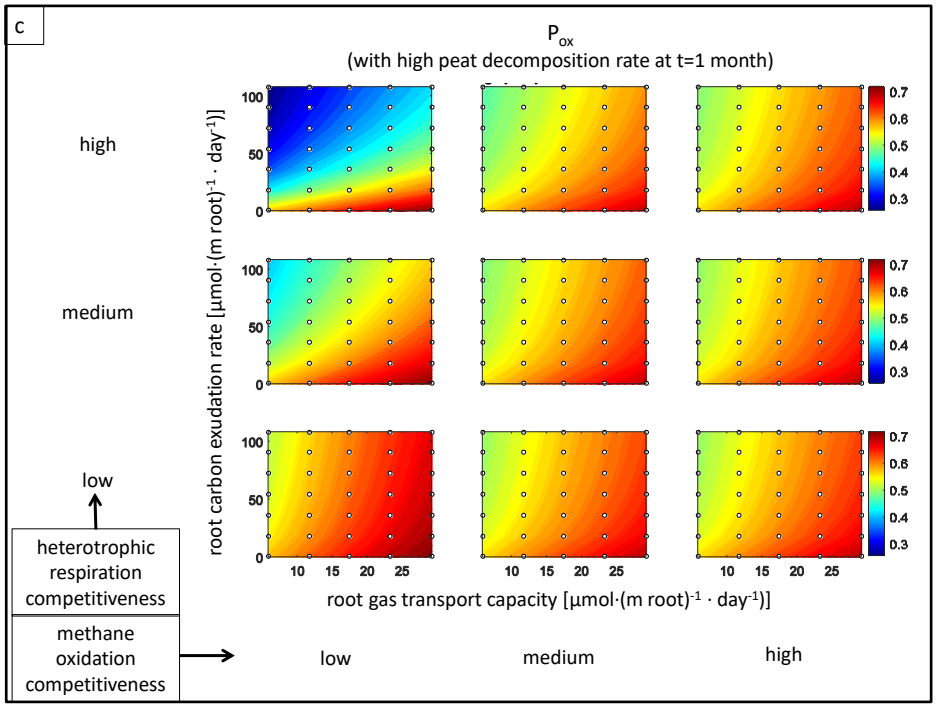

Figure 3-8 Dependence of P_{ox} on root gas transport capacity and root carbon exudation rate in different levels of competition between methanotrophic and heterotrophic bacteria, zero root oxygen consumption and a) low, b) medium and c) high peat decomposition rate at t=1 month

Chapter 4. NEW P_{OX} DEVELOPMENT

Walter and Heimann's methane emission model defined a static P_{ox} equal to 0.5 (Walter and Heimann, 2000). The mechanistic model developed in this study however showed that P_{ox} is not a constant static parameter and that it changes as a function of other processes that impact root zone methane oxidation and plant-mediated methane transport. In this chapter, a new P_{ox} equation for use in large-scale methane models was developed based on the mechanistic modeling results for P_{ox} to replace the existing static P_{ox} in Walter and Heimann's model. As shown in Figure 4-1, the P_{ox} pattern observed in the mechanistic root-scale model had consistent characteristics.

4.1 ROOT GAS TRANSPORT CAPACITY'S IMPACT ON P_{OX}

Mechanistic modeling results indicated that P_{ox} increased as root gas transport capacity increased. Higher root gas transport capacity allowed more oxygen to diffuse to the soil from the root which increased methane oxidation as shown in Figure 3-6. Higher root gas transport capacity also allowed more methane to diffuse into aerenchymatous tissues of the root and be transported to the atmosphere as shown in Figure 3-7. The resulting P_{ox} values were shown in Figure 3-8 which indicate that higher root gas transport led to an increase in P_{ox} values.

4.2 ROOT CARBON EXUDATION'S IMPACT ON P_{OX}

P_{ox} decreased as root carbon exudation rate increased. Higher root carbon exudation rate provided more fuel for methanogenesis and consequently higher methane concentrations in the root zone and higher plant-mediated emission as shown in Figure 3-7. By contrast, higher root

carbon exudation rate did not significantly impact methane oxidation rates as shown in Figure 3-6. As a result, P_{ox} values decreased as root carbon exudation increased.

P_{ox} gradient with respect to root carbon exudation rate decreased with increasing carbon exudation rate which means at higher rates of carbon exudation P_{ox} will only depend on root gas transport capacity (upward concave curvature).

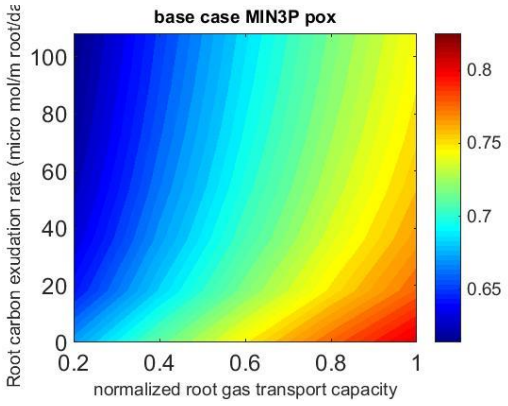

Figure 4-1 P_{ox} patterns for base case with average peat decomposition rate at the end of growing season

4.3 Empirical Dynamic P_{OX} Equation

The goal was to develop an equation that captured all of the above mentioned criteria. The following equation satisfied all of those conditions.

$$dyn\_pox = (A_0 + (A_1 - A_0)\exp(-\frac{Q_c}{Q_{cref}})) \times \frac{Q_o}{Q_{o\max}} + \min\_pox \quad (4\text{-}1)$$

where:

Q_0 is the root oxygen release rate as described in section 2.2.8.

$Q_{0\max}$ is the maximum root oxygen release rate. This rate was defined as the root oxygen release rate that created a 1 cm layer of oxygen saturation around the root in median condition for all other processes and was the maximum rate used in the mechanistic root-scale model.

$\frac{Q_0}{Q_{0\max}}$ is the normalized root oxygen release rate.

Q_c is the rate of root carbon exudation.

Q_{cref} is a fitting parameter for root carbon exudation which represents typical values of root carbon exudation in the growing season. The fitted values of Q_{cref} can be found in Table B-1 in Appendix B.

P_{ox} results from the mechanistic root-scale model were fitted to Equation 4-1 in order to find fitting parameters A_1, A_0, Q_{cref} and *min_pox*. A_1 and A_0 represent P_{ox} gradients with respect to low and high root carbon exudation rates respectively. *min_pox* represents the minimum P_{ox} value observed in each MIN3P model simulation. *Qcref* represents the typical value of root carbon exudation in the growing season. Fitting was performed separately for each of the sensitivity tests in the rhizosphere-scale model. Parameter fittings were performed for 351 simulations (shown in Table B-1 in Appendix B) which consisted of different scenarios of microbial competitiveness, root oxygen consumption and peat decomposition levels and different time points in the simulation.

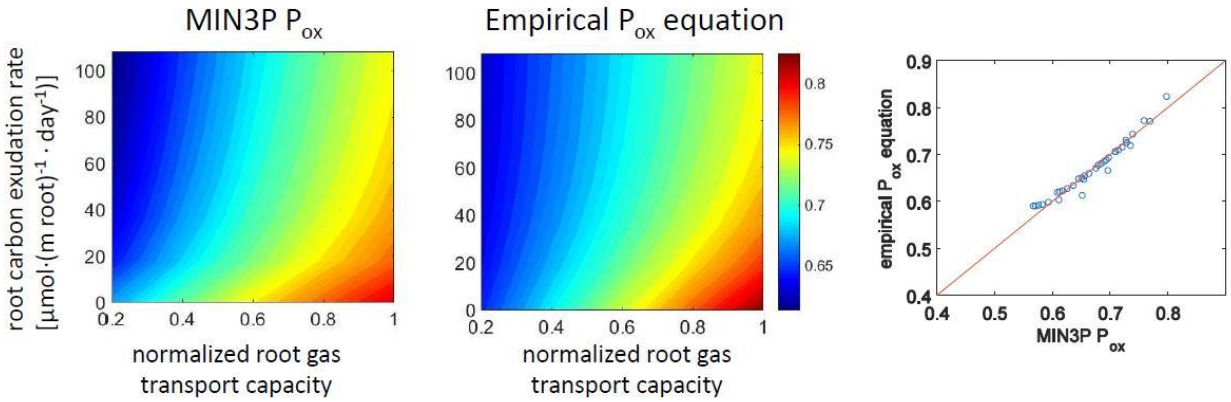

Figure 4-2 P_{ox} contour plots resulted from mechanistic root-scale model and Empirical dynamic P_{ox} equation shown for simulation MMM with medium peat decomposition rate and zero root oxygen consumption rate

As shown in Figure 4-2 the empirical P_{ox} equation was able to capture the characteristics of the mechanistic model P_{ox} results. Fitting results for simulation MMM with medium peat decomposition rate and zero root oxygen consumption rate is shown as a reference.

Chapter 5. LARGE-SCALE MODEL METHODS

5.1 DESCRIPTION OF MODEL

As described in chapter 1, the goal of this study was to introduce a dynamic representation of rhizospheric methane oxidation (P_{ox}) in large-scale methane emission models. To achieve this goal, an empirical equation (called dynamic P_{ox}) was developed using mechanistic modeling (described in Chapter 4) to describe methane oxidation in the rhizosphere of wetland plants. This representation of methane oxidation was then incorporated into Walter and Heimann's process-based methane emission model (Walter and Heimann 2000). In this chapter, integration of dynamic methane oxidation into Walter and Heimann's methane emission model is described.

Walter and Heimann's methane emissions model is a process-based, climate-sensitive model developed for natural wetland systems (Walter and Heimann, 2000). This model includes fundamental processes that occur in natural methanogenic environments (including methane production, deep soil methane oxidation, rhizospheric methane oxidation) and three main methane transport mechanisms to the atmosphere (diffusion, ebullition and plant-mediated transport). Soil temperature, water table depth and net primary productivity (NPP) are fed into the model as time series and the model calculates methane concentration for each time step based on the input parameters. Methane production is linked to NPP which is a measure of carbon availability and is also a function of water table position since water table determines the oxic and anoxic parts of the model domain. Deep soil methane oxidation is a function of water table position and soil temperature. Rhizospheric methane oxidation is defined as a constant fraction of plant-mediated methane transport.

Dynamic P_{ox} equation was added to the Walter and Heimann methane emission model's internal code in FORTRAN programming language. Dynamic P_{ox} equation was translated into Walter and Heimann model's parameters. $\frac{Q_0}{Q_{0\max}}$ from Equation 4-1 was replaced with $\frac{tveg}{tveg_{\max}}$. *tveg* is a parameter of Walter and Heimann methane emissions model that "describes the quality of plant-mediated methane transport at a site which depends on density and type of plant stands" and varies between 1 to 15, 1 representing plants with low methane transport capacity and 15 representing the highest capacity for methane transport (Walter and Heimann, 2000). *tveg* was similar to the Gas Transport Capacity parameter in the mechanistic model developed in this study since Gas Transport Capacity also directly controls the plant connectivity with the atmosphere and has an inverse relationship with the resistance to methane transport through the root to the atmosphere. During translation of dynamic P_{ox} equation into Walter and Heimann model's scripts, $\frac{Q_c}{Q_{cref}}$ was replaced with $\frac{NPP}{NPP_{ref}}$. Typical values of Q_c (chosen as the median of root carbon exudation rates used in the mechanistic model simulations, 50 μmol·(m root)$^{-1}$.day^{-1}) was used to normalize Q_{cref} and covert it to NPP_{ref} using typical values of NPP (average of NPP values observed during growing season) according to Equation 4-2.

$$\frac{Q_{cref}}{typical\,Q_c\,value} = \frac{NPP_{ref}}{typical\,NPP\,value}$$

Hereinafter, we refer to the Walter and Heimann model with dynamic P_{ox} as "dynamic model" versus the original model which we refer to as "static model" since it has a static constant P_{ox}. Methane emission rates from four boreal wetlands in Southwestern Siberia were then simulated using both the static and dynamic models. Four years of measured methane emission data were provided by our collaborators Glagolev et al. for these four sites (Glagolev et

al. 2011). The Glagolev et al. 2011 database consists of measurements over almost 700 sites across west Siberia, most consisting of a single time point. The four study sites used in this work were chosen due to the availability of a large number of data points (121 methane emission rates measured) during June to September growing season over multiple years (years 1997, 1998, 2006 and 2008), which allowed exploration of the model's response to seasonal and inter-annual variation in environmental conditions such as temperature, water table depth and net primary productivity.

5.2 MODEL INPUTS

The Walter-Heimann methane model is a process-based climate-sensitive model with the ability to calculate methane emission from natural wetlands (Walter and Heimann, 2000). Forcings of the Walter-Heimann model include monthly time series of soil temperature in different depths, water table position and net primary productivity. These inputs were generated using simulations of Variable Infiltration Capacity (VIC) 4.1.2 land surface hydrology (Liang et al., 1994) model over West Siberia (Bohn et al., 2007). Figure 5-1 shows a schematic representation of coupling of VIC and Walter-Heimann models and how they are interacting with each other. The VIC model requires climate forcings such as air temperature, precipitation, wind speed, humidity, shortwave and longwave radiation, and atmospheric CO_2 concentration. Methods described in (Bohn et al., 2013a) were used to derive hourly values of all of these variables. Historic values of these variables were derived over the 100-km gridcells (all 4 study sites in this study were located in one grid-cell) from daily meteorological fields of Sheffield et al. and gridded monthly observations (Mitchell and Jones, 2005; Sheffield et al., 2006, Willmott and Matsuura 2001) via the methods of (Adam and Lettenmaier, 2003; Adam et al., 2006). For future simulations, these values were derived from model projections from the fifth phase of the

Coupled Model Intercomparison Project (CMIP5) (Taylor et al., 2011). For each of the 31 different climate models from CMIP5 the input variables were calculated to run the VIC model and generate time series of soil temperature, water table position and net primary productivity. Many CMIP5 models contained a dynamic vegetation component to predict geographical distribution of vegetation (in form of Leaf Area Index or LAI) in the future. In order to account for changes in future NPP, each climate model's predicted LAI was converted to an equivalent VIC LAI via quantile mapping and mapped to corresponding MODIS LAI for both historic and future values (Bohn et al., 2013b). Other kinetic parameters in the Walter and Heimann model were calibrated as described in section 5.3.

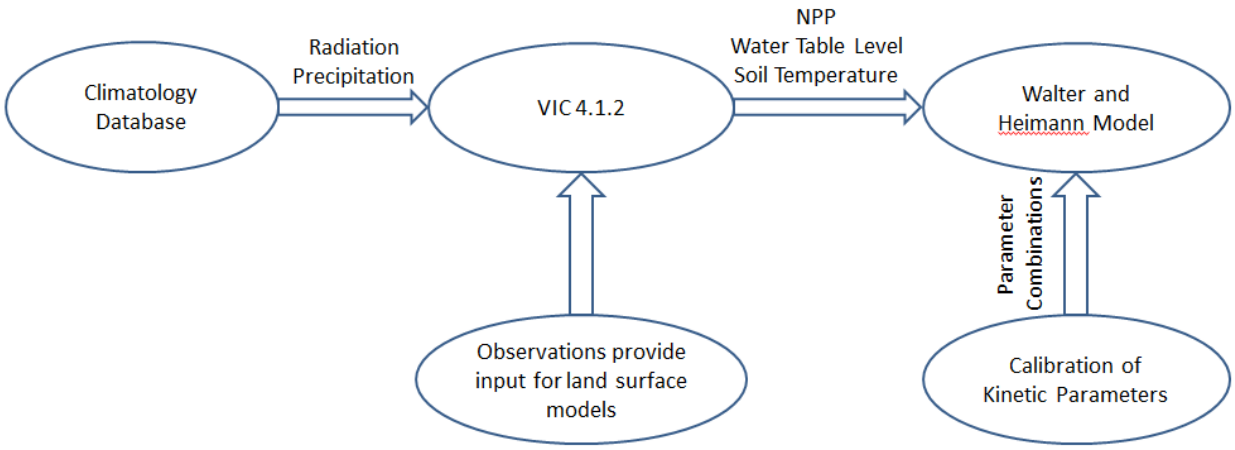

Figure 5-1 Schematic representation of coupling of VIC, BETHY and Walter-Heimann models

5.3 Model Calibration

Nine model parameters were calibrated for dynamic model according to Bohn et al. (2013b): five of these parameters were Walter and Heimann model parameters r0, xvmax, rkm, rq10, oxq10 and the other four were dynamic P_{ox} equation parameters A0, A1, NPPref and min_pox. r0 is measure of absolute substrate availability and quality. It is a tuning parameter that enables the model to be adjusted to each data set to achieve the desired amplitude of methane emissions.

xvmax is the maximum methane oxidation rate in the unsaturated soil zone. rkm is the half saturation of methane in the Michaelis-Menten kinetic equation for methane oxidation rate. rq10 is the Q10 value for methane production rate. oxq10 is the Q10 value for methane oxidation rate.

Measured methane emission rates from the four sites located in West Siberia (provided by Glagolev et al) were used to calibrate the parameters (Glagolev et al., 2011). These sites were located within the eastern part of Bakchar Bog in Tomsk area, Western Siberia. Bakchar Bog is a continuous peatland with spatial heterogeneity in environmental conditions and vegetation cover (Panikov and Dedysh, 2000). The four study sites are located along a 200 meter boardwalk and they allowed for sampling a few different types of wetlands (Carex sedge dominated, Menyanthes dominated, Equisetum dominated, and Ereophorum sedge dominated). Methane emission measurements were provided by Galogolev et al and were available for years 1997, 1998, 2006 and 2008 during rowing season (June to August) Calibration was performed by running the dynamic model for random combinations of these parameter values and calculation of a likelihood score for each parameter combination based on Equation 5-1. Observed and simulated methane emissions were divided into 10-day periods and average of observed and simulated methane emissions were calculated for each 10-day period. The standard error for observed and simulated methane emissions was also calculated (These 10-day period are shown in Figure 6-2 in Chapter 6). Observations and simulation from the four different sites were lumped since they had similar temperature measurement and water table depth in the Glagolev database. The similar environmental conditions in the four sites was probably due to the fact that they were located in a 200 meter transect (shown in Figure 5-2). The likelihood score was calculated based on the assumption that standard error on means of emissions on 10-day periods across sites has a normal distribution. The likelihood score calculated here is a measure of

likelihood of a parameter combination resulting in emissions that match observations which was a result of calculating the probability density function for the resulted x_{mid}.

$$x_{mid} = \frac{simulated\,emission - observed\,esmission}{error\,of\,observed\,emission}$$

$$x(0) = \text{int}(x_{mid} \times 100)/100$$

$$x(1) = x(0) + 0.01$$

$$\phi(z) = \frac{1}{2\pi}\int_{-\infty}^{z} e^{-\frac{x^2}{2}}\,dx \qquad (5\text{-}1)$$

$$likelihood = \phi(x(1)) - \phi(x(0))$$

A probability distribution for each parameter was then produced by taking all simulations that fell between the 1st and 99th percentile of cumulative likelihood of matching observations.

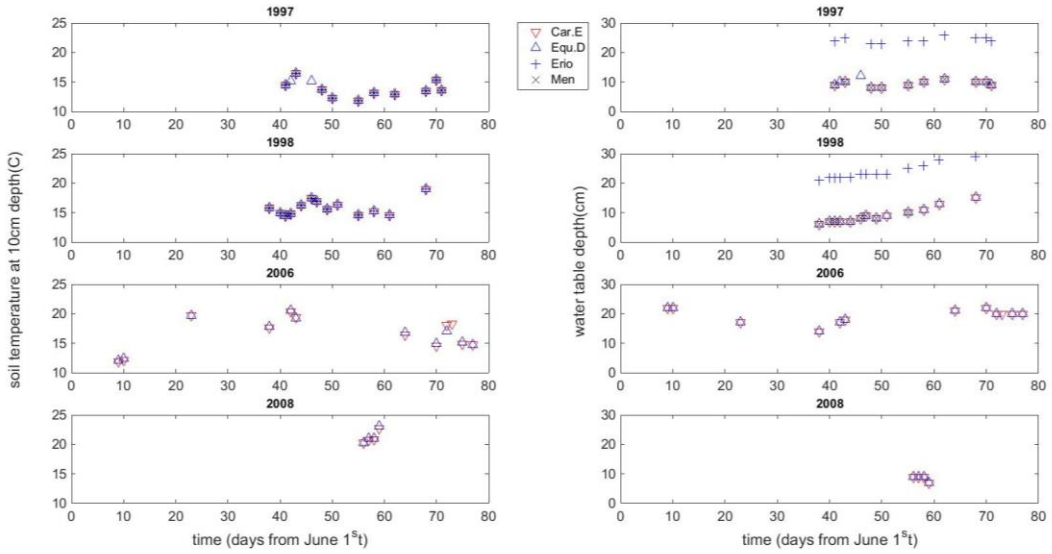

Figure 5-2 Measured soil temperature and water table depth for the four study sites. source:(Glagolev et al., 2011)

The model parameters were calibrated using the measured CH_4 emissions from these four sites for dynamic models (calibrations results discussed in section 6-1). Historic and future simulations of methane emission were then performed using each model. The goal of integration of dynamic P_{ox} into Walter and Heimann's methane model was to test the performance of the dynamic P_{ox} equation in the setting of a large-scale methane emission model by comparing the changes in historic and future emissions caused by dynamic P_{ox} compared to static P_{ox}. Changes in distributions of calibrated model parameters were also of interest.

5.4 Model Simulations

Historic and future methane emissions were simulated using the static and dynamic models. Each historic model simulation consisted of a 20 year period (from 1991 to 2010). Thirty different parameter combinations (generated from calibrated parameter distributions) were used to simulate historic methane emissions. Future simulations consisted of a 20 year period (from

2081 to 2100). Future simulations covered 31 different climates models from CMIP-5 climate models (Taylor et al., 2011) which were fed into VIC model in order to generate time series of Net Primary Productivity (NPP), soil temperature profiles and water table depth profiles. Parameter combinations used in the future model simulations were the same as the historic simulations.

The Walter and Heimann model was only calibrated using the dynamic model. The rationale behind this approach was for the static and dynamic model results to be comparable. Both static and dynamic model simulations were performed using the dynamic model's calibrated parameters. Instead of using a static P_{ox} of 0.5 (as in original Walter and Heimann model) an average P_{ox} of historic dynamic model simulation was calculated and used as the value for static P_{ox} (equal to 0.5876). This method allowed a fair comparison between static and dynamic model results.

Chapter 6. LARGE-SCALE MODEL RESULTS

6.1 CALIBRATION RESULTS

In order to estimate the optimal values of each calibrated parameter, likelihood score was plotted as a function of each parameter. Figure 6-1 shows the plots that were generated in the calibration process and were used to minimize the ranges of search for each parameter. Table 6-1 shows the final probability distribution for each parameter based on parameter combinations that lied between 1st and 99th percentile of total relative likelihood for both static and dynamic models.

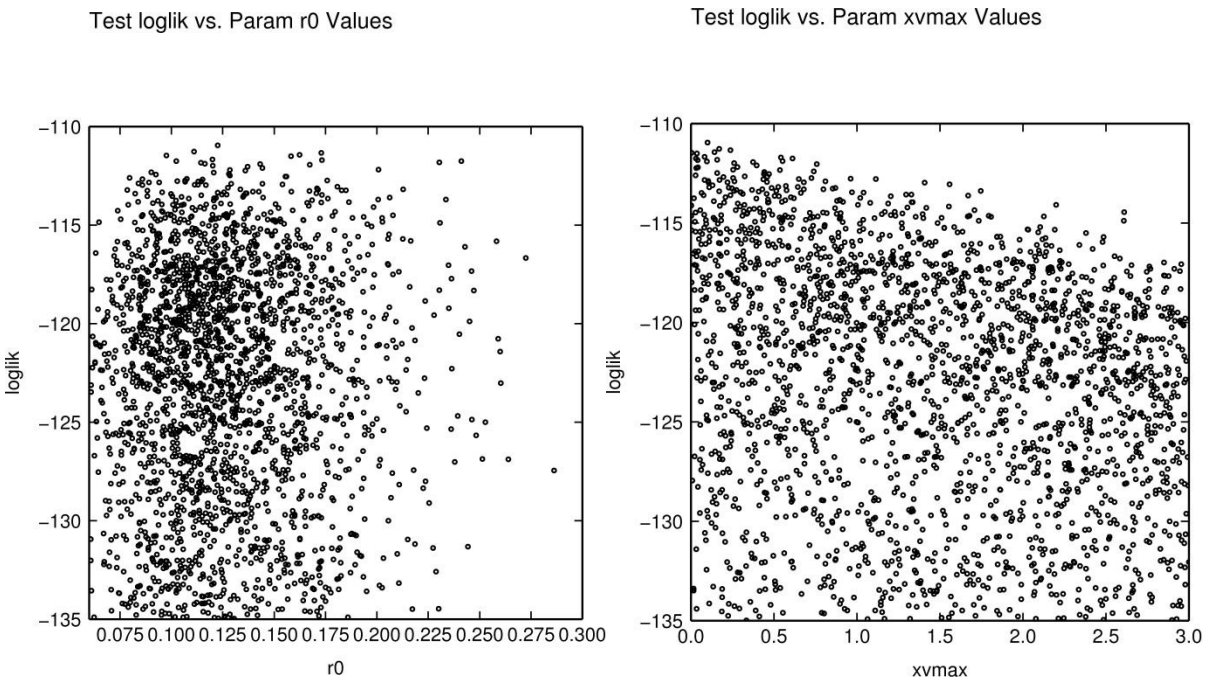

Test loglik vs. Param rkm Values

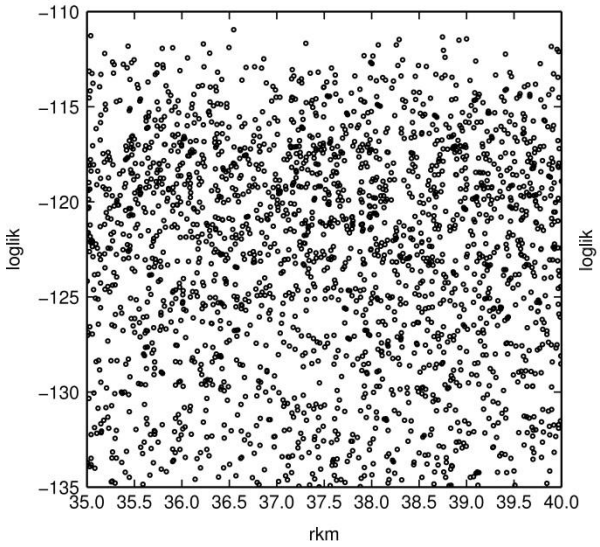

Test loglik vs. Param rq10 Values

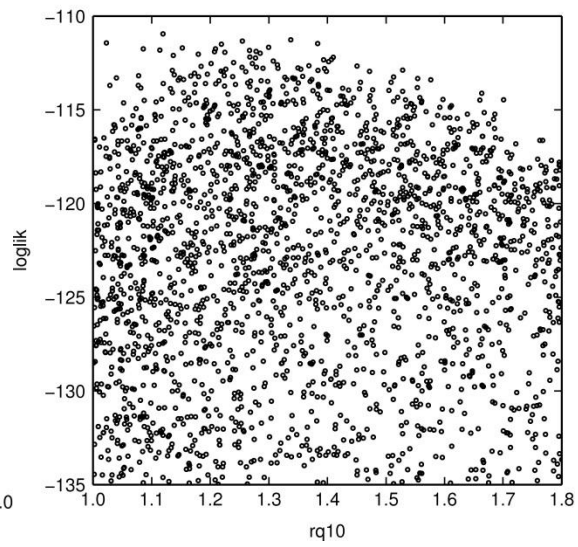

Test loglik vs. Param tveg Values

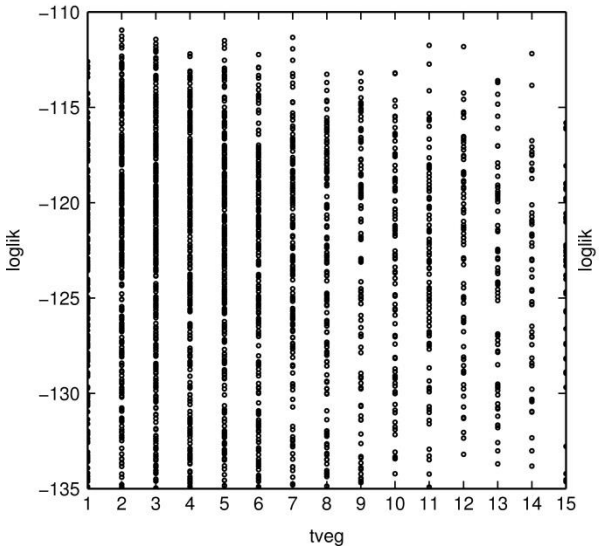

Test loglik vs. Param at0 Values

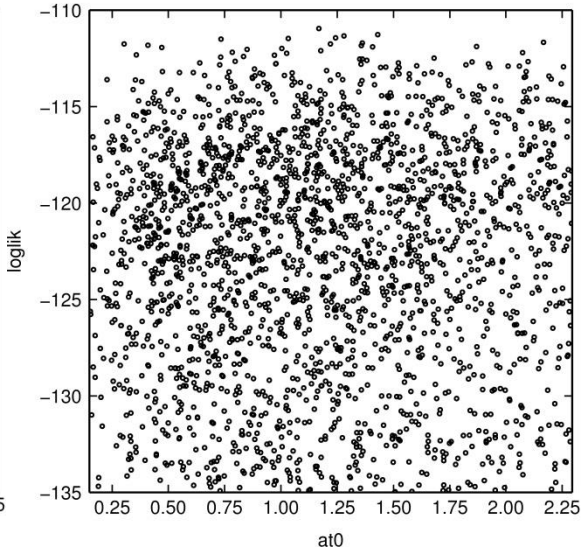

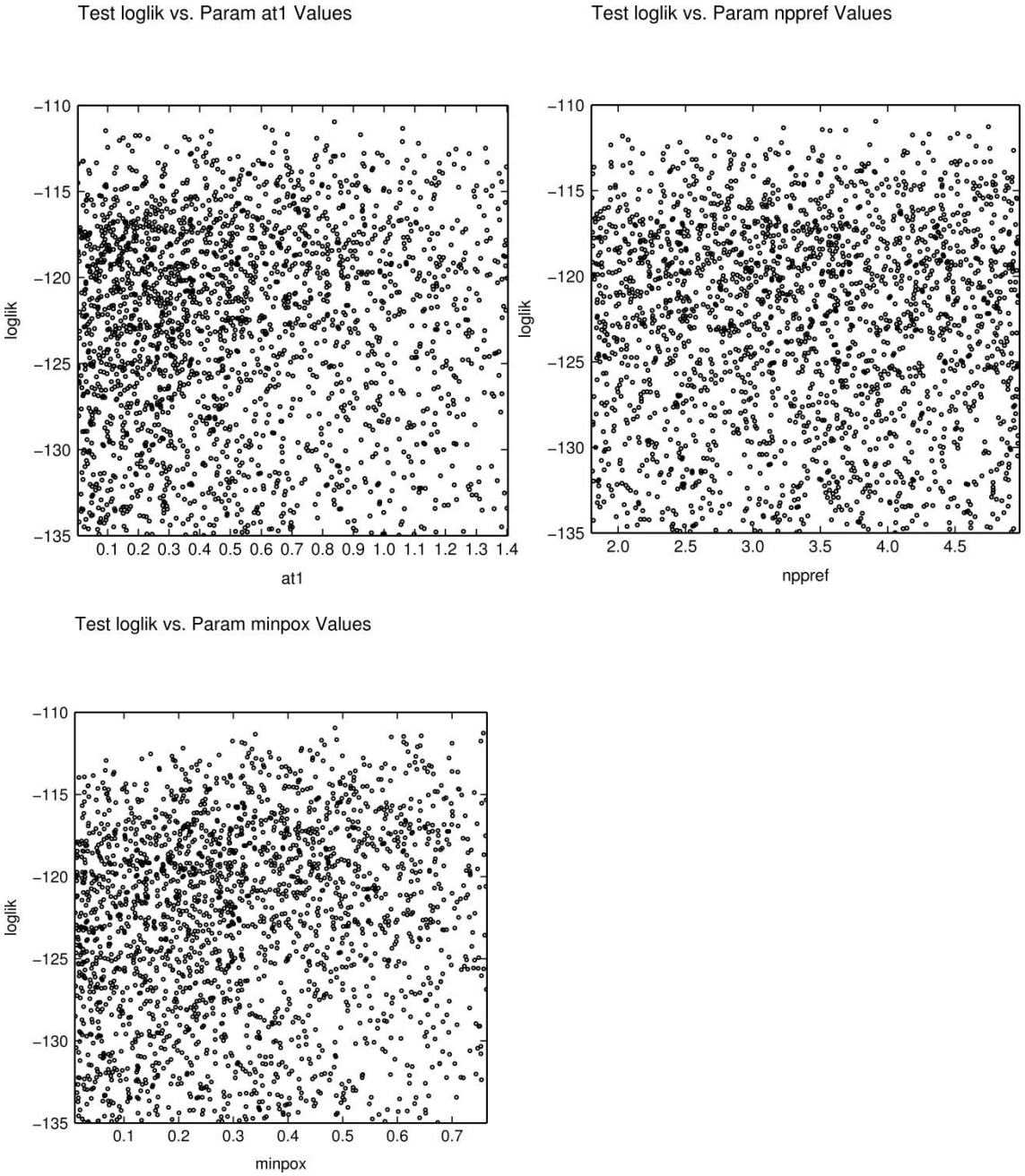

Figure 6-1 Plots of likelihood score of dynamic model simulations in the calibration process

Table 6-1 Dynamic model calibration results

percentile	r0	xvmax	rkm	rq10	tveg	AT0	AT1	NPPref	min_pox
1st	0.077	0.003	35.00	1.01	1.26	0.293	0.016	1.92	0.035
25th	0.109	0.105	36.25	1.18	1.75	0.839	0.322	2.78	0.316
50th	0.127	0.295	37.50	1.26	2.87	1.204	0.605	3.48	0.448
75th	0.157	0.608	38.75	1.36	5.09	1.495	0.833	4.19	0.605
99th	0.240	2.175	40.00	1.65	13.36	2.231	1.338	4.91	0.758

Table 6-2 shows the parameter combinations for which static model simulations were performed.

Table 6-2 Dynamic model simulations' ensemble members

Simulation number	Walter and Heiman model parameters					Dynamic Pox equation parameters				Static Pox
	r0	xvmax	rkm	rq10	tveg	AT0	AT1	NPPref	min_pox	P_{ox}
1	0.138335	0.295199	35.03343	1.230617	4	1.174797	0.661163	2.560012	0.587466	0.5876
2	0.115206	0.196041	35.47048	1.184496	2	1.849473	0.326187	4.124276	0.63392	0.5876
3	0.107443	0.324929	35.27073	1.368553	3	0.797177	0.180226	4.93545	0.499792	0.5876
4	0.090318	0.254831	37.9195	1.407126	2	0.357836	0.166807	3.866865	0.440155	0.5876
5	0.119969	0.081922	37.30714	1.299973	3	2.167293	0.685518	4.519587	0.489178	0.5876
6	0.082365	0.170963	38.46049	1.576335	3	0.883351	0.608631	4.226206	0.164559	0.5876
7	0.097638	0.003865	38.29072	1.383441	2	1.032133	0.093562	3.689262	0.611756	0.5876
8	0.111346	0.679403	35.42351	1.398595	3	1.465381	0.841088	3.515502	0.464363	0.5876
9	0.125579	0.901827	36.99194	1.341732	5	1.278211	0.914627	3.729176	0.248396	0.5876
10	0.095294	0.379145	37.78575	1.426542	4	1.48555	0.502465	4.694395	0.061322	0.5876
11	0.104953	1.295631	35.45194	1.350209	2	2.201263	0.785025	2.582906	0.52328	0.5876
12	0.079731	0.028117	39.09716	1.314503	1	1.380959	0.808169	3.127657	0.27414	0.5876
13	0.085845	0.459018	37.98836	1.450577	2	2.097758	0.679228	3.447211	0.187804	0.5876
14	0.110976	0.170005	35.03866	1.337346	2	1.429667	0.613387	4.748157	0.757263	0.5876
15	0.145067	2.609563	39.66605	1.26974	3	1.473882	0.765793	4.58793	0.68071	0.5876
16	0.106068	1.330759	36.35518	1.279738	2	0.794947	0.558428	4.113668	0.382852	0.5876
17	0.101277	0.490032	38.88535	1.107913	1	1.715598	0.797885	3.37631	0.415984	0.5876
18	0.125576	0.273538	39.30673	1.344793	6	0.919416	0.063937	4.717674	0.356207	0.5876
19	0.122639	0.099875	36.54563	1.119261	2	1.168358	0.838311	3.911951	0.485793	0.5876
20	0.100545	0.312633	37.26043	1.456345	4	0.874612	0.390279	2.036104	0.234533	0.5876
21	0.143269	0.095641	35.90249	1.207402	5	1.407173	0.780622	2.668055	0.320989	0.5876
22	0.116393	0.551836	36.49818	1.278408	2	1.868652	0.150723	2.828966	0.700141	0.5876
23	0.114337	0.039596	39.89411	1.267177	3	1.356738	0.351427	4.605388	0.315719	0.5876
24	0.200815	0.279223	36.29226	1.26773	14	0.783984	0.644581	2.458002	0.207915	0.5876
25	0.182818	0.48622	35.2808	1.238322	10	0.549249	0.020533	4.339153	0.622305	0.5876
26	0.24114	0.612979	38.25848	1.085624	11	0.303922	0.204802	4.184929	0.752917	0.5876
27	0.173209	0.542905	36.22564	1.152522	5	1.361584	0.92283	4.307744	0.461188	0.5876
28	0.120189	0.260693	39.954	1.285583	3	1.00406	0.365241	3.024019	0.466948	0.5876
29	0.158437	0.430958	38.67816	1.148275	5	1.524925	1.334725	3.505242	0.194723	0.5876
30	0.212727	0.526467	36.376	1.077666	9	0.473738	0.455445	2.578823	0.539175	0.5876

Another set of model simulations for both static and dynamic model were performed to assess the impact of *tveg* parameter in the model results. This "mega-ensemble" consisted of the

parameter combinations shown in Table 6-2 with model simulations performed for each parameter combination with all possible values of *tveg* (integer numbers from 1 to 15). As a result, mega-ensemble had 30×15 parameter combinations.

6.2 HISTORIC SIMULATIONS

Observed methane emissions, along with static and dynamic model's simulations of the 30-member ensemble are shown in Figure 6-2. As a metric of goodness-of-fit, the bias in methane emission was calculated to compare each model to the observations. Percentage of bias was calculated as ratio of difference between modeled and observed emission to observed emission (shown in Table 6-3). Weighted average of magnitudes of biases was 46% and 48% for static and dynamic model respectively. Both models matched year 2 and year 3 with much less bias compared to year 1 and year 4. It should be noted that the number of observations in year 4 was significantly less than the other 3 years.

Table 6-3 Bias percentage for methane emission simulations of static and dynamic model in comparison to observed methane emissions

	Mean ($mg/m^2/hr$)			difference in mean ($mg/m^2/hr$)		% bias		
Year	observed	static model	dynamic model	difference between static model and observation	difference between dynamic model and observation	% bias of static model	% bias of static model	number of observations
1	4.322	8.809	8.267	4.487	4	104	91	42
2	9.916	8.321	7.73	-1.595	-2	-16	-22	48
3	9.935	8.394	7.829	-1.541	-2	-16	-21	13
5	20.021	9.193	8.645	-10.828	-11	-54	-57	8

Monthly aggregate methane emissions for historic simulations are shown for years 1991 to 2010 in Figure 6-3. This figure demonstrates the results of 20-year simulations of both static and dynamic model, for the four modeling sites, using 30 different parameter combinations shown in

Table 6-2 These parameter combinations were generated based on the posterior parameter distributions resulted from model parameter calibration (posterior distributions shown in Table 6-1). As described in section 5.3, calibration was performed by grouping simulations into 10-day observation groups.

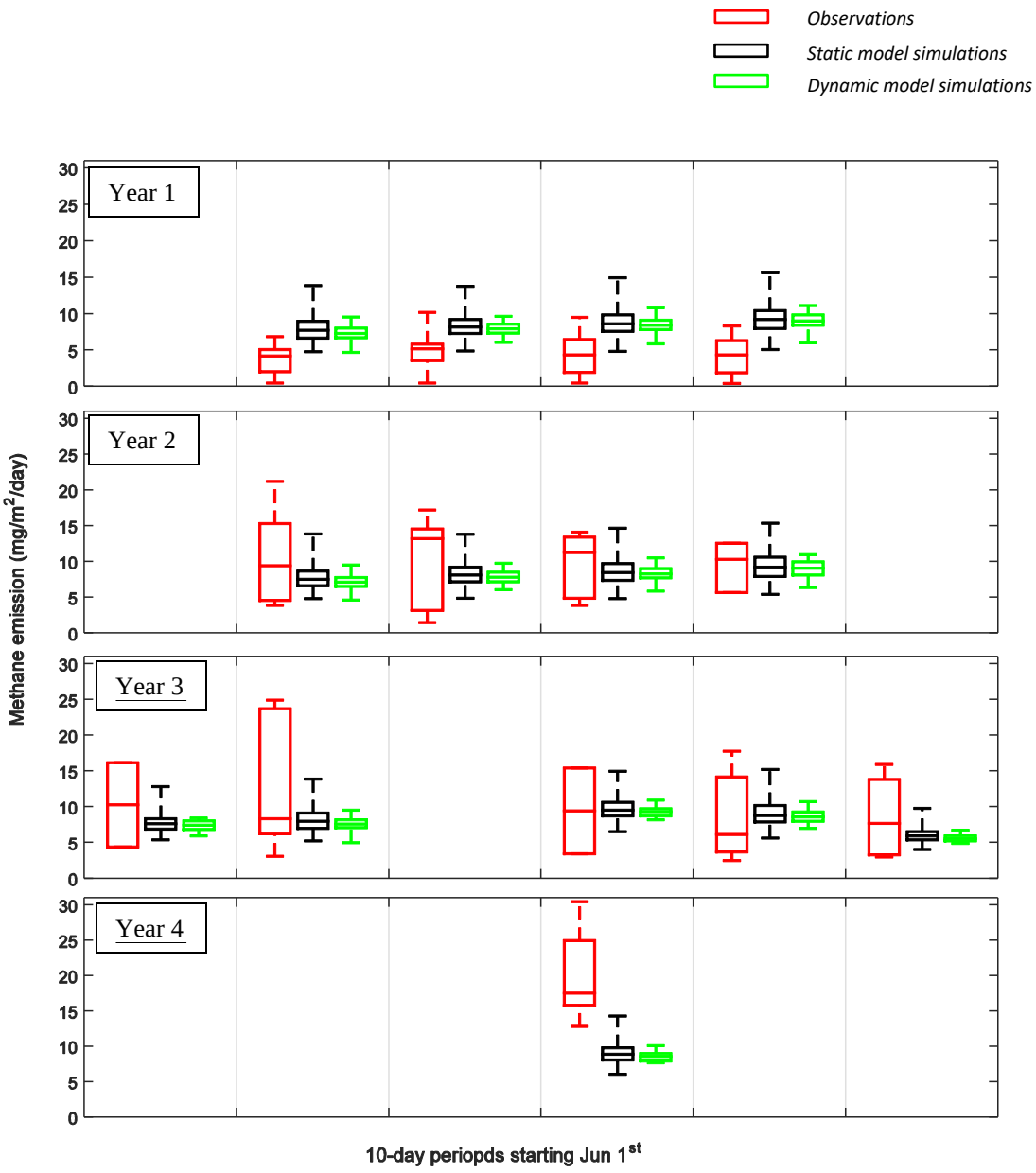

Figure 6-2 Methane emissions observations from Glagolev et al 2011 (in red), ensemble of static model simulations (in black) and ensemble of dynamic model simulations (in green) based on the 30 member ensemble of model simulations

6.3 FUTURE SIMULATIONS

Future simulations of static and dynamic model were performed for years 2081 to 2100. Methane emission rates were plotted in Figure 6-3. This figure shows the input variables for the Walter and Heimann model for historic and future simulations. Dynamic P_{ox} was lower for future

emissions compared to historic values due to lower NPP. Future temperatures were higher than historic temperatures as a result of future climate scenarios in the CMIP5 climate models. Future soil temperature was up to 2 °C higher than median historic soil temperature. NPP values went up slightly from historic to future and its impact on dynamic P_{ox} can be observed in Figure 6-3. The distribution of methane emission for each month is based on the 30 different parameter combinations and averaged over the 20 year simulation period. Methane emission rates are mostly influenced by NPP rates and therefore are highest in the month of July which is the peak of growing season in boreal wetlands of western Siberia. This pattern of maximum methane emissions is also shown by previous studies (Bohn et al., 2007; Ringeval et al., 2010; Walter and Heimann, 2000). July has the peak of methane emissions in all fours sites. Similar to historic simulations, future methane emissions also peak at the month of July, which is reasonable considering that NPP also reaches its peak in July.

Historic mean annual emission was 33.7 g/m^2 from static model versus 31.4 g/m^2 from dynamic model. Future mean annual emission on the other hand was 55.9 g/m^2 for static mode versus 53.7 g/m^2 for dynamic model. Switching from static to dynamic model resulted in 6.8% reduction in annual emission for historic simulation versus 4.0% for future emissions. The absolute change in total emissions resulted from switching to dynamic model was approximately the same (2.2 g/m^2) for both future and historic simulations. Ratio of future to historic mean annual emission was 1.66 and 1.71 for static and dynamic model respectively. These results indicate that the annual emissions are very similar for static and dynamic model.

Plots of seasonal variation in emissions for static and dynamic model (shown in Figure 6-3) indicated that the static and dynamic model differentiate in the shoulder season. The largest difference between the two models occurs in August, September and October. Based on the P_{ox}

graph shown in Figure 6-3, P_{ox} was higher for dynamic model (compare values to static P_{ox} value of 0.5876). The higher P_{ox} values in dynamic model do not result in a seasonally uniform decrease in methane emissions. The months of August, September and October which showed the largest difference between static and dynamic model, had the highest temperatures along with deepest water table level which would result in high deep soil oxidation and a more pronounced decrease in emissions.

Dynamic model results demonstrated smaller uncertainty intervals compared to static model in both historic and future simulations which could be due to four additional dynamic P_{ox} equation's calibrated parameters in the dynamic model.

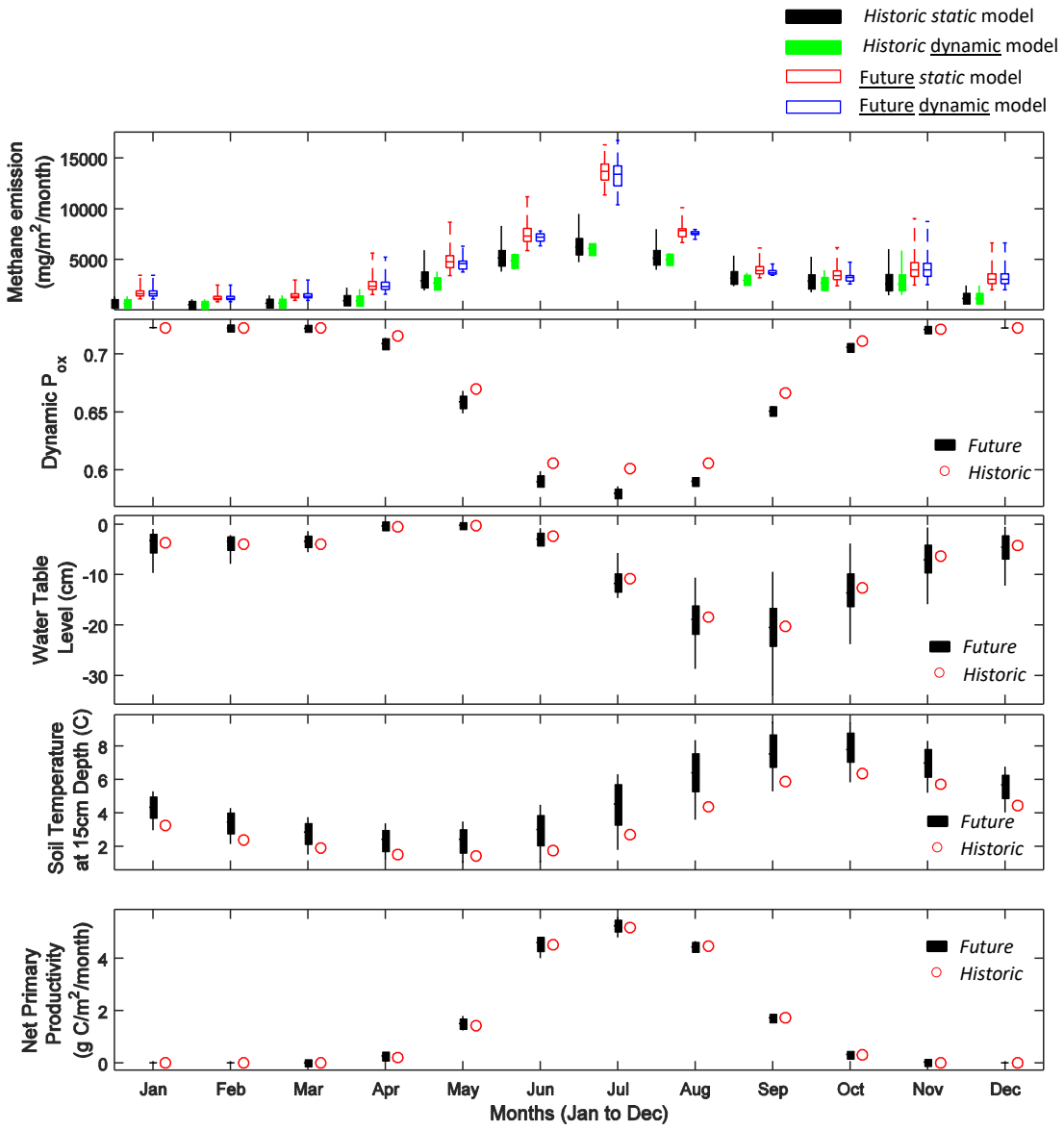

Figure 6-3 Methane emission for historic and future simulations using static and dynamic model along with input variables for historic and future simulations

6.3.1 *Plant-mediated Transport*

In order to further understand the impact of static model versus dynamic model in different conditions of root gas transport capacity (*tveg*). another series of simulations were performed. This set of simulations were 15 times larger in terms of number of single simulations since all of the previous parameter combinations were included in this set with varying *tveg*

values from 1 to 15. The results of this set of simulations showed the variation caused solely by *tveg*. Figure 6-4 shows methane emission ranges for months of June, July and August for different values of *tveg*. As seen in Figure 6-4, while uncertainty of methane emission did not seem to be changing from static to dynamic model, the rate of change of emissions with respect to *tveg* was different. Table 6-4 shows that while at low *tveg* dynamic model results in higher plant-mediated and higher total emission in all months, in higher *tveg*, this relationship becomes reverse. In higher *tveg* static model shows a higher plant-mediated transport rate and thus higher total emissions. Note that sites with higher *tveg* show a more pronounced change in emissions when comparing static model to dynamic model.

Dynamic model has a wider variation of methane emissions from small to large values of *tveg*. With lower values of *tveg*, dynamic model results in higher methane emissions, while with higher values of *tveg*, dynamic model yields lower methane emission rates. This means that the dynamic model has higher sensitivity to *tveg* compared to static model. Note that box and whiskers in Figure 6-4 show the variation in methane emissions due to different parameter combinations and the plotted values are averages of methane emissions from different climate model forcings, four different study sites and 20 years of simulations.

Table 6-4 Changes in plant-mediated, non-plant-mediated and total methane emission due to switch from static to dynamic model, in different conditions of *tveg* for June, July and August (Emissions are in mg/m^2/hour)

	static model	dynamic model	% change due to switching from static model to dynamic model	static model	dynamic model	% change due to switching from static model to dynamic model	static model	dynamic model	% change due to switching from static model to dynamic model
	June plant-mediated emission			July plant-mediated emission			August plant-mediated emission		
low tveg	1169	1452	24%	898	1123	25%	551	685	24%
high tveg	3675	463	-87%	3820	591	-85%	2430	305	-87%
	June non-plant mediated emission			July non-plant mediated emission			August non-plant mediated emission		
low tveg	9827	9827	0%	1759	1759	0%	10150	10150	0%
high tveg	2499	2499	0%	5900	5900	0%	3360	3360	0%
	June total emission			July total emission			August total emission		
low tveg	10996	11279	3%	2657	2882	8%	10701	10835	1%
high tveg	6174	2962	-52%	9720	6491	-33%	5790	3665	-37%

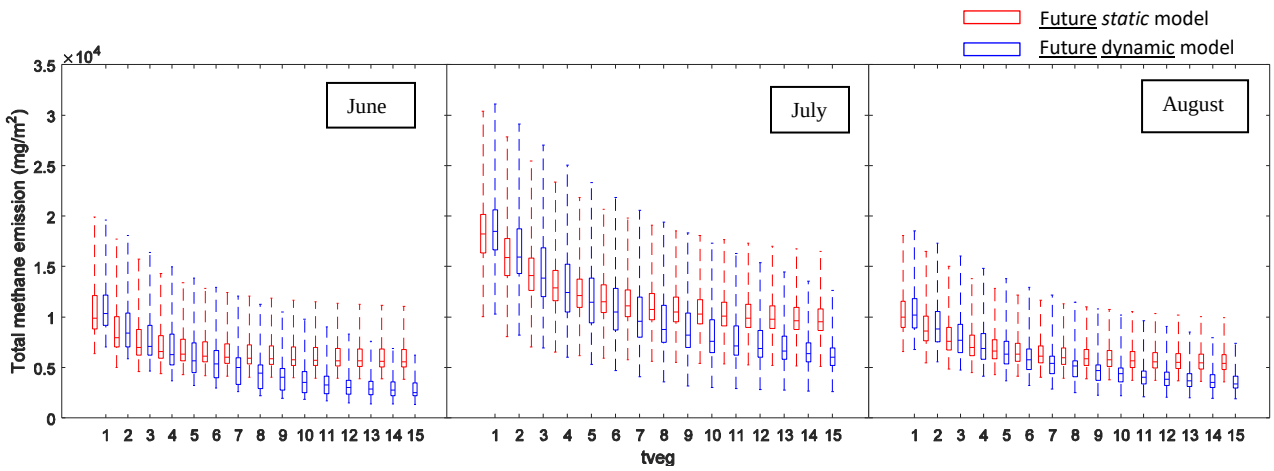

Figure 6-4 Total methane emission in for varying *tveg* values in the Mega Ensemble in June, July and August

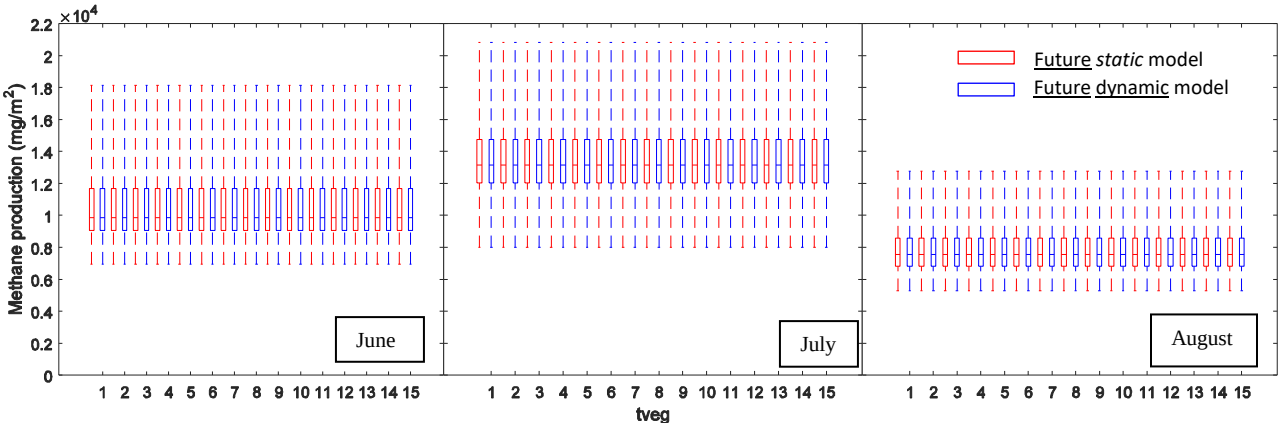

Figure 6-5 Methane production for varying *tveg* values in the Mega Ensemble in June, July and August

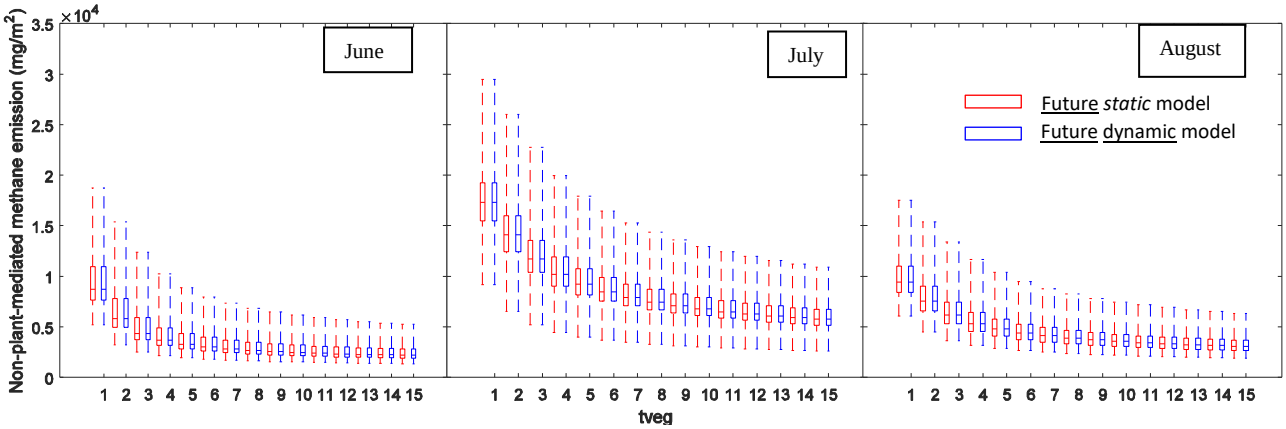

Figure 6-6 Non-plant methane emission in month of July for varying *tveg* values in the Mega Ensemble

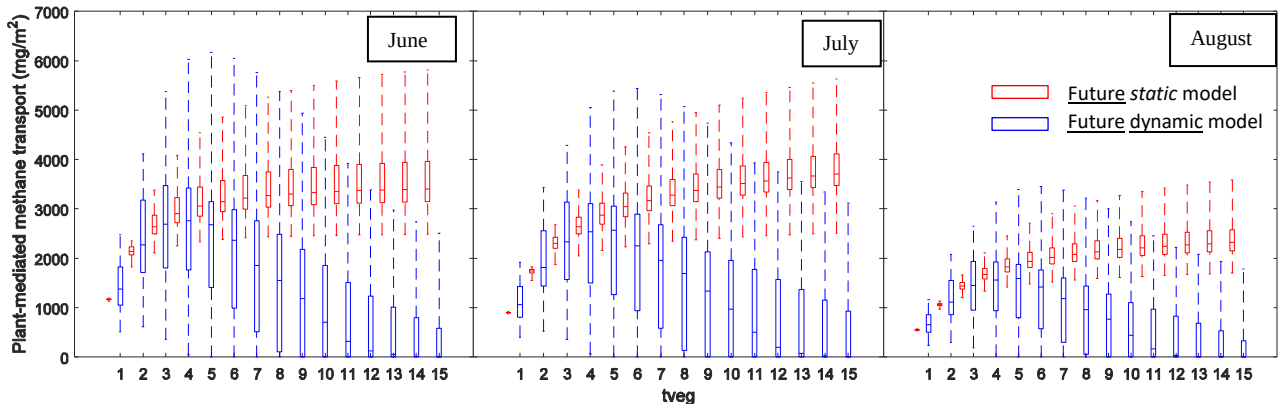

Figure 6-7 Plant-aided methane emission for varying *tveg* values in the Mega Ensemble in June, July and August

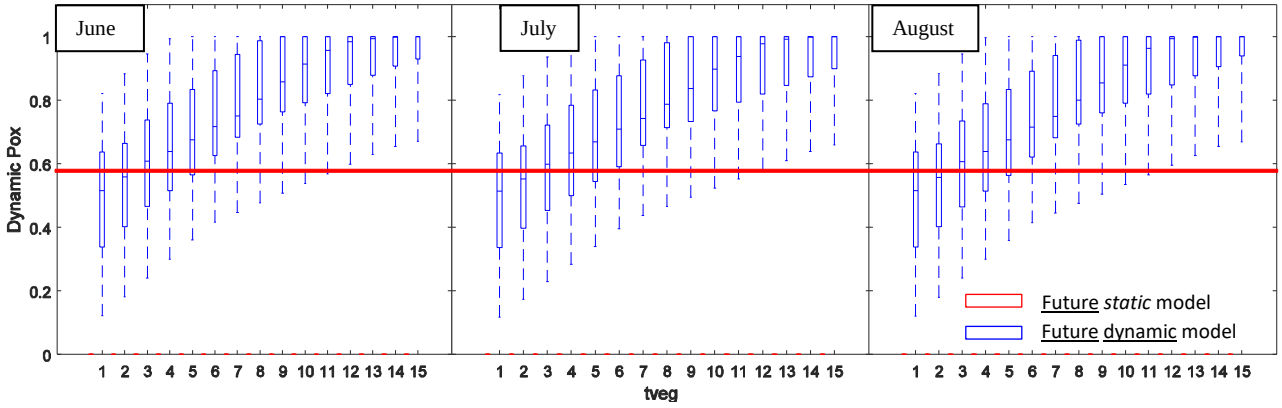

Figure 6-8 Dynamic P_{ox} for varying *tveg* values in the Mega Ensemble in June, July and August

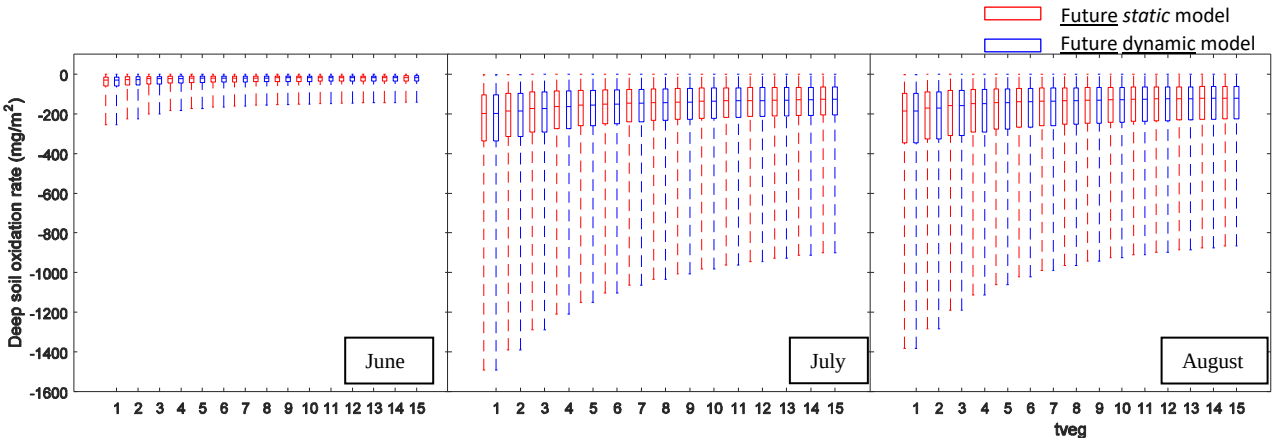

Figure 6-9 Deep soil methane oxidation for varying *tveg* values in the Mega Ensemble in June, July and August

The resulted decrease in total methane emission for high values of *tveg* (shown in Figure 6-4) can be explained by looking into details of mechanisms of methane transport to the

atmosphere. Figure 6-7 shows diffusion and ebullition portion of methane emissions. As shown in this figure, rate of methane transport decreases as *tveg* increases in both static and dynamic model. This pattern could be explained by the fact that a high *tveg* value means there is more connectivity between deep soil and atmosphere and methane concentrations in the soil can drop faster, resulting in lower ebullition and diffusion rates.

Plant-mediated transport shows completely different patterns in static and dynamic model. As Figure 6-8 indicates, with static model, higher *tveg* results in higher plant-mediated transport which is in line with the assumption that a constant portion of methane goes to oxidation. However, with dynamic model, at higher *tveg* values, P_{ox} increases and thus rate of plant-mediated transport goes down. As a result, plant-mediated methane transport has a maximum point. Interestingly, this pattern can be observed in some of the rhizosphere-scale modeling simulations performed in MIN3P (described in Chapter 2 and 3) depending on the microbial competition between the processes. Figure 6-10 shows plant-mediated methane emission rates for a scenario of non-competitive heterotrophic respiration and highly competitive methane oxidation, with medium peat production and zero root oxygen consumption (figure taken from Figure 3-7-a). Although the effect is not very strong, it is observed that at high competitiveness of methane oxidizing bacteria, methane emissions can decrease as root oxygen leakage (equivalent to *tveg* in Walter and Heimann model) increases. This effect is more pronounced in lower root carbon exudation rates. Further evaluation of microbial competitiveness scenarios can be beneficial in validating root-scale model results that show this optimum *tveg* effect.

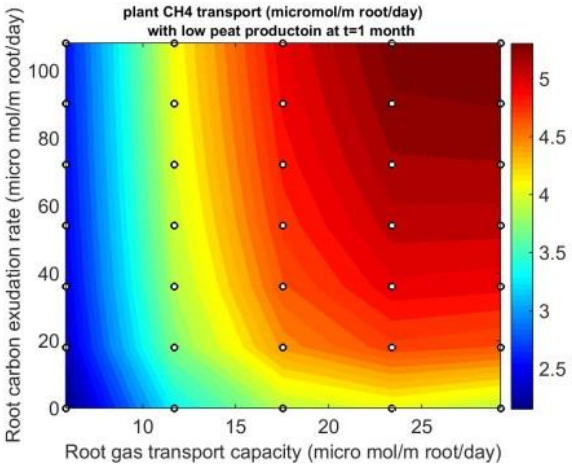

Figure 6-10 Example plot of simulated plant-mediated methane emission from MIN3P rhizosphere-scale model showing the optimum *tveg* effect

Figure 6-9 shows the dynamic P_{ox} (for dynamic model simulations) along with the static P_{ox} value (which was a calculated average of growing season dynamic P_{ox} values from historic simulations) used in the static model. Dynamic P_{ox} has a wide range (from 0.1 to 1) and static P_{ox} is lying in the middle of the range.

Chapter 7. DISCUSSION

7.1 IMPLICATIONS OF RHIZOSPHERE-SCALE MODEL FOR WALTER AND HEIMANN METHANE EMISSIONS MODEL P_{OX}

Based on the rhizosphere-scale model developed in this study, factors that controlled methane oxidation in the rhizosphere were the amount of oxygen and methane available for methanotrophic bacteria. The available methane is directly controlled by methane production rate and the root methane uptake rate through its aerenchymatous tissue (root gas transport capacity). The available oxygen is controlled by root oxygen leakage rate (root gas transport capacity) but it's also controlled by the rate of other processes that use oxygen as a substrate (for example heterotrophic respiration). Rate of heterotrophic respiration is on the other hand controlled by root carbon exudation rate as well as root oxygen leakage. This means the rate of carbon exudation from the root can indirectly impact P_{ox} since it can affect heterotrophic respiration rate which competes with methane oxidation for the limited available oxygen. This result was observed in Figure 3-8 where varying competitiveness levels of heterotrophic respiration resulted in varying P_{ox} values. In other words, when more oxygen is consumed by heterotrophic bacteria, the rate of rhizospheric methane oxidation and hence P_{ox} decreases.

Rhizosphere-scale simulations in this study confirmed the dependence of P_{ox} on root gas transport capacity and root carbon exudation. Plots of modeled P_{ox}, shown in Figure 3-8 indicate that P_{ox} increased as a function of root gas transport capacity. Root gas transport capacity in our rhizosphere-scale model had a similar definition to *tveg* parameter in the Walter and Heimann methane emission model. Although *tveg* only has a qualitative description in the Walter and Heimann model, it provided an already existing parameter that could be used in the dynamic P_{ox}

equation. Another environmental factor that controlled P_{ox} was root oxygen consumption. This parameter was not included in the dynamic P_{ox} since there was no suitable parameter in the Walter and Heimann model to mimic this process. Instead, the fitted P_{ox} parameters from several different levels of root oxygen consumption were included in the calibration process to account for its impact.

This study investigated the impact of microbial competition on rhizospheric methane oxidation using a mechanistic model. Previous process-based methane emission models had assumed a constant static rate for this process or assumed a seasonal relationship for it since field observations indicated that rhizospheric methane oxidation increases in the peak of the growing season (Riley et al., 2011). The results of the rhizosphere-scale model in this study were in line with previous studies that assessed rhizospheric methane oxidation's representation in process-based models. Riley et al performed a global simulation to calculate the ratio of rhizospheric methane oxidation (P_{ox}) and found a global average P_{ox} of 0.6 (Riley et al., 2011). This lies in line with the average growing season P_{ox} from the dynamic model in this study which was 0.58 for historic simulations.

7.2 Historic and Future Methane Emissions Prediction

Seasonal pattern of historic methane emissions shown in Figure 6-3 followed the previously observed and modeled methane emissions in the northern wetlands (Glagolev et al., 2011; Meng et al., 2015). Methane emission started to rise as temperatures rise in the site and reached its peak in July. Although there are not methane emissions measurements outside of the growing season in the Glagolev database, this model suggests that the shoulder season contributes a significant portion of total annual methane emissions, although global methane models showed a lot of disagreement with each other and with observations as to shoulder season emissions in West

Siberia (Bohn et al 2015). Zona et al showed that contribution of cold season could be contributing a significant portion of the total methane emissions from arctic tundra (Zona et al., 2016). Contribution of cold season emission was confirmed by our modeling simulations which showed that up to 40% of total annual methane emission occurs in the shoulder season. Another interesting observation was the ratio of future to historic methane emissions (shown in Figure 7-1) which was higher on average for cold season compared to growing season. More observations during the cold season could be useful for future validations of this phenomenon.

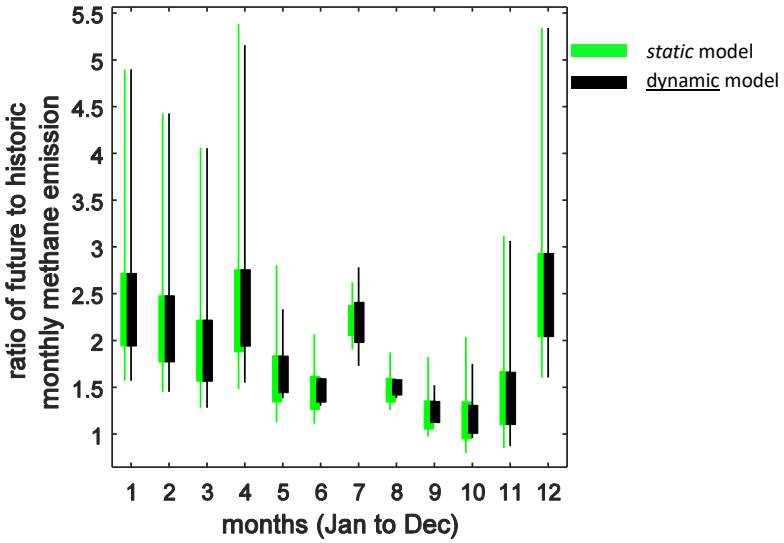

Figure 7-1 Ratio of future to historic methane emissions for static and dynamic model

As shown in Figure 7-1 future model simulations showed that methane emission are going to increase by a median factor of 1.2 to 2.5 for different month of the year based on the 30 member ensemble end of the century simulations. The factor of increase in median methane emission rate was 1.7 for both static and dynamic model based on the 30 member ensemble simulations. This prediction lies within the range of predictions reported by previous modeling studies. Chen et al predicted an increase in pan-arctic methane emissions by a factor of 1.38 to

1.53 by the end of the century (Chen et al., 2015). Gedney et al reported a factor of increase of 2 for the increase of methane emissions from northern latitude wetlands by the end of century (Gedney et al., 2004), while Koven et al reported that global methane emissions are going to increase from 34 Tg/year in 20th century to 71-74 Tg/year by end of 21st century (Koven et al., 2011). Note that the present study's prediction may be overestimated since this modeling simulation did not account for acclimatization and because of the fact that only 4 study sites were included in the model.

The large-scale modeling work in this study showed that seasonal pattern of methane emission can be shifted with use of dynamic model. While the 30-member ensemble of dynamic model simulations for the four study sites didn't show a significant change in annual emissions, it shifted the seasonal patterns by having a more pronounced impact on shoulder season emissions. This effect can even be more pronounced for sites with high *tveg* as shown in section 6.3.1. As a result, global scale emissions can benefit from this modeling framework due to its ability to capture the effect of varying *tveg* (which is a function vegetation type) on global estimates of methane emissions.

The dynamic model results showed smaller uncertainties compared to static model (see Figure 6-1) which because of the fact that four new calibration parameters were added to the Walter and Heimann model with the dynamic P_{ox} equation. Also the Walter and Heimann model calibration was performed for dynamic model only.

7.3 Implications for Future Studies and Field Investigations

The modeling framework developed in this study only utilized observation data from four study sites during the growing season. Therefore the data base did not contain shoulder season observation to examine the observed seasonality of the modeled methane emissions. The

difference between static and dynamic model's methane emission rates in shoulder season (August, September and October) could be further investigated in the future studies using observations performed in these months. Another drawback of the dataset was the limited number of sites and the limited variation in *tveg* factor in spite of choosing sites with heterogeneous vegetation types. Incorporating more sites with higher variety in *tveg* factor can be beneficial in validating the impact of *tveg* modeled methane emissions (discussed in section 6.3.1). Field investigations in sites with highly aerenchymatous plant types is more favorable since the current modeling framework showed a higher sensitivity of plant-mediated methane transport in sites with high *tveg*.

Chapter 8. CONCLUSION

P_{ox} is an important factor determining the plant-mediated methane transport from wetlands. This modeling study showed that the assumption of a constant P_{ox} for all environmental conditions does not capture all of the variations observed in the measured methane emissions. This study showed not only the dependence of P_{ox} on root carbon exudation and root gas transport capacity, it also showed that the competition between microbial activities is an important factor impacting P_{ox}.

There was not a significant difference between the predicted future emissions from the static and dynamic model for the 30 member ensemble. Both models predicted an increase of a factor of 1.7 in methane emissions in end of century projections. However a significant difference was observed for high *tveg* simulations in the Mega Ensemble. It must be noted that while static and dynamic model are resulting in similar emissions for the 30member ensemble, dynamic model developed in this study provides a method to quantify a potentially important but currently uncertain sink of methane.

The future methane simulations with the Mega Ensemble and using static model indicated that there is a consistent increase in plant-mediated methane transport with increase of *tveg*. However dynamic model showed a different interesting trend. Switching from static to dynamic model resulted in reduction of total annual methane emissions by 4% and reduction of plant-mediated methane transport by 17% in the four study sites. The reduction is more pronounced for sites with higher density of aerenchymatous plants (such as sedges) due to an increase in root zone methane oxidation in the dynamic model. As *tveg* was increased plant-mediated methane transport increased up to an "optimum *tveg*" and then started decreasing. This effect could be very important in estimating methane emissions from sites with high density of aerenchymatous

plants. Current approach of large-scale models could potentially be overestimating methane emissions from such sites due to neglecting the effect of high *tveg* on P_{ox} as it is proposed in this study.

BIBLIOGRAPHY

IPCC, 2013: Climate Change 2013: The Physical Science Basis. Contribution of Working Group I to the Fifth Assessment Report of the Intergovernmental Panel on Climate Change [Stocker, T.F., D. Qin, G.-K. Plattner, M. Tignor, S.K. Allen, J. Boschung, A. Nauels, Y. Xia, V. Bex and P.M. Midgley (eds.)]. Cambridge University Press, Cambridge, United Kingdom and New York, NY, USA, 1535 pp, doi:10.1017/CBO9781107415324.

Ferry, J. G. Methanogenesis: Ecology, Physiology, Biochemistry & Genetics. New York: Chapman & Hall, 1993. Print.

Kiene, R. P.: Production and consumption of methane in aquatic systems, in: Microbial production and consumption of greenhouse gases: methane, nitrogen oxides, and halomethanes, edited by: Rogers, J. E. and Whitman, W. E., American Society for Microbiology Press, Washington, DC, 111–146, 1991.

Willmott, C. J., and Matsuura, K.: Terrestrial air temperature and precipitation: monthly and annual time series (1950-1999) (version 1.02), Center for Climate Research, University of Delaware, Newark, DE. [Available online at http://climate.geog.udel.edu/~climate/html_pages/archive.html.], last access December 4 2016, 2001.

Aceti, D.J., and Ferry, J.G. (1988). Purification and characterization of acetate kinase from acetate-grown Methanosarcina thermophila. Evidence for regulation of synthesis. J. Biol. Chem. *263*, 15444–15448.

Adam, J.C., and Lettenmaier, D.P. (2003). Adjustment of global gridded precipitation for systematic bias. J. Geophys. Res.-Atmospheres *108*, 4257.

Adam, J.C., Clark, E.A., Lettenmaier, D.P., and Wood, E.F. (2006). Correction of global precipitation products for orographic effects. J. Clim. *19*, 15–38.

Arah, J.R.M., and Stephen, K.D. (1998). A model of the processes leading to methane emission from peatland. Atmos. Environ. *32*, 3257–3264.

Armstrong, W. (1964). Oxygen Diffusion from the Roots of Some British Bog Plants. Nature *204*, 801–802.

Armstrong, W., Cousins, D., Armstrong, J., Turner, D.W., and Beckett, P.M. (2000). Oxygen distribution in wetland plant roots and permeability barriers to gas-exchange with the rhizosphere: a microelectrode and modelling study with Phragmites australis. Ann. Bot. *86*, 687–703.

Artolozaga, M.J., Kubátová, E., Volc, J., and Kalisz, H.M. (1997). Pyranose 2-oxidase from Phanerochaete chrysosporium- further biochemical characterisation. Appl. Microbiol. Biotechnol. *47*, 508–514.

Aulakh, M.S., Wassmann, R., Bueno, C., and Rennenberg, H. (2001). Impact of root exudates of different cultivars and plant development stages of rice (Oryza sativa L.) on methane production in a paddy soil. Plant Soil *230*, 77–86.

Bartlett, K.B., Crill, P.M., Sebacher, D.I., Harriss, R.C., Wilson, J.O., and Melack, J.M. (1988). Methane flux from the central Amazonian floodplain. J. Geophys. Res. Atmospheres *93*, 1571–1582.

Bender, M., and Conrad, R. (1992). Kinetics of CH4 oxidation in oxic soils exposed to ambient air or high CH4 mixing ratios. FEMS Microbiol. Ecol. *10*, 261–269.

Bender, M., and Conrad, R. (1993). Kinetics of methane oxidation in oxic soils. Chemosphere *26*, 687–696.

Bhullar, G.S., Edwards, P.J., and Venterink, H.O. (2013). Variation in the plant-mediated methane transport and its importance for methane emission from intact wetland peat mesocosms. J. Plant Ecol. rts045.

Bodegom, P.V., Goudriaan, J., and Leffelaar, P. (2001). A Mechanistic Model on Methane Oxidation in a Rice Rhizosphere. Biogeochemistry *55*, 145–177.

van Bodegom, P.M., and Scholten, J.C.M. (2001). Microbial processes of CH4 production in a rice paddy soil: model and experimental validation. Geochim. Cosmochim. Acta *65*, 2055–2066.

Bodelier, P.L.E., and Laanbroek, H.J. (1997). Oxygen uptake kinetics of Pseudomonas chlororaphis grown in glucose- or glutamate-limited continuous cultures. Arch. Microbiol. *167*, 392–395.

Bohn, T.J., Lettenmaier, D.P., Sathulur, K., Bowling, L.C., Podest, E., McDonald, K.C., and Friborg, T. (2007). Methane emissions from western Siberian wetlands: heterogeneity and sensitivity to climate change. Environ. Res. Lett. *2*, 045015.

Bohn, T.J., Podest, E., Schroeder, R., Pinto, N., McDonald, K.C., Glagolev, M., Filippov, I., Maksyutov, S., Heimann, M., Chen, X., et al. (2013a). Modeling the large-scale effects of surface moisture heterogeneity on wetland carbon fluxes in the West Siberian Lowland. Biogeosciences *10*, 6559–6576.

Bohn, T.J., Podest, E., Schroeder, R., Pinto, N., McDonald, K.C., Glagolev, M., Filippov, I., Maksyutov, S., Heimann, M., Chen, X., et al. (2013b). Modeling the large-scale effects of surface moisture heterogeneity on wetland carbon fluxes in theWest Siberian Lowland. Biogeosciences *10*, 6559–6576.

Bohn, T.J., Melton, J.R., Ito, A., Kleinen, T., Spahni, R., Stocker, B.D., Zhang, B., Zhu, X., Schroeder, R., Glagolev, M.V., et al. (2015). WETCHIMP-WSL: intercomparison of wetland methane emissions models over West Siberia. Biogeosciences *12*, 3321–3349.

Boucher, O., Friedlingstein, P., Collins, B., and Shine, K.P. (2009). The indirect global warming potential and global temperature change potential due to methane oxidation. Environ. Res. Lett. *4*, 044007.

Chen, X., Bohn, T.J., and Lettenmaier, D.P. (2015). Model estimates of climate controls on pan-Arctic wetland methane emissions. Biogeosciences *12*, 6259–6277.

Clarens, M., and Moletta, R. (1990). Kinetic-Studies of Acetate Fermentation by Methanosarcina Sp Msta-1. Appl. Microbiol. Biotechnol. *33*, 239–244.

Crow, S.E., and Wieder, R.K. (2005). Sources of CO2 Emission from a Northern Peatland: Root Respiration, Exudation, and Decomposition. Ecology *86*, 1825–1834.

D'Angelo, E.M., and Reddy, K.R. (1999). Regulators of heterotrophic microbial potentials in wetland soils. Soil Biol. Biochem. *31*, 815–830.

Danneel, H., Rossner, E., Zeeck, A., and Giffhorn, F. (1993). Purification and Characterization of a Pyranose Oxidase from the Basidiomycete Peniophora-Gigantea and Chemical-Analyses of Its Reaction-Products. Eur. J. Biochem. *214*, 795–802.

Duddleston, K.N., Kinney, M.A., Kiene, R.P., and Hines, M.E. (2002). Anaerobic microbial biogeochemistry in a northern bog: Acetate as a dominant metabolic end product. Glob. Biogeochem. Cycles *16*, 1063.

Dunfield, P., knowles, R., Dumont, R., and Moore, T.R. (1993). Methane production and consumption in temperate and subarctic peat soils: Response to temperature and pH. Soil Biol. Biochem. *25*, 321–326.

Fischer, R., and Thauer, R.K. (1988). Methane formation from acetyl phosphate in cell extracts of Methanosarcina barkeri Dependence of the reaction on coenzyme A. FEBS Lett. *228*, 249–253.

Gedney, N., Cox, P.M., and Huntingford, C. (2004). Climate feedback from wetland methane emissions. Geophys. Res. Lett. *31*, L20503.

Gerard, G., and Chanton, J. (1993). Quantification of Methane Oxidation in the Rhizosphere of Emergent Aquatic Macrophytes - Defining Upper Limits. Biogeochemistry *23*, 79–97.

Glagolev, M., Kleptsova, I., Filippov, I., Maksyutov, S., and Machida, T. (2011). Regional methane emission from West Siberia mire landscapes. Environ. Res. Lett. *6*, 045214.

Green, J., and Dalton, H. (1986). Steady-state kinetic analysis of soluble methane mono-oxygenase from Methylococcus capsulatus (Bath). Biochem. J. *236*, 155–162.

Harrison, D.E.F. (1973). Studies on the Affinity of Methanol- and Methane-utilizing Bacteria for their Carbon Substrates. J. Appl. Bacteriol. *36*, 301–308.

He, M., Guo, Y., Zhong, Q., and Zhang, Y. (2010). Determination of Binary Gas Diffusion Coefficients Using Digital Holographic Interferometry. J. Chem. Eng. Data *55*, 3318–3321.

Huser, B., Wuhrmann, K., and Zehnder, A. (1982). Methanothrix-Soehngenii Gen-Nov-Sp-Nov, a New Acetotrophic Non-Hydrogen-Oxidizing Methane Bacterium. Arch. Microbiol. *132*, 1–9.

Hütsch, B.W., Augustin, J., and Merbach, W. (2002). Plant rhizodeposition — an important source for carbon turnover in soils. J. Plant Nutr. Soil Sci. *165*, 397–407.

J. Gerritse, J.C.G. (1993). Two-membered mixed cultures of methanogenic and aerobic bacteria in O2-limited chemostats. Microbiol.-Sgm *139*, 1853–1860.

Jähne, B., Heinz, G., and Dietrich, W. (1987). Measurement of the diffusion coefficients of sparingly soluble gases in water. J. Geophys. Res. Oceans *92*, 10767–10776.

Jetten, M., Stams, A., and Zehnder, A. (1990). Acetate Threshold Values and Acetate Activating Enzymes in Methanogenic Bacteria. Fems Microbiol. Ecol. *73*, 339–344.

Joergensen, L. (1985). The methane mono-oxygenase reaction system studied in vivo by membrane-inlet mass spectrometry. Biochem. J. *225*, 441–448.

Jørgensen, T.R., vanKuyk, P.A., Poulsen, B.R., Ruijter, G.J.G., Visser, J., and Iversen, J.J.L. (2007). Glucose uptake and growth of glucose-limited chemostat cultures of Aspergillus niger and a disruptant lacking MstA, a high-affinity glucose transporter. Microbiol. Read. Engl. *153*, 1963–1973.

Karadagli, F., and Rittmann, B.E. (2005). Kinetic Characterization of Methanobacterium bryantii M.o.H. Environ. Sci. Technol. *39*, 4900–4905.

Kenealy, W.R., and Zeikus, J.G. (1982). One-Carbon Metabolism in Methanogens: Evidence for Synthesis of a Two-Carbon Cellular Intermediate and Unification of Catabolism and Anabolism in Methanosarcina barkeri. J. Bacteriol. *151*, 932–941.

King, G.M. (1994). Associations of methanotrophs with the roots and rhizomes of aquatic vegetation. Appl. Environ. Microbiol. *60*, 3220–3227.

King, G.M., Roslev, P., and Skovgaard, H. (1990). Distribution and Rate of Methane Oxidation in Sediments of the Florida Everglades. Appl. Environ. Microbiol. *56*, 2902–2911.

Koelbener, A., Ström, L., Edwards, P.J., and Venterink, H.O. (2009). Plant species from mesotrophic wetlands cause relatively high methane emissions from peat soil. Plant Soil *326*, 147–158.

Kotsyurbenko, O.R., Friedrich, M.W., Simankova, M.V., Nozhevnikova, A.N., Golyshin, P.N., Timmis, K.N., and Conrad, R. (2007). Shift from Acetoclastic to H2-Dependent Methanogenesis in a West Siberian Peat Bog at Low pH Values and Isolation of an Acidophilic Methanobacterium Strain. Appl. Environ. Microbiol. *73*, 2344–2348.

Koven, C.D., Ringeval, B., Friedlingstein, P., Ciais, P., Cadule, P., Khvorostyanov, D., Krinner, G., and Tarnocai, C. (2011). Permafrost carbon-climate feedbacks accelerate global warming. Proc. Natl. Acad. Sci. U. S. A. *108*, 14769–14774.

Krämer, H., and Conrad, R. (1993). Measurement of dissolved H2 concentrations in methanogenic environments with a gas diffusion probe. FEMS Microbiol. Ecol. *12*, 149–158.

Kristjansson, J., Schonheit, P., and Thauer, R. (1982). Different Ks-Values for Hydrogen of Methanogenic Bacteria and Sulfate Reducing Bacteria - an Explanation for the Apparent Inhibition of Methanogenesis by Sulfate. Arch. Microbiol. *131*, 278–282.

Krooneman, J., Moore, E.R.., van Velzen, J.C.., Prins, R.A., Forney, L.J., and Gottschal, J.C. (1998). Competition for oxygen and 3-chlorobenzoate between two aerobic bacteria using different degradation pathways. FEMS Microbiol. Ecol. *26*, 171–179.

Laanbroek, H.J. (2010). Methane emission from natural wetlands: interplay between emergent macrophytes and soil microbial processes. A mini-review. Ann. Bot. *105*, 141–153.

Lai, D.Y.F. (2009). Methane Dynamics in Northern Peatlands: A Review. Pedosphere *19*, 409–421.

Liang, X., Lettenmaier, D.P., Wood, E.F., and Burges, S.J. (1994). A simple hydrologically based model of land surface water and energy fluxes for general circulation models. J. Geophys. Res. Atmospheres *99*, 14415–14428.

Lidstrom, M.E., and Somers, L. (1984). Seasonal Study of Methane Oxidation in Lake Washington. Appl. Environ. Microbiol. *47*, 1255–1260.

Linton, J., and Buckee, J. (1977). Interactions in a Methane-Utilizing Mixed Bacterial Culture in a Chemostat. J. Gen. Microbiol. *101*, 219–225.

Lokshina, L.Y., Vavilin, V.A., Kettunen, R.H., Rintala, J.A., Holliger, C., and Nozhevnikova, A.N. (2001). Evaluation of kinetic coefficients using integrated monod and haldane models for low-temperature acetoclastic methanogenesis. Water Res. *35*, 2913–2922.

Lovley, D.R., Dwyer, D.F., and Klug, M.J. (1982). Kinetic Analysis of Competition Between Sulfate Reducers and Methanogens for Hydrogen in Sediments. Appl. Environ. Microbiol. *43*, 1373–1379.

Lupton, F., and Zeikus, J. (1984). Physiological-Basis for Sulfate-Dependent Hydrogen Competition Between Sulfidogens and Methanogens. Curr. Microbiol. *11*, 7–12.

Machida, Y., and Nakanishi, T. (1984). Purification and Properties of Pyranose Oxidase from Coriolus-Versicolor. Agric. Biol. Chem. *48*, 2463–2470.

Masuda-Nishimura, I., Minamihara, T., and Koyama, Y. (1999). Improvement in thermal stability and reactivity of pyranose oxidase from Coriolus versicolor by random mutagenesis. Biotechnol. Lett. *21*, 203–207.

Mayer, K.U., Frind, E.O., and Blowes, D.W. (2002). Multicomponent reactive transport modeling in variably saturated porous media using a generalized formulation for kinetically controlled reactions. Water Resour. Res. *38*, 1174.

Megraw, S., and Knowles, R. (1987). Methane Production and Consumption in a Cultivated Humisol. Biol. Fertil. Soils *5*, 56–60.

Melton, J.R., Wania, R., Hodson, E.L., Poulter, B., Ringeval, B., Spahni, R., Bohn, T., Avis, C.A., Beerling, D.J., Chen, G., et al. (2013). Present state of global wetland extent and wetland methane modelling: conclusions from a model inter-comparison project (WETCHIMP). Biogeosciences *10*, 753–788.

Meng, L., Paudel, R., Hess, P.G.M., and Mahowald, N.M. (2015). Seasonal and interannual variability in wetland methane emissions simulated by CLM4Me' and CAM-chem and comparisons to observations of concentrations. Biogeosciences *12*, 4029–4049.

Meyer, D.J., and Jones, C.W. (1973). Reactivity with oxygen of bacterial cytochrome oxidases a1, aa3 and o. FEBS Lett. *33*, 101–105.

Mitchell, T.D., and Jones, P.D. (2005). An improved method of constructing a database of monthly climate observations and associated high-resolution grids. Int. J. Climatol. *25*, 693–712.

Nagai, S., Mori, T., and Aiba, S. (1973). Investigation of the energetics of methane-utilising bacteria in methane- and oxygen-limited chemostat cultures. J. Appl. Chem. Biotechnol. *23*, 549–562.

Nat, F.-J.W.A.V.D., and Middelburg, J.J. (1998). Effects of Two Common Macrophytes on Methane Dynamics in Freshwater Sediments. Biogeochemistry *43*, 79–104.

Nedwell, D.B., and Watson, A. (1995). CH4 production, oxidation and emission in a U.K. ombrotrophic peat bog: Influence of SO42− from acid rain. Soil Biol. Biochem. *27*, 893–903.

Neumann, R.B., Blazewicz, S.J., Conaway, C.H., Turetsky, M.R., and Waldrop, M.P. (2015). Modeling CH4 and CO2 cycling using porewater stable isotopes in a thermokarst bog in Interior Alaska: results from three conceptual reaction networks. Biogeochemistry *127*, 57–87.

Nouchi, I., Mariko, S., and Aoki, K. (1990). Mechanism of Methane Transport from the Rhizosphere to the Atmosphere through Rice Plants. Plant Physiol. *94*, 59–66.

Oberlies, G., Fuchs, G., and Thauer, R. (1980). Acetate Thiokinase and the Assimilation of Acetate in Methanobacterium-Thermoautotrophicum. Arch. Microbiol. *128*, 248–252.

Ohtsubo, S., Demizu, K., Kohno, S., Miura, I., Ogawa, T., and Fukuda, H. (1992). Comparison of acetate utilization among strains of an aceticlastic methanogen, Methanothrix soehngenii. Appl. Environ. Microbiol. *58*, 703–705.

Oneill, J., and Wilkinson, J. (1977). Oxidation of Ammonia by Methane-Oxidizing Bacteria and Effects of Ammonia on Methane Oxidation. J. Gen. Microbiol. *100*, 407–412.

Panikov, N.S., and Dedysh, S.N. (2000). Cold season CH4 and CO2 emission from boreal peat bogs (West Siberia): Winter fluxes and thaw activation dynamics. Glob. Biogeochem. Cycles *14*, 1071–1080.

Pankratov, T.A. (2012). Acidobacteria in microbial communities of the bog and tundra lichens. Microbiology *81*, 51–58.

Phillips, R.P., Bernhardt, E.S., and Schlesinger, W.H. (2009). Elevated CO2 increases root exudation from loblolly pine (Pinus taeda) seedlings as an N-mediated response. Tree Physiol. *29*, 1513–1523.

Powell, G., Hilton, M., Archer, D., and Kirsop, B. (1983). Kinetics of the Methanogenic Fermentation of Acetate. J. Chem. Technol. Biotechnol. B-Biotechnol. *33*, 209–215.

Riley, W.J., Subin, Z.M., Lawrence, D.M., Swenson, S.C., Torn, M.S., Meng, L., Mahowald, N.M., and Hess, P. (2011). Barriers to predicting changes in global terrestrial methane fluxes: analyses using CLM4Me, a methane biogeochemistry model integrated in CESM. Biogeosciences *8*, 1925–1953.

Ringeval, B., Noblet-Ducoudré, N. de, Ciais, P., Bousquet, P., Prigent, C., Papa, F., and Rossow, W.B. (2010). An attempt to quantify the impact of changes in wetland extent on methane emissions on the seasonal and interannual time scales. Glob. Biogeochem. Cycles *24*.

Robinson, J., and Tiedje, J. (1984). Competition Between Sulfate-Reducing and Methanogenic Bacteria for H-2 Under Resting and Growing Conditions. Arch. Microbiol. *137*, 26–32.

Saari, A., Rinnan, R., and Martikainen, P.J. (2004). Methane oxidation in boreal forest soils: Kinetics and sensitivity to pH and ammonium. Soil Biol. Biochem. *36*, 1037–1046.

Schipper, L.A., and Reddy, K.R. (1996). Determination of methane oxidation in the rhizosphere of Sagittaria lancifolia using methyl fluoride. Soil Sci. Soc. Am. J. *60*, 611–616.

Schonheit, P., Kristjansson, J., and Thauer, R. (1982). Kinetic Mechanism for the Ability of Sulfate Reducers to Out-Compete Methanogens for Acetate. Arch. Microbiol. *132*, 285–288.

Schütz, H., Seiler, W., and Conrad, R. (1989). Processes involved in formation and emission of methane in rice paddies. Biogeochemistry *7*, 33–53.

Segers, R. (1998). Methane production and methane consumption: a review of processes underlying wetland methane fluxes. Biogeochemistry *41*, 23–51.

Sheffield, J., Goteti, G., and Wood, E.F. (2006). Development of a 50-Year High-Resolution Global Dataset of Meteorological Forcings for Land Surface Modeling. J. Clim. *19*, 3088–3111.

Shieh, J.S., and Whitman, W.B. (1987). Pathway of acetate assimilation in autotrophic and heterotrophic methanococci. J. Bacteriol. *169*, 5327–5329.

Shoemaker, J.K., and Schrag, D.P. (2010). Subsurface characterization of methane production and oxidation from a New Hampshire wetland. Geobiology *8*, 234–243.

Sipkema, E.M., de Koning, W., Ganzeveld, K.J., Janssen, D.B., and Beenackers, A.A.C.M. (1998). Experimental pulse technique for the study of microbial kinetics in continuous culture. J. Biotechnol. *64*, 159–176.

Smatlak, C.R., Gossett, J.M., and Zinder, S.H. (1996). Comparative Kinetics of Hydrogen Utilization for Reductive Dechlorination of Tetrachloroethene and Methanogenesis in an Anaerobic Enrichment Culture. Environ. Sci. Technol. *30*, 2850–2858.

Smith, M.R., and Mah, R.A. (1978). Growth and Methanogenesis by Methanosarcina Strain 227 on Acetate and Methanol. Appl. Environ. Microbiol. *36*, 870–879.

Strayer, R.F., and Tiedje, J.M. (1978). Kinetic Parameters of the Conversion of Methane Precursors to Methane in a Hypereutrophic Lake Sediment. Appl. Environ. Microbiol. *36*, 330–340.

Taylor, K.E., Stouffer, R.J., and Meehl, G.A. (2011). An Overview of CMIP5 and the Experiment Design. Bull. Am. Meteorol. Soc. *93*, 485–498.

Trojanowicz, K., Styka, W., and Baczynski, T. (2009). Experimental Determination of Kinetic Parameters for Heterotrophic Microorganisms in Biofilm under Petrochemical Wastewater Conditions. Pol. J. Environ. Stud. *18*, 913–921.

Tros, M.E., Bosma, T.N.P., Schraa, G., and Zehnder, A.J.B. (1996). Measurement of minimum substrate concentration (S-min) in a recycling fermenter and its prediction from the kinetic parameters of Pseudomonas sp strain B13 from batch and chemostat cultures. Appl. Environ. Microbiol. *62*, 3655–3661.

Walkiewicz, A., Bulak, P., Brzeziñska, M., Włodarczyk, T., and Polakowski, C. (2012). Kinetics of methane oxidation in selected mineral soils. Int. Agrophysics *26*, 401–406.

Walter, B.P., and Heimann, M. (2000). A process-based, climate-sensitive model to derive methane emissions from natural wetlands: Application to five wetland sites, sensitivity to model parameters, and climate. Glob. Biogeochem. Cycles *14*, 745–765.

Westermann, P., Ahring, B.K., and Mah, R.A. (1989). Temperature Compensation in Methanosarcina barkeri by Modulation of Hydrogen and Acetate Affinity. Appl. Environ. Microbiol. *55*, 1262–1266.

Whalen, S.C., and Reeburgh, W.S. (1988). A methane flux time series for tundra environments. Glob. Biogeochem. Cycles *2*, 399–409.

Whiting, G.J., and Chanton, J.P. (1993). Primary production control of methane emission from wetlands. Nature *364*, 794–795.

Wu, F.Y., Chung, A.K.C., Tam, N.F.Y., and Wong, M.H. (2012). Root Exudates of Wetland Plants Influenced by Nutrient Status and Types. Int. J. Phytoremediation *14*, 543–553.

Zehnder, A.J.B., and Brock, T.D. (1980). Anaerobic Methane Oxidation: Occurrence and Ecology. Appl. Environ. Microbiol. *39*, 194–204.

Zhai, X., Piwpuan, N., Arias, C.A., Headley, T., and Brix, H. (2013). Can root exudates from emergent wetland plants fuel denitrification in subsurface flow constructed wetland systems? Ecol. Eng. *61*, 555–563.

Zona, D., Gioli, B., Commane, R., Lindaas, J., Wofsy, S.C., Miller, C.E., Dinardo, S.J., Dengel, S., Sweeney, C., Karion, A., et al. (2016). Cold season emissions dominate the Arctic tundra methane budget. Proc. Natl. Acad. Sci. U. S. A. *113*, 40–45.

APPENDIX A: MECHANISTIC MODEL KINETIC PARAMETERS DATABASE

			Methane oxidation reaction Vmax						
µmol of CH4 /g of dry matter soil /hr	**mmol of CH4 /g of cells /hr**	**nmol of CH4 /g of slurry /hr**	**nmol of Ch4 /h / g dry weight soil**	**log PMO (Potential Methane Oxidation) (PMO in micro mol/m3/s)**	**nmol of CH4 /mg of protein /min**	**mol/L/s**	**source**	**primary or secondary source**	**median of parameter value from each primary source**
			0.61			4.83E-11	(Bender and Conrad, 1993)	primary	
			0.76			6.02E-11	(Bender and Conrad, 1993)	primary	
			0.74			5.86E-11	(Bender and Conrad, 1993)	primary	
			1.05			8.32E-11	(Bender and Conrad, 1993)	primary	
			3.6			2.85E-10	(Bender and Conrad, 1993)	primary	6.02E-11
			0.7			5.54E-11	(Bender and Conrad, 1992)	primary	
			15			1.19E-09	(Bender and Conrad, 1992)	primary	
			270			2.14E-08	(Bender and Conrad, 1992)	primary	
			0.9			7.13E-11	(Bender and Conrad, 1992)	primary	
			2.1			1.66E-10	(Bender and Conrad, 1992)	primary	
			410			3.25E-08	(Bender and Conrad, 1992)	primary	
			3.6			2.85E-10	(Bender and Conrad, 1992)	primary	
			41			3.25E-09	(Bender and Conrad, 1992)	primary	
			450			3.56E-08	(Bender and Conrad, 1992)	primary	1.19E-09
					290	4.35E-10	(Sipkema et al., 1998)	primary	4.35E-10
					70	1.05E-10	(Joergensen, 1985)	primary	
					80	1.20E-10	(Joergensen, 1985)	primary	1.13E-10
	2.15					3.59E-10	(Harrison, 1973)	primary	3.59E-10
					56	8.40E-11	(Green and Dalton, 1986)	primary	8.40E-11
0.55						4.36E-08	(Walkiewicz et al., 2012)	primary	
0.443						3.51E-08	(Walkiewicz et al., 2012)	primary	
0.137						1.09E-08	(Walkiewicz et al., 2012)	primary	3.51E-08
		43.7				1.21E-08	(Dunfield et al., 1993)	primary	
		48				1.33E-08	(Dunfield et al., 1993)	primary	
		54.9				1.53E-08	(Dunfield et al., 1993)	primary	1.33E-08
				0.75		5.62E-09	(Segers, 1998)	secondary	5.62E-09
				0.74		5.50E-09	(Segers, 1998)	secondary	5.50E-09
				0.48		3.02E-09	(Segers, 1998)	secondary	3.02E-09
				0.91		8.13E-09	(Segers, 1998)	secondary	8.13E-09
								min	**8.40E-11**
								1st quartile	**3.97E-10**
								median	**2.10E-09**
								3rd quartile	**5.50E-09**
								max	**3.51E-08**
								mean	**6.63E-09**

Methane oxidation reaction Km for methane							
mg of CH4 /L of water	ppmv (µL of CH4 /L of air)	nmol of CH4/L of water	µmol of CH4/L of water	mol of CH4/L of water	source	prtimary or secondary source of data	median of parameter valules from each primary source
	3.20E+01			4.48E-08	(Bender and Conrad, 1993)	primary	
	4.30E+01			6.02E-08	(Bender and Conrad, 1993)	primary	
	2.80E+01			3.92E-08	(Bender and Conrad, 1993)	primary	
	4.60E+01			6.44E-08	(Bender and Conrad, 1993)	primary	
	2.20E+01			3.08E-08	(Bender and Conrad, 1993)	primary	4.48E-08
		50.16		5.02E-08	(Bender and Conrad, 1992)	primary	
		91		9.10E-08	(Bender and Conrad, 1992)	primary	
		1740		1.74E-06	(Bender and Conrad, 1992)	primary	
		49.9		4.99E-08	(Bender and Conrad, 1992)	primary	
		12.6		1.26E-08	(Bender and Conrad, 1992)	primary	
		4560		4.56E-06	(Bender and Conrad, 1992)	primary	
		29.7		2.97E-08	(Bender and Conrad, 1992)	primary	
		470		4.70E-07	(Bender and Conrad, 1992)	primary	
		27900		2.79E-05	(Bender and Conrad, 1992)	primary	9.10E-08
			37	3.70E-05	(Sipkema et al., 1998)	primary	3.70E-05
			44.5	4.45E-05	(Nedwell and Watson, 1995)	primary	4.45E-05
	5.2			2.29E-07	(Saari et al., 2004)	primary	
	17			7.50E-07	(Saari et al., 2004)	primary	
	18			7.94E-07	(Saari et al., 2004)	primary	
	16			7.06E-07	(Saari et al., 2004)	primary	
	18			7.94E-07	(Saari et al., 2004)	primary	
	18			7.94E-07	(Saari et al., 2004)	primary	
	510			2.25E-05	(Saari et al., 2004)	primary	7.94E-07
			26	2.60E-05	(Harrison, 1973)	primary	2.60E-05
			2.5	2.50E-06	(Joergensen, 1985)	primary	2.50E-06
			32	3.20E-05	(Linton and Buckee, 1977)	primary	
			44	4.40E-05	(Linton and Buckee, 1977)	primary	3.80E-05
			45	4.50E-05	(Oneill and Wilkinson, 1977)	primary	
			48	4.80E-05	(Oneill and Wilkinson, 1977)	primary	4.65E-05
			3	3.00E-06	(Green and Dalton, 1986)	primary	3.00E-06
			2	2.00E-06	(Joergensen, 1985)	primary	2.00E-06
			66.2	6.62E-05	(Megraw and Knowles, 1987)	primary	6.62E-05
			2.2	2.20E-06	(King et al., 1990)	primary	
			2.8	2.80E-06	(King et al., 1990)	primary	
			3.7	3.70E-06	(King et al., 1990)	primary	2.80E-06
			30.66	3.07E-05	(Walkiewicz et al., 2012)	primary	
			19.79	1.98E-05	(Walkiewicz et al., 2012)	primary	
			5.98	5.98E-06	(Walkiewicz et al., 2012)	primary	1.98E-05
6.60E-02				4.13E-06	(Nagai et al., 1973)	primary	4.13E-06
			1.05	1.05E-06	(Dunfield et al., 1993)	primary	

			0.949	9.49E-07	(Dunfield et al., 1993)	primary	
			0.951	9.51E-07	(Dunfield et al., 1993)	primary	9.51E-07
						min	**9.10E-08**
						1st quartile	**2.25E-06**
						median	**4.13E-06**
						3rd quartile	**3.75E-05**
						max	**6.62E-05**
						mean	**2.67E-05**

	Methane oxidation reaction Km for Oxygen				
mg /L	**µmol/L**	**mol/L**	**source**	**primary or secondary**	**median of kinetic parameters from each source**
	1	1.00E-06	(Sipkema et al., 1998)	primary	1.00E-06
	4.7	4.70E-06	(J. Gerritse, 1993)	primary	4.70E-06
	37	3.70E-05	(Segers, 1998)	no source metioned in Segers 1998	3.70E-05
	0.3	3.00E-07	(Joergensen, 1985)	primary	3.00E-07
0.04		1.25E-06	(Nagai et al., 1973)	primary	1.25E-06
	20	2.00E-05	(Lidstrom and Somers, 1984)	primary	2.00E-05
				min	**3.00E-07**
				1st quartile	**1.06E-06**
				median	**2.98E-06**
				3rd quartile	**1.62E-05**
				max	**3.70E-05**
				mean	**1.07E-05**

	acetate kinetics in Methane production reaction Vmax						
activity (µmol /min/mg protein)	**activity (nmol /min/mg protein)**	**q max (mmol/g cell/hour)**	**Vmax µmol/ gdw cell/ min)**	**Vmax(mol/L/S)**	**source**		median of parameter values from each primary source
	2700			2.53E-09	(Jetten et al., 1990)	primary	
	97			9.10E-11	(Jetten et al., 1990)	primary	
	44			4.13E-11	(Jetten et al., 1990)	primary	
	264			2.48E-10	(Jetten et al., 1990)	primary	1.69E-10
	90			8.44E-11	(Oberlies et al., 1980)	primary	8.44E-11
	757			7.10E-10	(Shieh and Whitman, 1987)	primary	
	425			3.99E-10	(Shieh and Whitman, 1987)	primary	5.54E-10
16				1.50E-08	(Fischer and Thauer, 1988)	primary	
9				8.44E-09	(Fischer and Thauer, 1988)	primary	1.17E-08
		26.3		2.74E-09	(Clarens and Moletta, 1990)	primary	
		24.8		2.58E-09	(Clarens and Moletta, 1990)	primary	
		23.9		2.49E-09	(Clarens and Moletta, 1990)	primary	2.58E-09
				3.80E-09	(van Bodegom and Scholten, 2001)	primary	3.80E-09
			16.13	2.02E-11	(Ohtsubo et al., 1992)	primary	
			37.84	4.73E-11	(Ohtsubo et al., 1992)	primary	
			84.74	1.06E-10	(Ohtsubo et al., 1992)	primary	
			48.54	6.07E-11	(Ohtsubo et al., 1992)	primary	
			42.01	5.25E-11	(Ohtsubo et al., 1992)	primary	5.25E-11
6.4				6.00E-09	(Aceti and Ferry, 1988)	primary	6.00E-09
						min	**5.25E-11**
						Q1	**1.48E-10**
						median	**1.57E-09**
						mean	**3.12E-09**
						Q3	**4.35E-09**
						max	**1.17E-08**

Methane production reaction acetate Km					
Km (mmol /L)	**Km (µmol/L)**	**Km (mol/L of water)**	**source**	**primary or secondary**	**median of parameter values from each primary source**
0.46		4.60E-04	(Zehnder and Brock, 1980)	primary	4.60E-04
	0.3	3.00E-07	Zinder et al 1984	primary	3.00E-07
0.7		7.00E-04	(Huser et al., 1982)	primary	7.00E-04
	40	4.00E-05	(Oberlies et al., 1980)	primary	4.00E-05
	860	8.60E-04	(Jetten et al., 1990)	primary	
	78	7.80E-05	(Jetten et al., 1990)	primary	
	280	2.80E-04	(Jetten et al., 1990)	primary	
	90	9.00E-05	(Jetten et al., 1990)	primary	1.85E-04
10		1.00E-02	(Clarens and Moletta, 1990)	primary	
10.7		1.07E-02	(Clarens and Moletta, 1990)	primary	
11.6		1.16E-02	(Clarens and Moletta, 1990)	primary	1.07E-02
2.4		2.40E-03	(Powell et al., 1983)	primary	2.40E-03
7		7.00E-03	(Fischer and Thauer, 1988)	primary	7.00E-03
22		2.20E-02	(Aceti and Ferry, 1988)	primary	2.20E-02
3		3.00E-03	(Kenealy and Zeikus, 1982)	primary	3.00E-03
	90	9.00E-05	(Shieh and Whitman, 1987)	primary	9.00E-05
3		3.00E-03	(Schonheit et al., 1982)	primary	3.00E-03
6.75		6.75E-03	(Lokshina et al., 2001)	primary	
0.3		3.00E-04	(Lokshina et al., 2001)	primary	
2.55		2.55E-03	(Lokshina et al., 2001)	primary	
1.3		1.30E-03	(Lokshina et al., 2001)	primary	1.93E-03
5		5.00E-03	(Smith and Mah, 1978)	primary	5.00E-03
2.5		2.50E-03	(Westermann et al., 1989)	primary	2.50E-03
0.84		8.40E-04	(Ohtsubo et al., 1992)	primary	
0.39		3.90E-04	(Ohtsubo et al., 1992)	primary	
0.49		4.90E-04	(Ohtsubo et al., 1992)	primary	
1.17		1.17E-03	(Ohtsubo et al., 1992)	primary	
1.19		1.19E-03	(Ohtsubo et al., 1992)	primary	8.40E-04
				min	**3.00E-07**
				Q1	**3.91E-04**
				median	**2.16E-03**
				mean	**2.07E-03**
				Q3	**3.50E-03**
				max	**2.20E-02**

Inhibition factor of O2 in Methane production reaction	2.5E-6 mol/L	(Arah and Stephen, 1998)

Methane production from H2/CO2, Vmax						
activity (nmol /min/mg protein)	**Vmax(µmol/g dry sediment/hr)**	**q max (mol/g cell/day)**	**Vmax(mol/L/S)**			median of parameter values from each source
		2.36	1.02E-08	(Karadagli and Rittmann, 2005)	primary	1.02E-08
140			1.31E-10	(Robinson and Tiedje, 1984)	primary	
180			1.69E-10	(Robinson and Tiedje, 1984)	primary	
13			1.22E-11	(Robinson and Tiedje, 1984)	primary	
220			2.06E-10	(Robinson and Tiedje, 1984)	primary	1.50E-10
			7.60E-09	(van Bodegom and Scholten, 2001)	primary	7.60E-09
	0.45		3.56E-08	(Strayer and Tiedje, 1978)	primary	
	2.44		1.93E-07	(Strayer and Tiedje, 1978)	primary	
	3		2.38E-07	(Strayer and Tiedje, 1978)	primary	
	1.18		9.35E-08	(Strayer and Tiedje, 1978)	primary	
	1.14		9.03E-08	(Strayer and Tiedje, 1978)	primary	
	4.27		3.38E-07	(Strayer and Tiedje, 1978)	primary	
	0.47		3.72E-08	(Strayer and Tiedje, 1978)	primary	
	5.51		4.36E-07	(Strayer and Tiedje, 1978)	primary	
	0.49		3.88E-08	(Strayer and Tiedje, 1978)	primary	
	5.88		4.66E-07	(Strayer and Tiedje, 1978)	primary	
	0.69		5.46E-08	(Strayer and Tiedje, 1978)	primary	
	4.73		3.75E-07	(Strayer and Tiedje, 1978)	primary	
	1.12		8.87E-08	(Strayer and Tiedje, 1978)	primary	
	6.38		5.05E-07	(Strayer and Tiedje, 1978)	primary	
	6.01		4.76E-07	(Strayer and Tiedje, 1978)	primary	1.93E-07
			9.38E-11	(Oberlies et al., 1980)	primary	9.38E-11
					min	**9.38E-11**
					Q1	**1.50E-10**
					median	**7.60E-09**
					mean	**4.23E-08**
					Q3	**1.02E-08**
					max	**1.93E-07**

Inhibition factor of O2 in Methane production reaction	2.5E-6 mol/L	(Arah and Stephen, 1998)

Methane production from H2/CO2, Km for Hydrogen							
µmol/L	**mol/L**	**Pa**	**mmol/L**	**mol/L**	**source**		**median of parameter values from each primary source**
18				1.80E-05	(Karadagli and Rittmann, 2005)	primary	1.80E-05
5				5.00E-06	(Robinson and Tiedje, 1984)	primary	
2.5				2.50E-06	(Robinson and Tiedje, 1984)	primary	
4.1				4.10E-06	(Robinson and Tiedje, 1984)	primary	
13				1.30E-05	(Robinson and Tiedje, 1984)	primary	4.55E-06
		2.4		3.33E-08	(Strayer and Tiedje, 1978)	primary	
		2.2		3.05E-08	(Strayer and Tiedje, 1978)	primary	
		2.4		3.33E-08	(Strayer and Tiedje, 1978)	primary	
		2.1		2.91E-08	(Strayer and Tiedje, 1978)	primary	
		2.2		3.05E-08	(Strayer and Tiedje, 1978)	primary	
		3.7		5.13E-08	(Strayer and Tiedje, 1978)	primary	
		4.5		6.24E-08	(Strayer and Tiedje, 1978)	primary	
		3.8		5.27E-08	(Strayer and Tiedje, 1978)	primary	
		1.3		1.80E-08	(Strayer and Tiedje, 1978)	primary	
		4.7		6.51E-08	(Strayer and Tiedje, 1978)	primary	
		3.8		5.27E-08	(Strayer and Tiedje, 1978)	primary	
		2.9		4.02E-08	(Strayer and Tiedje, 1978)	primary	
		4		5.54E-08	(Strayer and Tiedje, 1978)	primary	
		4.8		6.65E-08	(Strayer and Tiedje, 1978)	primary	
		4.3		5.96E-08	(Strayer and Tiedje, 1978)	primary	5.13E-08
		130		1.80E-06	(Kotsyurbenko et al., 2007)	primary	
		170		2.36E-06	(Kotsyurbenko et al., 2007)	primary	2.08E-06
		597		8.28E-06	(Lovley et al., 1982)	primary	8.28E-06
	8.00E-06			8.00E-06	(Kristjansson et al., 1982)	primary	
	6.00E-06			6.00E-06	(Kristjansson et al., 1982)	primary	7.00E-06
	1.40E-05			1.40E-05	(Lupton and Zeikus, 1984)	primary	1.40E-05
	1.33E-05			1.33E-05	(van Bodegom and Scholten, 2001)	primary	1.33E-05
1				1.00E-06	(Smatlak et al., 1996)	primary	1.00E-06
			3	3.00E-06	(Schonheit et al., 1982)	primary	3.00E-06
						min	**5.13E-08**
						Q1	**2.31E-06**
						median	**5.78E-06**
						mean	**7.13E-06**
						Q3	**1.20E-05**
						max	**1.80E-05**

Heterotrophic bacteria kinetics , acetate Km							
Km for acetate	**Km for glucose**	**Km**	**Ks**	**Km**			
m mol /L	**mmol/L**	**µ mol/L**	**mg COD/L**	**mol/L**	**source**	**primary or secondary**	**median of parameter values from each source**
1.56				1.56E-03	(Tros et al., 1996)	primary	1.56E-03
			6.8	5.67E-04	(Trojanowicz et al., 2009)	primary	
			11.2	9.33E-04	(Trojanowicz et al., 2009)	primary	
			9.8	8.17E-04	(Trojanowicz et al., 2009)	primary	
			10.99	9.16E-04	(Trojanowicz et al., 2009)	primary	
			6.8	5.67E-04	(Trojanowicz et al., 2009)	primary	
			10.96	9.13E-04	(Trojanowicz et al., 2009)	primary	8.65E-04
		17.6		1.76E-05	(Bodelier and Laanbroek, 1997)	primary	1.76E-05
	0.74			7.40E-04	(Masuda-Nishimura et al., 1999)	primary	
	1.4			1.40E-03	(Masuda-Nishimura et al., 1999)	primary	1.07E-03
	1.7			1.70E-03	(Machida and Nakanishi, 1984)	primary	
	0.9			9.00E-04	(Machida and Nakanishi, 1984)	primary	
	1			1.00E-03	(Machida and Nakanishi, 1984)	primary	
	1.8			1.80E-03	(Machida and Nakanishi, 1984)	primary	1.35E-03
	1.43			1.43E-03	(Artolozaga et al., 1997)	primary	1.43E-03
						min	1.76E-05
						average	1.05E-03
						median	1.21E-03
						max	1.56E-03
						1st quartile	9.16E-04
						3rd quartile	1.41E-03

Heterotrophic respiration , Km for O2						
µ mol/L	**mol/ m3**	**mmol/L**	**mol/L**	**source**	**primary or secondary**	**median of parameter values from each primary source**
24			2.40E-05	(Krooneman et al., 1998)	primary	
15			1.50E-05	(Krooneman et al., 1998)	primary	
16			1.60E-05	(Krooneman et al., 1998)	primary	
17			1.70E-05	(Krooneman et al., 1998)	primary	
7			7.00E-06	(Krooneman et al., 1998)	primary	
8			8.00E-06	(Krooneman et al., 1998)	primary	1.55E-05
	1.07E-02		1.07E-05	(Bodegom et al., 2001)	secondary	1.07E-05
5.63			5.63E-06	(Bodelier and Laanbroek, 1997)	primary	5.63E-06
		83.2	8.32E-02	(Artolozaga et al., 1997)	primary	8.32E-02
		0.65	6.50E-04	(Danneel et al., 1993)	primary	
		0.13	1.30E-04	(Danneel et al., 1993)	primary	3.90E-04
0.33			3.30E-07	(Meyer and Jones, 1973)	primary	
6.5			6.50E-06	(Meyer and Jones, 1973)	primary	
2.8			2.80E-06	(Meyer and Jones, 1973)	primary	
1.8			1.80E-06	(Meyer and Jones, 1973)	primary	
7.7			7.70E-06	(Meyer and Jones, 1973)	primary	2.80E-06
					min	2.80E-06
					average	1.39E-02
					median	1.31E-05
					max	8.32E-02
					1st quartile	6.90E-06
					3rd quartile	2.96E-04

Heterotrophic respiration Vmax						
specific growth rate	**Vmax**		**Vmax**	**source**	**primary or secondary source**	**median of parameter from each primary source**
1/hr	**fmol / cell / hr**	**micro mol/gdw cell/s**	**mol/L/S**			
			1.23E-10	(Krooneman et al., 1998)	primary	
			1.49E-10	(Krooneman et al., 1998)	primary	
			2E-10	(Krooneman et al., 1998)	primary	
			2.81E-10	(Krooneman et al., 1998)	primary	
			3.57E-10	(Krooneman et al., 1998)	primary	
			3.6E-10	(Krooneman et al., 1998)	primary	2.4E-10
	0.79		1.31E-10	(Bodelier and Laanbroek, 1997)	primary	
	0.14		2.32E-11	(Bodelier and Laanbroek, 1997)	primary	7.72E-11
		0.49	3.68E-11	(Jørgensen et al., 2007)	primary	
		0.48	3.6E-11	(Jørgensen et al., 2007)	primary	
		0.73	5.48E-11	(Jørgensen et al., 2007)	primary	
		0.9	6.75E-11	(Jørgensen et al., 2007)	primary	
		1.01	7.58E-11	(Jørgensen et al., 2007)	primary	
		0.93	6.98E-11	(Jørgensen et al., 2007)	primary	6.11E-11
				min		6.11E-11
				average		1.26E-10
				median		7.72E-11
				max		2.40E-10
				1st quartile		5.79E-11
				3rd quartile		1.87E-10

µ mol/m2 /day CO2 emission	µ mol /hr/ g root dw	mg C m-1 h-1	µ g / g rood dry mass/hr	mol/s / m length of root	source	note
51.5				9.4E-12	(Crow and Wieder, 2005)	
	202.5			9.2E-10	(Wu et al., 2012)	
			10.2	7.8E-13	(Zhai et al., 2013)	
			280	2.1E-11	(Phillips et al., 2009)	*Pinus taeda* seedlings
			260	2.0E-11	(Phillips et al., 2009)	*Pinus taeda* seedlings
			15	1.1E-12	(Phillips et al., 2009)	*Pinus taeda* seedlings
			10	7.6E-13	(Phillips et al., 2009)	*Pinus taeda* seedlings
			average	2.09E-10		

MECHANISTIC MODEL KINETIC PARAMTER DATABASE

UNIT CONVERSIONS AND ASSUMPTOINS

1-Methane oxidation V_{max}

$$\frac{\mu mol}{g\ of\ dry\ matter\ soil * hr} = \frac{\mu mol}{g\ dry\ matter\ soil * hr} * \frac{mol}{10^6\ \mu mol} * \frac{hr}{3600 s} * \frac{0.114 g\ of\ dry\ matter\ soil}{1 mL\ bulk} * \frac{1000 mL}{1 L}$$

$$* \frac{1\ L\ bulk}{0.4 L\ H_2O} = 7.92E-8 \frac{mol}{L s}$$

dry density of soil = 0.114 g/cm^3 according to Colby's field data
porosity=0.4 (our own assumption)

$$\frac{mmol}{g\ of\ cells * hr} = \frac{mmol}{g\ of\ cells * hr} * \frac{mol}{10^3 mmol} * \frac{10^{-12} g\ of\ cells}{1 cell} * \frac{2.1E+6 cells}{1 g\ dry\ weight\ soil} * \frac{0.114 g\ of\ dry\ matter\ soil}{1 mL\ bulk}$$

$$* \frac{1000 mL}{1 L} * \frac{1\ L\ bulk}{0.4 L\ H_2O} * \frac{1 hr}{3600 s} = 1.67E-10 \frac{mol}{L s}$$

Mass of a cell = I picogram (Wikipedia)
Number of cells in mL of sediment taken from Elias et al. 1999

TABLE 3. CoM levels in various sediments and CoM levels per cell for sediments

Environmental sample	Depth (ft)	Amt of CoM		MPN estimation procedure	
		nmol/g of sediment	nmol/ml	No. of cells/ml	fmol of CoM/cell
Pond sediment		0.02	0.06	1.5×10^5	0.40
Landfill sediment		0.01	0.02	1.1×10^5	0.18
Sewage sludge		0.09	0.22	4.6×10^5	0.48
Hydrocarbon-contaminated sediment	2.5	0.00	ND[a]	ND	
	3.0	0.02	0.05	7.5×10^4	0.67
	4.0	0.08	0.20	3.3×10^5	0.47
	5.5	0.07	0.18	2.2×10^5	0.65
	7.5	0.08	0.20	3.6×10^5	0.43
	8.5	0.07	0.19	2.7×10^5	0.55
	10.0	0.07	0.17	1.6×10^5	0.74

[a] ND, not determined.

Table from from Elias et al. 1999

$$\frac{nmol}{g\,of\,slurry*hr}=\frac{nmol}{g\,of\,slurry*hr}*\frac{mol}{10^9\,nmol}*\frac{g\,of\,slurry}{mL\,of\,bulk}*\frac{10^3\,mL\,of\,bulk}{L}*\frac{1hr}{3600s}=2.78E-10\frac{mol}{Ls}$$

$$\frac{nmol}{g\,of\,dry\,weight\,soil*hr}=\frac{nmol}{g\,of\,dry\,weight\,soil*hr}*\frac{mol}{10^9\,nmol}*\frac{hr}{3600s}*\frac{0.114g\,of\,dry\,matter\,soil}{1mL\,bulk}*\frac{1000mL}{1L}$$
$$*\frac{1\,L\,bulk}{0.4L\,H_2O}=7.92E-11\frac{mol}{Ls}$$

$$\frac{\mu mol}{m^3\,s}=\frac{mol}{m^3\,s}*\frac{10^{-6}\,mol}{1\mu mol}*\frac{m^3}{1000L}=1.0E-9\frac{mol}{Ls}$$

$$\frac{nmol}{mg\,of\ protein*\min}=\frac{nmol}{mg\,of\ protein*\min}*\frac{mol}{10^9\,nmol}*\frac{0.15mg\,of\ protein}{1mg\,of\,cell}*\frac{1mg\,of\,cell}{10^{-3}\,g\,of\,cell}*\frac{10^{-12}\,g\,of\,cell}{1cell}$$
$$*\frac{2.1E+6cells}{1g\,dry\,weight\,soil}*\frac{0.114g\,of\,dry\,matter\,soil}{1mL\,bulk}*\frac{1000mL}{1L}*\frac{1\,L\,bulk}{0.4L\,H_2O}*\frac{1\min}{60s}=1.50E-12\frac{mol}{Ls}$$

Table 2
Numbers of methanotrophic bacteria (±SE%) in various soils assayed in fresh state (exposed to ambient CH_4) and after preincubation under 20% CH_4

Soils	Numbers of methanotrophs (±SE%) (cells g^{-1} dw)	
	Fresh	Preincubated
CC	$3.6\times10^6\pm14$	$10\times10^6\pm14$
MC	$3.6\times10^5\pm17$	$3.3\times10^6\pm21$
FL	$2.4\times10^5\pm34$	$6.4\times10^5\pm20$
PS	$4.2\times10^6\pm13$	$2.3\times10^7\pm19$
NG [a]		$2.1\times10^7\pm16$

The numbers were significantly different in the two treatments (*t*-test; $p<0.05$).
[a] Forest soil over a natural gas source in Switzerland.

Table from Bender and Conrad 1993

2-Methane production from acetate V_{max}

$$\frac{\mu mol}{mg\ of\ protein*\min}=\frac{\mu mol}{mg\ of\ protein*\min}*\frac{mol}{10^{6}\ \mu mol}*\frac{0.15mg\ of\ protein}{1mg\ of\ cell}*\frac{1mg\ of\ cell}{10^{-3}\ g\ of\ cell}*\frac{10^{-12}\ g\ of\ cell}{1cell}$$
$$*\frac{1.5E+5cells}{1\ mL\ bulk}*\frac{1000mL}{1L}*\frac{1\ L\ bulk}{0.4\ L\ H_2O}*\frac{1\min}{60s}=9.38E-10\frac{mol}{L\ s}$$

$$\frac{nmol}{mg\ of\ protein*\min}=\frac{nmol}{mg\ of\ protein*\min}*\frac{mol}{10^{9}\ nmol}*\frac{0.15mg\ of\ protein}{1mg\ of\ cell}*\frac{1mg\ of\ cell}{10^{-3}\ g\ of\ cell}*\frac{10^{-12}\ g\ of\ cell}{1cell}$$
$$*\frac{1.5E+5cells}{1mL\ bulk}*\frac{1000mL}{1L}*\frac{1\ L\ bulk}{0.4\ L\ H_2O}*\frac{1\min}{60s}=9.38E-13\frac{mol}{L\ s}$$

$$\frac{mmol}{g\ of\ cells*hr}=\frac{mmol}{g\ of\ cells*hr}*\frac{mol}{10^{3}\ mmol}*\frac{10^{-12}\ g\ of\ cells}{1cell}*\frac{1.5E+5cells}{1mL\ bulk}*\frac{1000mL}{1L}*\frac{1\ L\ bulk}{0.4\ L\ H_2O}*\frac{1hr}{3600s}=$$
$$1.04E-10\frac{mol}{L\ s}$$

$$\frac{\mu mol}{g\ of\ dry\ weight\ cell*\min}=\frac{\mu mol}{g\ of\ dry\ weight\ cell*\min}*\frac{mol}{10^{6}\ \mu mol}*\frac{20g\ of\ dry\ weight\ cell}{100g\ of\ cells}*\frac{10^{-12}\ g\ of\ cells}{1cell}$$
$$*\frac{1.5E+5cells}{1mL\ bulk}*\frac{1000mL}{1L}*\frac{1\ L\ bulk}{0.4\ L\ H_2O}*\frac{1\min}{60s}=1.25E-12\frac{mol}{L\ s}$$

It is assumed that 80% of a cell's mass is water and 20% is dry matter. (Wikipedia)

3-Methane production from H_2/CO_2 V_{max}

$$\frac{\mu mol}{mg\ of\ protein*\min}=\frac{\mu mol}{mg\ of\ protein*\min}*\frac{mol}{10^{6}\ \mu mol}*\frac{0.15mg\ of\ protein}{1mg\ of\ cell}*\frac{1mg\ of\ cell}{10^{-3}\ g\ of\ cell}*\frac{10^{-12}\ g\ of\ cell}{1cell}$$
$$*\frac{1.5E+5cells}{1\ mL\ bulk}*\frac{1000mL}{1L}*\frac{1\ L\ bulk}{0.4\ L\ H_2O}*\frac{1\min}{60s}=9.38E-10\frac{mol}{L\ s}$$

$$\frac{nmol}{mg\ of\ protein*\min}=\frac{nmol}{mg\ of\ protein*\min}*\frac{mol}{10^{9}\ nmol}*\frac{0.15mg\ of\ protein}{1mg\ of\ cell}*\frac{1mg\ of\ cell}{10^{-3}\ g\ of\ cell}*\frac{10^{-12}\ g\ of\ cell}{1cell}$$
$$*\frac{1.5E+5cells}{1mL\ bulk}*\frac{1000mL}{1L}*\frac{1\ L\ bulk}{0.4\ L\ H_2O}*\frac{1\min}{60s}=9.38E-13\frac{mol}{L\ s}$$

$$\frac{\mu mol}{g\ of\ dry\ sediment*hr}=\frac{\mu mol}{g\ dry\ sediment*hr}*\frac{mol}{10^{6}\ \mu mol}*\frac{hr}{3600s}*\frac{0.114g\ of\ dry\ sediment}{1mL\ bulk}*\frac{1000mL}{1L}$$
$$*\frac{1\ L\ bulk}{0.4\ L\ H_2O}=7.92E-8\frac{mol}{L\ s}$$

$$\frac{mol}{g\,of\,cells*day}=\frac{mol}{g\,of\,cells*day}*\frac{10^{-12}\,g\,of\,cells}{1cell}*\frac{1.5E+5cells}{1mL\,bulk}*\frac{1000mL}{1L}*\frac{1\,L\,bulk}{0.4\,L\,H_2O}*\frac{1day}{86400s}=$$

$$4.34E-9\frac{mol}{L\,s}$$

4-Heterotrophic Respiration's V_{max}

$$\frac{nmol}{mg\,of\ protein*\min}=\frac{nmol}{mg\,of\ protein*\min}*\frac{mol}{10^9\,nmol}*\frac{0.15mg\,of\ protein}{1mg\,of\,cell}*\frac{1mg\,of\,cell}{10^{-3}\,g\,of\,cell}*\frac{10^{-12}\ g\,of\,cell}{1cell}$$

$$*\frac{2.1E+6cells}{1g\,dry\,weight\,soil}*\frac{0.114g\,of\,dry\,matter\,soil}{1mL\,bulk}*\frac{1000mL}{1L}*\frac{1\,L\,bulk}{0.4\,L\,H_2O}*\frac{1\min}{60s}=1.50E-12\frac{mol}{L\,s}$$

$$\frac{fmol}{cell*hr}=\frac{fmol}{cell*hr}*\frac{10^{-15}\,mol}{1\,fmol}*\frac{2.1E+6cells}{1g\,dry\,weight\,soil}*\frac{0.114g\,of\,dry\,matter\,soil}{1mL\,bulk}*\frac{1000mL}{1L}*\frac{1\,L\,bulk}{0.4\,L\,H_2O}$$

$$*\frac{1hr}{3600s}=1.66E-10\frac{mol}{L\,s}$$

$$\frac{\mu mol}{g\,of\,dry\ weight\,cell\,*s}=\frac{\mu mol}{g\,of\,dry\ weight\,cell*s}*\frac{mol}{10^6\,\mu mol}*\frac{20g\,of\,dry\,weight\,cell}{100\,g\,of\,cells}*\frac{10^{-12}\,g\,of\,cells}{1cell}$$

$$*\frac{1.5E+5cells}{1mL\,bulk}*\frac{1000mL}{1L}*\frac{1\,L\,bulk}{0.4\,L\,H_2O}=7.5E-11\frac{mol}{L\,s}$$

APPENDIX B: POX FITTING PARAMETERS

M: Medium

H:High

L: Low

Table 8B-1: Dynamic Pox equation fitting paramters for eahc model simulation

Pox fitting	Methane Production	Heterotrophic Respiration	Methane Oxidation	Peat Production	Root Oxygen Consumption (%)	Time(months)	A0	A1	NPPref	Min_pox
1	M	M	M	L	0	1	0.1414	0.1992	0.0307	0.6995
2	M	M	M	M	0	1	0.1383	0.2218	0.0294	0.6034
3	M	M	M	H	0	1	0.1264	0.2303	0.0262	0.4787
4	M	M	M	L	0	2	0.1401	0.2615	0.0296	0.5615
5	M	M	M	M	0	2	0.1171	0.2615	0.0258	0.4285
6	M	M	M	H	0	2	0.0867	0.2220	0.0205	0.2989
7	M	M	M	L	0	3	0.1329	0.3017	0.0325	0.4575
8	M	M	M	M	0	3	0.0939	0.2704	0.0255	0.3223
9	M	M	M	H	0	3	0.0555	0.1997	0.0177	0.2110
10	M	M	H	L	0	1	0.1563	0.2063	0.0345	0.7042
11	M	M	H	M	0	1	0.1503	0.2246	0.0324	0.6080
12	M	M	H	H	0	1	0.1352	0.2282	0.0284	0.4830
13	M	M	H	L	0	2	0.1531	0.2639	0.0313	0.5667
14	M	M	H	M	0	2	0.1272	0.2598	0.0268	0.4332
15	M	M	H	H	0	2	0.0940	0.2176	0.0209	0.3026
16	M	M	H	L	0	3	0.1442	0.3017	0.0339	0.4627
17	M	M	H	M	0	3	0.1024	0.2673	0.0259	0.3265
18	M	M	H	H	0	3	0.0610	0.1954	0.0175	0.2140
19	M	M	L	L	0	1	0.0899	0.2705	0.0164	0.6408
20	M	M	L	M	0	1	0.0900	0.3122	0.0167	0.5458
21	M	M	L	H	0	1	0.0807	0.3360	0.0164	0.4266
22	M	M	L	L	0	2	0.0871	0.3599	0.0205	0.4925
23	M	M	L	M	0	2	0.0659	0.3662	0.0199	0.3678
24	M	M	L	H	0	2	0.0408	0.3180	0.0179	0.2526
25	M	M	L	L	0	3	0.0810	0.4057	0.0246	0.3888
26	M	M	L	M	0	3	0.0468	0.3668	0.0223	0.2686
27	M	M	L	H	0	3	0.0188	0.2769	0.0183	0.1741
28	H	M	M	L	0	1	0.1397	0.2188	0.0334	0.6501
29	H	M	M	M	0	1	0.1317	0.2409	0.0319	0.5330
30	H	M	M	H	0	1	0.1117	0.2370	0.0282	0.3948
31	H	M	M	L	0	2	0.1358	0.2747	0.0325	0.5203

32	H	M	M	M	0	2	0.1086	0.2669	0.0282	0.3816
33	H	M	M	H	0	2	0.0743	0.2163	0.0222	0.2541
34	H	M	M	L	0	3	0.1289	0.3080	0.0348	0.4276
35	H	M	M	M	0	3	0.0880	0.2691	0.0273	0.2929
36	H	M	M	H	0	3	0.0483	0.1927	0.0189	0.1858
37	L	M	M	L	0	1	0.1401	0.1811	0.0310	0.7581
38	L	M	M	M	0	1	0.1407	0.2004	0.0297	0.6955
39	L	M	M	H	0	1	0.1522	0.1902	0.0299	0.6254
40	L	M	M	L	0	2	0.1510	0.2354	0.0296	0.6777
41	L	M	M	M	0	2	0.1382	0.2551	0.0253	0.5748
42	L	M	M	H	0	2	0.1561	0.2178	0.0306	0.4763
43	L	M	M	L	0	3	0.1562	0.2833	0.0312	0.6010
44	L	M	M	M	0	3	0.1271	0.2899	0.0242	0.4779
45	L	M	M	H	0	3	0.1503	0.2237	0.0317	0.3764
46	M	H	M	L	0	1	0.1343	0.2170	0.0301	0.6863
47	M	H	M	M	0	1	0.1285	0.2413	0.0291	0.5890
48	M	H	M	H	0	1	0.1140	0.2496	0.0265	0.4645
49	M	H	M	L	0	2	0.1294	0.2820	0.0299	0.5463
50	M	H	M	M	0	2	0.1047	0.2808	0.0268	0.4142
51	M	H	M	H	0	2	0.0755	0.2377	0.0224	0.2873
52	M	H	M	L	0	3	0.1202	0.3220	0.0326	0.4425
53	M	H	M	M	0	3	0.0818	0.2872	0.0267	0.3099
54	M	H	M	H	0	3	0.0481	0.2117	0.0201	0.2020
55	M	L	M	L	0	1	0.1476	0.1913	0.0343	0.7054
56	M	L	M	M	0	1	0.1467	0.2131	0.0320	0.6099
57	M	L	M	H	0	1	0.1370	0.2215	0.0278	0.4852
58	M	L	M	L	0	2	0.1496	0.2522	0.0311	0.5684
59	M	L	M	M	0	2	0.1282	0.2527	0.0264	0.4350
60	M	L	M	H	0	2	0.0975	0.2148	0.0203	0.3041
61	M	L	M	L	0	3	0.1437	0.2924	0.0338	0.4644
62	M	L	M	M	0	3	0.1050	0.2627	0.0256	0.3280
63	M	L	M	H	0	3	0.0638	0.1941	0.0169	0.2150
64	M	H	H	L	0	1	0.1532	0.2109	0.0342	0.7008
65	M	H	H	M	0	1	0.1462	0.2297	0.0324	0.6043
66	M	H	H	H	0	1	0.1302	0.2332	0.0287	0.4793
67	M	H	H	L	0	2	0.1485	0.2692	0.0316	0.5628
68	M	H	H	M	0	2	0.1221	0.2648	0.0274	0.4295
69	M	H	H	H	0	2	0.0897	0.2216	0.0218	0.2996
70	M	H	H	L	0	3	0.1389	0.3069	0.0340	0.4588
71	M	H	H	M	0	3	0.0975	0.2716	0.0265	0.3233
72	M	H	H	H	0	3	0.0584	0.1985	0.0186	0.2116
73	M	H	L	L	0	1	0.0654	0.4505	0.0219	0.5089
74	M	H	L	M	0	1	0.0553	0.4892	0.0227	0.4166
75	M	H	L	H	0	1	0.0385	0.4923	0.0232	0.3129
76	M	H	L	L	0	2	0.0567	0.5328	0.0279	0.3659
77	M	H	L	M	0	2	0.0340	0.5097	0.0285	0.2631

78	M	H	L	H	0	2	0.0157	0.4228	0.0276	0.1763
79	M	H	L	L	0	3	0.0460	0.5567	0.0328	0.2784
80	M	H	L	M	0	3	0.0194	0.4782	0.0319	0.1873
81	M	H	L	H	0	3	0.0060	0.3514	0.0293	0.1197
82	M	L	L	L	0	1	0.1372	0.1751	0.0239	0.7110
83	M	L	L	M	0	1	0.1531	0.2108	0.0231	0.6205
84	M	L	L	H	0	1	0.1615	0.2383	0.0210	0.4984
85	M	L	L	L	0	2	0.1519	0.2507	0.0255	0.5729
86	M	L	L	M	0	2	0.1425	0.2670	0.0222	0.4406
87	M	L	L	H	0	2	0.1173	0.2413	0.0175	0.3088
88	M	L	L	L	0	3	0.1515	0.2995	0.0298	0.4670
89	M	L	L	M	0	3	0.1193	0.2824	0.0234	0.3305
90	M	L	L	H	0	3	0.0772	0.2189	0.0159	0.2167
91	M	L	H	L	0	1	0.1588	0.2043	0.0356	0.7057
92	M	L	H	M	0	1	0.1535	0.2224	0.0332	0.6097
93	M	L	H	H	0	1	0.1391	0.2260	0.0288	0.4846
94	M	L	H	L	0	2	0.1567	0.2616	0.0317	0.5685
95	M	L	H	M	0	2	0.1313	0.2576	0.0269	0.4348
96	M	L	H	H	0	2	0.0978	0.2158	0.0206	0.3039
97	M	L	H	L	0	3	0.1483	0.2994	0.0342	0.4644
98	M	L	H	M	0	3	0.1065	0.2655	0.0259	0.3279
99	M	L	H	H	0	3	0.0638	0.1941	0.0171	0.2150
100	M	M	M	L	50	1	0.2934	0.4410	0.0330	0.5289
101	M	M	M	M	50	1	0.2593	0.4469	0.0318	0.4257
102	M	M	M	H	50	1	0.2074	0.4037	0.0285	0.3107
103	M	M	M	L	50	2	0.2491	0.5071	0.0320	0.3846
104	M	M	M	M	50	2	0.1821	0.4376	0.0280	0.2695
105	M	M	M	H	50	2	0.1186	0.3175	0.0221	0.1742
106	M	M	M	L	50	3	0.2109	0.5266	0.0352	0.2929
107	M	M	M	M	50	3	0.1307	0.4029	0.0275	0.1904
108	M	M	M	H	50	3	0.0702	0.2579	0.0190	0.1172
109	M	M	M	L	25	1	0.1949	0.2827	0.0317	0.6317
110	M	M	M	M	25	1	0.1834	0.3038	0.0305	0.5298
111	M	M	M	H	25	1	0.1588	0.2982	0.0272	0.4057
112	M	M	M	L	25	2	0.1816	0.3526	0.0307	0.4870
113	M	M	M	M	25	2	0.1436	0.3320	0.0268	0.3581
114	M	M	M	H	25	2	0.1005	0.2632	0.0212	0.2413
115	M	M	M	L	25	3	0.1643	0.3896	0.0337	0.3854
116	M	M	M	M	25	3	0.1096	0.3263	0.0264	0.2619
117	M	M	M	H	25	3	0.0620	0.2260	0.0183	0.1666
118	M	M	H	L	95	1	1.0530	1.6299	0.0395	0.0981
119	M	M	H	M	95	1	0.6976	1.2315	0.0375	0.0678
120	M	M	H	H	95	1	0.4205	0.8139	0.0326	0.0428
121	M	M	H	L	95	2	0.6067	1.2900	0.0370	0.0579
122	M	M	H	M	95	2	0.3418	0.8190	0.0312	0.0354
123	M	M	H	H	95	2	0.1834	0.4627	0.0235	0.0207

124	M	M	H	L	95	3	0.4139	1.0764	0.0402	0.0394
125	M	M	H	M	95	3	0.2091	0.6278	0.0299	0.0230
126	M	M	H	H	95	3	0.0986	0.3309	0.0194	0.0132
127	H	H	H	L	0	1	0.1498	0.2293	0.0367	0.6512
128	H	H	H	M	0	1	0.1376	0.2472	0.0348	0.5338
129	H	H	H	H	0	1	0.1138	0.2385	0.0305	0.3953
130	H	H	H	L	0	2	0.1433	0.2818	0.0345	0.5215
131	H	H	H	M	0	2	0.1129	0.2696	0.0299	0.3825
132	H	H	H	H	0	2	0.0769	0.2158	0.0236	0.2548
133	H	H	H	L	0	3	0.1345	0.3128	0.0365	0.4289
134	H	H	H	M	0	3	0.0912	0.2702	0.0284	0.2938
135	H	H	H	H	0	3	0.0510	0.1917	0.0198	0.1864
136	H	H	H	L	95	1	0.8251	1.5129	0.0437	0.0804
137	H	H	H	M	95	1	0.5078	1.0739	0.0414	0.0521
138	H	H	H	H	95	1	0.2842	0.6645	0.0354	0.0309
139	H	H	H	L	95	2	0.5040	1.2080	0.0415	0.0495
140	H	H	H	M	95	2	0.2732	0.7434	0.0349	0.0293
141	H	H	H	H	95	2	0.1390	0.4080	0.0263	0.0166
142	H	H	H	L	95	3	0.3611	1.0202	0.0436	0.0350
143	H	H	H	M	95	3	0.1783	0.5853	0.0327	0.0200
144	H	H	H	H	95	3	0.0808	0.3040	0.0216	0.0112
145	H	H	L	L	0	1	0.0608	0.4766	0.0232	0.4577
146	H	H	L	M	0	1	0.0481	0.5022	0.0246	0.3531
147	H	H	L	H	0	1	0.0301	0.4732	0.0255	0.2474
148	H	H	L	L	0	2	0.0510	0.5369	0.0296	0.3311
149	H	H	L	M	0	2	0.0278	0.4943	0.0303	0.2293
150	H	H	L	H	0	2	0.0103	0.3891	0.0291	0.1476
151	H	H	L	L	0	3	0.0422	0.5508	0.0344	0.2566
152	H	H	L	M	0	3	0.0161	0.4594	0.0334	0.1685
153	H	H	L	H	0	3	0.0031	0.3256	0.0302	0.1048
154	H	H	L	L	95	1	no fit			
155	H	H	L	M	95	1				
156	H	H	L	H	95	1				
157	H	H	L	L	95	2				
158	H	H	L	M	95	2				
159	H	H	L	H	95	2				
160	H	H	L	L	95	3				
161	H	H	L	M	95	3				
162	H	H	L	H	95	3				
163	H	L	H	L	0	1	0.1563	0.2223	0.0384	0.6565
164	H	L	H	M	0	1	0.1457	0.2398	0.0358	0.5393
165	H	L	H	H	0	1	0.1229	0.2318	0.0307	0.4003
166	H	L	H	L	0	2	0.1519	0.2742	0.0349	0.5272
167	H	L	H	M	0	2	0.1221	0.2628	0.0296	0.3876
168	H	L	H	H	0	2	0.0845	0.2106	0.0226	0.2586
169	H	L	H	L	0	3	0.1439	0.3055	0.0368	0.4343

170	H	L	H	M	0	3	0.1000	0.2644	0.0279	0.2981
171	H	L	H	H	0	3	0.0563	0.1878	0.0185	0.1894
172	H	L	H	L	95	1	0.8586	1.4968	0.0438	0.0810
173	H	L	H	M	95	1	0.5301	1.0634	0.0412	0.0524
174	H	L	H	H	95	1	0.2975	0.6582	0.0350	0.0312
175	H	L	H	L	95	2	0.5256	1.1978	0.0410	0.0499
176	H	L	H	M	95	2	0.2858	0.7374	0.0343	0.0295
177	H	L	H	H	95	2	0.1454	0.4047	0.0254	0.0167
178	H	L	H	L	95	3	0.3771	1.0131	0.0433	0.0353
179	H	L	H	M	95	3	0.1868	0.5813	0.0320	0.0202
180	H	L	H	H	95	3	0.0841	0.3018	0.0206	0.0113
181	H	L	L	L	0	1	0.1420	0.1971	0.0258	0.6629
182	H	L	L	M	0	1	0.1532	0.2336	0.0249	0.5498
183	H	L	L	H	0	1	0.1499	0.2484	0.0224	0.4117
184	H	L	L	L	0	2	0.1476	0.2644	0.0280	0.5311
185	H	L	L	M	0	2	0.1312	0.2717	0.0243	0.3923
186	H	L	L	H	0	2	0.0990	0.2322	0.0190	0.2623
187	H	L	L	L	0	3	0.1456	0.3054	0.0321	0.4365
188	H	L	L	M	0	3	0.1092	0.2794	0.0250	0.3002
189	H	L	L	H	0	3	0.0646	0.2084	0.0168	0.1907
190	H	L	L	L	95	1	0.8649	1.5303	0.0399	0.0804
191	H	L	L	M	95	1	0.5482	1.1034	0.0381	0.0520
192	H	L	L	H	95	1	0.3135	0.6908	0.0327	0.0309
193	H	L	L	L	95	2	0.5244	1.2230	0.0392	0.0495
194	H	L	L	M	95	2	0.2883	0.7591	0.0331	0.0293
195	H	L	L	H	95	2	0.1472	0.4192	0.0247	0.0166
196	H	L	L	L	95	3	0.3748	1.0330	0.0421	0.0350
197	H	L	L	M	95	3	0.1864	0.5960	0.0314	0.0200
198	H	L	L	H	95	3	0.0836	0.3109	0.0204	0.0112
199	H	M	M	L	95	1	0.8067	1.5202	0.0421	0.0799
200	H	M	M	M	95	1	0.4975	1.0814	0.0402	0.0517
201	H	M	M	H	95	1	0.2785	0.6703	0.0346	0.0307
202	H	M	M	L	95	2	0.4926	1.2143	0.0407	0.0492
203	H	M	M	M	95	2	0.2668	0.7484	0.0345	0.0291
204	H	M	M	H	95	2	0.1352	0.4113	0.0260	0.0165
205	H	M	M	L	95	3	0.3532	1.0254	0.0430	0.0348
206	H	M	M	M	95	3	0.1738	0.5890	0.0324	0.0199
207	H	M	M	H	95	3	0.0782	0.3062	0.0215	0.0112
208	M	H	H	L	95	1	1.0252	1.6447	0.0399	0.0975
209	M	H	H	M	95	1	0.6778	1.2419	0.0380	0.0674
210	M	H	H	H	95	1	0.4078	0.8205	0.0331	0.0426
211	M	H	H	L	95	2	0.5894	1.2989	0.0376	0.0576
212	M	H	H	M	95	2	0.3316	0.8244	0.0319	0.0352
213	M	H	H	H	95	2	0.1782	0.4658	0.0242	0.0206
214	M	H	H	L	95	3	0.4016	1.0825	0.0407	0.0392
215	M	H	H	M	95	3	0.2026	0.6313	0.0305	0.0229

216	M	H	H	H	95	3	0.0964	0.3328	0.0202	0.0131
217	M	H	L	L	95	1	no fit			
218	M	H	L	M	95	1				
219	M	H	L	H	95	1				
220	M	H	L	L	95	2				
221	M	H	L	M	95	2				
222	M	H	L	H	95	2				
223	M	H	L	L	95	3				
224	M	H	L	M	95	3				
225	M	H	L	H	95	3				
226	M	H	M	L	95	1	0.8869	1.7570	0.0395	0.0930
227	M	H	M	M	95	1	0.5821	1.3239	0.0382	0.0643
228	M	H	M	H	95	1	0.3471	0.8743	0.0342	0.0406
229	M	H	M	L	95	2	0.5055	1.3701	0.0390	0.0548
230	M	H	M	M	95	2	0.2819	0.8694	0.0340	0.0335
231	M	H	M	H	95	2	0.1515	0.4924	0.0272	0.0196
232	M	H	M	L	95	3	0.3426	1.1321	0.0420	0.0373
233	M	H	M	M	95	3	0.1710	0.6606	0.0329	0.0218
234	M	H	M	H	95	3	0.0832	0.3495	0.0235	0.0125
235	M	M	L	L	95	1	0.3838	2.2938	0.0330	0.0740
236	M	M	L	M	95	1	0.2425	1.7087	0.0327	0.0515
237	M	M	L	H	95	1	0.1293	1.1223	0.0300	0.0328
238	M	M	L	L	95	2	0.2071	1.7026	0.0374	0.0432
239	M	M	L	M	95	2	0.1009	1.0747	0.0339	0.0267
240	M	M	L	H	95	2	0.0414	0.6109	0.0280	0.0158
241	M	M	L	L	95	3	0.1357	1.3613	0.0410	0.0294
242	M	M	L	M	95	3	0.0530	0.7933	0.0344	0.0173
243	M	M	L	H	95	3	0.0153	0.4237	0.0265	0.0101
244	L	H	H	L	0	1	0.1548	0.1953	0.0350	0.7598
245	L	H	H	M	0	1	0.1528	0.2122	0.0330	0.6968
246	L	H	H	H	0	1	0.1621	0.1982	0.0354	0.6264
247	L	H	H	L	0	2	0.1634	0.2471	0.0319	0.6793
248	L	H	H	M	0	2	0.1476	0.2632	0.0270	0.5760
249	L	H	H	H	0	2	0.1628	0.2219	0.0345	0.4774
250	L	H	H	L	0	3	0.1662	0.2927	0.0330	0.6025
251	L	H	H	M	0	3	0.1345	0.2954	0.0253	0.4791
252	L	H	H	H	0	3	0.1549	0.2255	0.0350	0.3774
253	L	H	H	L	95	1	1.3539	1.9542	0.0406	0.1247
254	L	H	H	M	95	1	1.0087	1.6350	0.0386	0.0959
255	L	H	H	H	95	1	0.8502	1.0799	0.0415	0.0730
256	L	H	H	L	95	2	0.9764	1.8143	0.0376	0.0888
257	L	H	H	M	95	2	0.6119	1.3170	0.0320	0.0603
258	L	H	H	H	95	2	0.5257	0.7426	0.0390	0.0419
259	L	H	H	L	95	3	0.7375	1.6469	0.0397	0.0661
260	L	H	H	M	95	3	0.4109	1.0875	0.0302	0.0422
261	L	H	H	H	95	3	0.3791	0.5667	0.0389	0.0285

262	L	H	L	L	0	1	0.0647	0.4092	0.0209	0.5729
263	L	H	L	M	0	1	0.0561	0.4469	0.0209	0.5069
264	L	H	L	H	0	1	0.0573	0.4501	0.0210	0.4409
265	L	H	L	L	0	2	0.0684	0.4980	0.0251	0.4745
266	L	H	L	M	0	2	0.0443	0.5208	0.0248	0.3813
267	L	H	L	H	0	2	0.0517	0.4720	0.0252	0.3035
268	L	H	L	L	0	3	0.0655	0.5573	0.0284	0.3958
269	L	H	L	M	0	3	0.0317	0.5454	0.0273	0.2982
270	L	H	L	H	0	3	0.0466	0.4506	0.0278	0.2263
271	L	H	L	L	95	1	no fit			
272	L	H	L	M	95	1				
273	L	H	L	H	95	1				
274	L	H	L	L	95	2				
275	L	H	L	M	95	2				
276	L	H	L	H	95	2				
277	L	H	L	L	95	3				
278	L	H	L	M	95	3				
279	L	H	L	H	95	3				
280	L	L	H	L	0	1	0.1593	0.1894	0.0372	0.7642
281	L	L	H	M	0	1	0.1585	0.2056	0.0344	0.7017
282	L	L	H	H	0	1	0.1689	0.1912	0.0409	0.6317
283	L	L	H	L	0	2	0.1697	0.2400	0.0323	0.6845
284	L	L	H	M	0	2	0.1558	0.2557	0.0268	0.5816
285	L	L	H	H	0	2	0.1718	0.2146	0.0371	0.4828
286	L	L	H	L	0	3	0.1742	0.2851	0.0334	0.6082
287	L	L	H	M	0	3	0.1438	0.2879	0.0248	0.4847
288	L	L	H	H	0	3	0.1647	0.2187	0.0371	0.3825
289	L	L	H	L	95	1	1.4034	1.9296	0.0407	0.1256
290	L	L	H	M	95	1	1.0483	1.6159	0.0383	0.0967
291	L	L	H	H	95	1	0.8830	1.0653	0.0431	0.0736
292	L	L	H	L	95	2	1.0141	1.7964	0.0371	0.0894
293	L	L	H	M	95	2	0.6373	1.3048	0.0312	0.0608
294	L	L	H	H	95	2	0.5464	0.7340	0.0392	0.0422
295	L	L	H	L	95	3	0.7671	1.6335	0.0392	0.0666
296	L	L	H	M	95	3	0.4286	1.0791	0.0294	0.0425
297	L	L	H	H	95	3	0.3940	0.5609	0.0391	0.0287
298	L	L	L	L	0	1	0.1223	0.1491	0.0240	0.7640
299	L	L	L	M	0	1	0.1355	0.1753	0.0234	0.7060
300	L	L	L	H	0	1	0.1556	0.1807	0.0241	0.6382
301	L	L	L	L	0	2	0.1447	0.2110	0.0254	0.6852
302	L	L	L	M	0	2	0.1460	0.2421	0.0219	0.5854
303	L	L	L	H	0	2	0.1725	0.2209	0.0279	0.4872
304	L	L	L	L	0	3	0.1598	0.2665	0.0287	0.6092
305	L	L	L	M	0	3	0.1431	0.2868	0.0222	0.4874
306	L	L	L	H	0	3	0.1720	0.2338	0.0304	0.3850
307	L	L	L	L	95	1	1.3574	1.9291	0.0359	0.1247

308	L	L	L	M	95	1	1.0420	1.6446	0.0348	0.0960
309	L	L	L	H	95	1	0.8876	1.1097	0.0352	0.0730
310	L	L	L	L	95	2	0.9898	1.8131	0.0351	0.0887
311	L	L	L	M	95	2	0.6323	1.3335	0.0300	0.0603
312	L	L	L	H	95	2	0.5466	0.7616	0.0352	0.0419
313	L	L	L	L	95	3	0.7536	1.6556	0.0379	0.0660
314	L	L	L	M	95	3	0.4249	1.1035	0.0289	0.0421
315	L	L	L	H	95	3	0.3931	0.5802	0.0360	0.0284
316	L	M	M	L	95	1	1.3177	1.9578	0.0384	0.1239
317	L	M	M	M	95	1	0.9839	1.6419	0.0369	0.0954
318	L	M	M	H	95	1	0.8321	1.0889	0.0374	0.0725
319	L	M	M	L	95	2	0.9517	1.8205	0.0367	0.0882
320	L	M	M	M	95	2	0.5962	1.3241	0.0314	0.0599
321	L	M	M	H	95	2	0.5150	0.7493	0.0365	0.0416
322	L	M	M	L	95	3	0.7201	1.6536	0.0390	0.0656
323	L	M	M	M	95	3	0.4002	1.0936	0.0299	0.0419
324	L	M	M	H	95	3	0.3717	0.5717	0.0369	0.0283
325	M	L	H	L	95	1	1.0652	1.6252	0.0397	0.0982
326	M	L	H	M	95	1	0.7062	1.2282	0.0376	0.0679
327	M	L	H	H	95	1	0.4261	0.8118	0.0325	0.0429
328	M	L	H	L	95	2	0.6142	1.2871	0.0370	0.0580
329	M	L	H	M	95	2	0.3464	0.8173	0.0311	0.0355
330	M	L	H	H	95	2	0.1859	0.4617	0.0233	0.0207
331	M	L	H	L	95	3	0.4193	1.0745	0.0402	0.0395
332	M	L	H	M	95	3	0.2121	0.6267	0.0298	0.0230
333	M	L	H	H	95	3	0.0998	0.3303	0.0192	0.0132
334	M	L	L	L	95	1	1.0664	1.6619	0.0359	0.0975
335	M	L	L	M	95	1	0.7292	1.2800	0.0346	0.0674
336	M	L	L	H	95	1	0.4502	0.8592	0.0303	0.0425
337	M	L	L	L	95	2	0.6145	1.3180	0.0354	0.0575
338	M	L	L	M	95	2	0.3514	0.8453	0.0301	0.0351
339	M	L	L	H	95	2	0.1898	0.4814	0.0227	0.0206
340	M	L	L	L	95	3	0.4182	1.0979	0.0391	0.0391
341	M	L	L	M	95	3	0.2130	0.6446	0.0294	0.0228
342	M	L	L	H	95	3	0.1004	0.3416	0.0191	0.0131
343	M	L	M	L	95	1	1.0577	1.6165	0.0395	0.0982
344	M	L	M	M	95	1	0.7042	1.2257	0.0374	0.0679
345	M	L	M	H	95	1	0.4263	0.8122	0.0324	0.0429
346	M	L	M	L	95	2	0.6117	1.2840	0.0369	0.0580
347	M	L	M	M	95	2	0.3459	0.8169	0.0311	0.0355
348	M	L	M	H	95	2	0.1860	0.4621	0.0232	0.0207
349	M	L	M	L	95	3	0.4181	1.0731	0.0401	0.0395
350	M	L	M	M	95	3	0.2118	0.6267	0.0298	0.0230
351	M	L	M	H	95	3	0.0998	0.3306	0.0192	0.0132